

540 HAZ  
T 152

49645 →

CENTRAL LIBRARY  
TEZPUR UNIVERSITY

Accession No. 49645

Date 14/9/11

CENTRAL LIBRARY, T. U.  
ACC. NO. T. 152

No

REFERENCE BOOK  
NOT TO BE ISSUED  
TEZPUR UNIVERSITY LIBRARY

**REACTIVITY OF SOME BIO-ACTIVE NATURAL  
PRODUCTS AND THEIR SYNTHETIC ANALOGS  
TOWARDS BIO-MOLECULES:  
A MOLECULAR MODELING APPROACH**

**A THESIS SUBMITTED IN PARTIAL FULFILLMENT OF THE  
REQUIREMENTS FOR THE DEGREE OF**

**DOCTOR OF PHILOSOPHY**

**By**

*Kalyan Kumar Hazarika*

**Registration No.: 002 of 2006**



**DEPARTMENT OF CHEMICAL SCIENCES  
SCHOOL OF SCIENCE AND TECHNOLOGY  
TEZPUR UNIVERSITY  
NAPAAM, TEZPUR-784028  
ASSAM, INDIA**

**July 2010**

*Dedicated to...*

*My centenarian grandma,*

*Parents,*

*Wife*

*&*

*Daughter*

## *Declaration*

I hereby declare that the thesis entitled “**Reactivity of some bio-active natural products and their synthetic analogs towards bio-molecules: a Molecular modeling approach**” being submitted to the Department of Chemical Sciences, Tezpur University, is a record of original research work carried out by me. Any text, figures, results or designs that are not of own devising are appropriately referenced in order to give credit to the original author(s). All sources of assistance have been assigned due acknowledgement. I also declare that neither this work as a whole nor a part of it has been submitted to any other university or institute for any other degree, diploma or award.

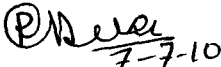
Date: *07.07.2010*

Place: *Tezpur*

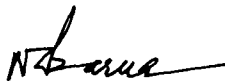
*Kalyan Kr. Hazarika*  
(*Kalyan Kumar Hazarika*)

## *CERTIFICATE*

This is to certify that the work incorporated in the thesis entitled, **“Reactivity of some bio-active natural products and their synthetic analogs towards bio-molecules: a Molecular modeling approach”** submitted to Tezpur University by **Mr. Kalyan Kr Hazarika, M.Sc**, for the Degree of **Doctor of Philosophy** was carried out by the candidate under our joint supervision in the Department of Chemical Sciences, Tezpur University, Assam, India and the Natural Products Chemistry Division, CSIR-North East Institute of Science and Technology, Jorhat, Assam, India. He has been duly registered and the thesis presented is worthy of being considered for the Ph. D. degree. It is certified that the work embodied in this thesis has not been submitted for any degree of any other University/Organization. Any material that has been obtained from other sources is duly acknowledged in the thesis.

  
(Dr. R. C. Debra)  
Supervisor

**Associate Professor**  
**Dept. of Chemical Sciences**  
**Tezpur University- 784028**

  
(Dr. N. C. Barua)  
Co-supervisor

**Dr. N. C. Barua**  
**Scientist "G"**  
**Council of Scientific & Industrial Research**  
**North East Institute of Science & Technology**  
**Govt of India**  
**Jorhat-785006 Assam**

## ACKNOWLEDGEMENTS

*It is a pleasure for me to acknowledge Dr. R. C. Deka, Associate Professor, Department of Chemical Sciences, Tezpur University (T.U.) for his valuable guidance and support during the course of this work. His guidance and association have been very friendly rather than like a formal student-guide relationship. His critical analysis always helped me to improve myself.*

*I am also deeply indebted to Dr. N. C. Barua, Scientist G and the Head of the Natural Products Chemistry Division, CSIR-North East Institute of Science and Technology, (formerly RRL), Jorhat for his motivation, support and guidance.*

*I, as an in-service scholar, extend my sincere gratitude to Prof. S. K. Dolui, (former Dean, Science and Technology, T.U.) and Prof. M. Ahom (former Registrar, T.U.) for their timely administrative supports in some critical period where their help was really required. I also thank Prof. N. S. Islam, Dean, R & D, T.U. for her constant inspiration throughout my PhD period.*

*I express my sincere regards to Prof. A. K. Buragohain, Registrar, T.U. for his encouragement. I wish to express my thanks to Prof. B. K. Konwar, Prof. A. K. Mukherjee and all other members of the Department of Molecular Biology & Biotechnology, and faculty members of the Department of Chemical Sciences, T.U., for their cooperation in completing my research work successfully.*

*My special thanks go to Sourav Mahanta who assisted me in learning some of the relevant techniques. A very special thanks to Dr Paritosh Mondal, for his interest on my research and sharing time for valuable discussions and suggestions.*

*I take this opportunity to express my thanks to Mr Dhiraj Sarma, Computer Engineer; my colleagues Suvenji, Tapasji, Naba, Manab, Pranab, Gohainda, and my all other friends for their wholehearted moral support and help.*

*I would like to thank all labmates (Pubalee, Ajanta-bou, Bulumoni, Subhi, Nabanita, Kusum) for their active co-operation.*

*Above all, words are not enough to say about my family member's love and supports, tremendous patience, trust and encouragement that they have shown to me.*

*Finally, my thanks are due to Prof. M. K. Choudhury, Vice Chancellor, T.U. for developing an ambient environment of research at T.U. and allowing me to submit this work in the form of a thesis.*

*Kalyan K. Hazarika*  
(Kalyan Kumar Hazarika)

**REACTIVITY OF SOME BIO-ACTIVE NATURAL PRODUCTS AND  
THEIR SYNTHETIC ANALOGS TOWARDS BIO-MOLECULES:  
A MOLECULAR MODELING APPROACH**

**ABSTRACT**

In the present thesis we have investigated structure and properties of two categories of organic bio-active molecules having antitubercular and antimalarial activities using several molecular modeling techniques. Density functional theory (DFT) based global and local reactivity descriptors have been utilized to study chemical reactivity and site selectivity of the molecules. We have theoretically verified the molecular structures of the established antitubercular drug isoniazid (INH) and pyrazinamide (PZA) with experimental data and predicted the molecular structure of a novel molecule, 2-methylheptylisonicotinate (MHI). Subsequently, reactivity of INH and PZA are compared with that of MHI and the comparison has been extended to a series of theoretically designed as well as synthetic derivatives of MHI. We also studied the mode of interaction of INH that involves binding of isoniazid-NAD adducts to the active site of *Mycobacterium tuberculosis* enoyl-ACP reductase (InhA) with docking and quantum mechanics/molecular mechanics (QM/MM) approaches. We used DFT based reactivity descriptors alongwith some molecular mechanics (MM) parameters to investigate the antimalarial activities of artemisinin and some of its synthetic derivatives with quantitative structure activity relationship (QSAR) method. We also explored the geometrical parameters, electronic states and interaction energies of heme-artemisinin complexes to have an insight on their mode of interaction. The contents of the thesis are distributed into seven chapters.

**Chapter 1:**

In this chapter we present a brief introduction of TB and malaria diseases as well as some of the important drug molecules used for their treatment. Theoretical works carried out in this field is also reviewed.

World Health Organization (WHO) has identified TB, malaria and AIDS as the three primary diseases of poverty and declared TB as a global health emergency in 1993. TB is a common and often deadly infectious disease caused by *M. tuberculosis*. Approximately 8 million people are infected by TB worldwide which takes 2 million lives every year. Effective control of TB has not been successful mainly because of its lethal combination with AIDS, each speeding the other's progress and also because of the emergence of strains with multi drug resistance (MDR). Although children could be protected from TB by vaccination, no vaccine is available till date for providing reliable protection for adults. INH and PZA are two of the established drugs used for the treatment of TB. Structural features of these two antitubercular drugs are similar to that of MHI which is a novel compound isolated from the culture filtrate of *Streptomyces sp.* 201.

Malaria, another infectious disease caused by the unicellular parasite *Plasmodium sp.*, remains one of the world's greatest public health challenges. Malaria is widespread in 109 countries of tropical and subtropical regions, including parts of the Americas, Asia, and Africa. More than one million people die each year out of approximately 350–500 million cases of malaria. Artemisinin, isolated from the plant *Artemisia annua*, and its synthetic derivatives have been increasingly used over the last two decades in the treatment of MDR malaria causes by *Plasmodium falciparum*. Molecular modeling techniques are very important for designing and developing new drug molecules with antitubercular and antimalarial activities.

**Chapter 2:**

This chapter provides the background of various computational methods such as molecular mechanics (MM), quantum mechanics (QM) and hybrid QM/MM used in the present work. We define various global and local DFT based reactivity parameters which are frequently used in this thesis to predict and compare activity of different antitubercular and anti malarial drug molecules. Importance of DFT based reactivity descriptors as well as some structural



parameters to develop QSAR equations for several drug molecules have been explained.

The need of docking method to describe how two molecules fit together in a three dimensional space has been stressed. Using docking method it is possible to predict the structure of receptor ligand complexes where the receptor is usually a protein and the ligand is either a small molecule or another protein.

### Chapter 3:

In chapter 3, we present the quantum chemical calculations performed to determine the structure and reactivity of two of the most commonly used antitubercular drug molecules, INH and PZA. Having found good agreement with the available experimental data for these two compounds, we extended DFT calculation to predict the properties of MHI which is a novel natural analogue of INH. DFT based reactivity descriptors global softness, global electrophilicity, Fukui function and philicity have been utilized to predict chemically active sites of these three compounds and compare their reactivity. Reactivity of few more synthetic and theoretically designed derivatives of MHI are also presented in this chapter.

### Chapter 4:

In this chapter we investigate the most favorable sites of MHI, INH and PZA in *M. tuberculosis* enoyl-ACP reductase (InhA) using docking method. Interaction of INH-NAD (nicotinamide adenine dinucleotide) and PZA-NAD adducts with the active site of the enzyme are reported by performing docking as well as hybrid QM/MM techniques. The coordinates of INH-NAD adduct to InhA are taken from the Brookhaven Protein Data Bank (PDB code 1ZID) for docking calculation performed using AutoDock Vina. The most favorable docking in the active site of InhA is for MHI followed by INH and PZA. However, the docking of corresponding NAD adducts with InhA are energetically more favorable and follow the trend INH-NAD>PZA-NAD>NADH. The more relevant docked conformations are then used to compute the interaction energy between the ligands and the InhA cavity. Hybrid QM/MM calculations are carried out with QMERA, a program that is integrated with Materials Studio.

**Chapter 5:**

Chapter 5 deals with the comparison of structure and chemical reactivity of artemisinin and some of its selected derivatives using conceptual DFT. We have used the DMol<sup>3</sup> program for optimization of various derivatives of artemisinin. Calculated geometry of artemisinin is in good agreement with the available X-ray data. DFT based global reactivity descriptors such as global softness and global electrophilicity calculated at the optimized geometries are used to investigate the usefulness of these descriptors for understanding the reactive nature of the molecules. Local descriptors, Fukui function and philicity values successfully describe the reactive sites of the molecules which are in agreement with experimental results. Antimalarial activities of artemisinin derivatives against the chloroquine-resistant, mefloquine-sensitive *Plasmodium falciparum* W-2 clone were investigated by QSAR analysis using DFT based descriptors as well as some molecular mechanics (MM) parameters.

**Chapter 6:**

In chapter 6, we focus on the interaction of artemisinin and its derivatives with heme. Artemisinin, a sesquiterpene lactone, possesses a unique structure among the natural products and its endoperoxide bridge is primarily responsible for the antimalarial activity. The interaction of the peroxide group with intracellular heme group of human hemoglobin constitutes the initial stage of the mechanism of action of artemisinin. We have performed a systematic study on interaction and geometrical arrangements of artemisinin with respect to heme by means of DFT calculations. Theoretically calculated geometrical arrangements of the heme-artemisinin complex are found to be in good agreement with available experimental results. Calculated values of interaction energies and electronic states have provided an insight on the mechanism of action of artemisinin with heme.

**Chapter 7:**

The salient conclusions derived in this thesis are summarized in this chapter. Important points emerging out of the present investigation are mentioned on the basis of the results of the work.

# Table

## OF CONTENTS

ABSTRACT .....	i
Table of Contents.....	v
List of Abbreviations .....	ix
List of Figures.....	xi
List of Tables.....	xiii

### **CHAPTER 1 Introduction**

Abstract	1
1.1 Tuberculosis	2
1.1.1 Symptoms and Transmission of TB	3
1.1.2 Prevention and Control of TB	4
1.1.2.1 Vaccination	4
1.1.2.2 Treatment of TB	5
1.1.3 Theoretical efforts in development of new antitubercular drug	7
1.2 Malaria	8
1.2.1 History of Malaria	9
1.2.2 Global Scenario of Malaria	10
1.2.3 Causes of Malaria	11
1.2.4 Control and Treatment of Malaria	11
1.2.4.1 Vaccination	12
1.2.4.2 Treatment of Malaria	13
1.2.5 New Antimalarials and Artemisinin	15
1.2.6 Theoretical efforts in development of new antimalarial	17
References	18

### **CHAPTER 2 Theoretical Methods**

2.1 Computational Chemistry	28
2.1.1 Molecular Mechanics	29

2.1.2	Quantum Chemical Methods	30
2.1.2.1	Density Functional Theory	32
2.1.2.1.1	The Kohn-Sham Equations	34
2.1.2.2	DFT based reactivity descriptors	35
2.1.2.2.1	Global reactivity descriptors	35
2.1.2.2.2	Local reactivity descriptors	37
2.1.3	Hybrid QM/MM methods	39
2.1.4	Quantitative Structure Activity Relationship (QSAR)	42
2.1.4.1	Model Building	44
2.1.4.2	Model Validation	46
2.1.5	Docking	47
2.1.5.1	Docking Approaches	47
	References	48

### **CHAPTER 3 Molecular Structure and Reactivity of Anti-tuberculosis Drug Molecules Isoniazid, Pyrazinamide and 2-Methylheptylisonicotinate: a Density Functional Approach**

	Abstract	54
3.1	Introduction	55
3.2	Theoretical background	57
3.3	Methodology and Computational Details	57
3.4	Results and discussion	58
3.4.1	Geometry Optimization	58
3.4.2	Experimental Reactivity	61
3.4.3	Global Descriptors	62
3.4.3.1	Global Softness/Hardness/Chemical potential	62
3.4.3.2	Electrophilicity Index	62
3.4.4	Local Descriptors	64
3.4.4.1	Fukui function	65
3.4.4.2	Local softness and philicity	66
3.4.4.3	Relative nucleophilicity	66
3.5	Conclusions	66
	References	67

## Table of contents

### **CHAPTER 4 Mode of interaction of anti TB drug molecules using docking and hybrid (QM/MM) methods**

Abstract	71
4.1 Introduction	72
4.2 Computational details	75
4.2.1 Protein and ligands structures	76
4.2.2 Docking studies	77
4.2.3 Hybrid QM/MM studies	78
4.3 Results and discussions	78
4.3.1 Docking calculations	78
4.3.2 Hybrid QM/MM	80
4.3.2.1 Interaction Energy	85
4.4 Conclusions	85
References	86

### **CHAPTER 5 Density Functional Theory Studies on Reactivity of Artemisinin and Some of its Derivatives**

Abstract	91
5.1 Introduction	92
5.2 Computational details	94
5.3 Results and discussion	96
5.3.1 Geometry of Artemisinin	96
5.3.2 Global Descriptors	98
5.3.3 Local Descriptors	100
5.3.3.1 Fukui function	100
5.3.3.2 Local philicity	101
5.3.3.3 Relative electrophilicity	101
5.3.4 QSAR studies	103
5.3.5 Conclusions	106
References	106

**CHAPTER 6 DFT Studies on Heme Artemisinin Interaction**

Abstract	111
6.1 Introduction	112
6.2 Computational details	115
6.3 Results and discussion	116
6.3.1 DFT calculations of artemisinin	116
6.3.1.1 Optimized geometry of artemisinin	116
6.3.1.2 Atomic charges	117
6.3.1.3 Fukui function	118
6.3.1.4 Relative electrophilicity	120
6.3.2 DFT calculations for the heme group	120
6.3.2.1 Geometry	121
6.3.2.2 Atomic charges and spin densities	122
6.3.2.3 Relative energies of heme	125
6.3.3 DFT calculations for heme–artemisinin complex	125
6.3.3.1 Heme–artemisinin interaction energies	127
6.4 Conclusions	128
References	130

**CHAPTER 7 General Conclusions**

General Conclusions	137
Future scopes	139

<b>List of Publications</b>	140
-----------------------------	-----

# List

## OF ABBREVIATIONS

AM1	Austin Model 1
AIDS	Acquired immunodeficiency syndrome
BLYP	Becke exchange functional (B88) in conjunction with the Lee-Yang-Parr correlation functional.
DFT	Density Functional Theory
DMol <sup>3</sup>	Molecular modeling package
DNP	Double Numerical with Polarization basis set
EA	Electron Affinity
$\eta$	Chemical hardness
$f$	Fukui function
$f_k^+ / f_k^-$	Relative electrophilicity
$f_k^- / f_k^+$	Relative nucleophilicity
GAMESS	General Atomic and Molecular Electronic Structure System
GGA	Generalized gradient approximation
HIV	Human Immunodeficiency Virus
HPA	Hirshfeld Population Analysis
HOMO	Highest Occupied Molecular Orbital
IC <sub>50</sub>	Half-maximal inhibitory concentration
IE	Ionization Energy
INH	Isoniazid

## List of Abbreviations

IP	Ionization Potential
IUPAC	International Union of Pure and Applied Chemistry
logP	log of octanol/water partition coefficient
LOO	Leave-One-Out
LUMO	Lowest Unoccupied Molecular Orbital
MHI	2-methylheptylisonicotinate
MIC	minimum inhibitory concentration
MM	Molecular Mechanics
MPA	Mulliken Population Analysis
$\mu$	chemical potential
$\omega, \omega_k^+$	Electrophilicity, local philicity
PZA	Pyrazinamide
QM/MM	Quantum Mechanics/Molecular Mechanics
QSAR	Quantitative Structure Activity Relationship
S	Global softness
TB	Tuberculosis
VWN	Vosko-Wilk-Nusair functional
WHO	World Health Organization



# List

## OF FIGURES

---

FIGURE		Page No.
1.1	Geographic distribution of TB in the world Source: <a href="http://www.cdc.gov/tb">http://www.cdc.gov/tb</a>	2
1.2	Geographic distribution of malaria in the world. Source: <a href="http://www.cdc.gov/malaria">http://www.cdc.gov/malaria</a>	10
2.1	Schematic representation of the calculation regions for a QM/MM treatment.	40
3.1	Schematic Representation of the Molecule of INH and MHI with Adopted Atom Numbering	56
3.2	Isoniazid, Pyrazinamide and 2-methylheptylisonicotinate molecules optimized at BLYP/DNP level.	58
4.1	Structures of isoniazid and of the two redox cofactors NAD <sup>+</sup> and NADH.	72
4.2	Structures of INH-NAD adduct.	74
4.3	INH-NAD adduct complexed to InhA taken from the Brookhaven Protein Data Bank (PDB code 1ZID)	76
4.4	Docked view of ligand (INH-NAD adduct) bound to protein receptor InhA. Hydrogen bonds with existing solvent and the protein	80
4.5	Geometry of INH in INH-NAD adduct in presence of protein environment (bold stick) and in isolation (thin stick).	84
4.6	Geometry of Isoniazid in presence of protein environment.	84
4.7	Geometry of Pyrazinamide in presence of protein environment.	84
5.1	Optimized geometries of 20 analogues of artemisinin	96
5.2	Optimized geometry of artemisinin	98

<b>FIGURE</b>		<b>Page No.</b>
<b>5.3</b>	Variation of hardness of the molecules calculated at BLYP/DNP level.	98
<b>5.4</b>	Variation of electrophilicity of the molecules calculated at BLYP/DNP level.	100
<b>5.5</b>	Variation of local reactivity parameters of the O1 and O2 atoms of all 21 artemisinin derivatives calculated at BLYP/DNP level using HPA.	101
<b>5.6</b>	A plot between experimental and calculated logRA values of all artemisinin derivatives.	105
<b>6.1</b>	Proposed mechanism of action of artemisinin	113
<b>6.2</b>	The optimized geometry of artemisinin.	116
<b>6.3</b>	Heme prosthetic group coordinated to a histidine residue.	121
<b>6.4</b>	Most stable complex between heme and artemisinin (triplet spin state).	126
<b>6.5</b>	Optimized complex between heme and artemisinin at quintet and septet spin state.	126

# List

## OF TABLES

Table		Page No.
3.1	Calculated and experimental geometric parameters of Isoniazid drug molecule. Bond lengths are in Å, bond angles are in degree.	59
3.2	Calculated and experimental geometric parameters of pyrazinamide drug molecule. Bond lengths are in Å, bond angles are in degree.	60
3.3	Geometric parameters of MHI molecule calculated using various functionals with DNP basis set. Bond lengths are in Å, bond angles are in degree.	61
3.4	Global reactivity descriptors for INH, PZA and MHI (in atomic units). The quantities are calculated at BLYP/DNP, BOP/DNP, HCTH/DNP, PW91/DNP, BLYP/TNP and MP2/6-31G** levels.	63
3.5	Calculated Fukui function ( $f_k^-$ ), local softness ( $s_k^-$ ), local philicity ( $\omega_k^-$ ) and relative nucleophilicity ( $f_k^-/f_k^+$ ) values for N3 atom of INH, PZA and MHI. These values are evaluated using BLYP/DNP, BOP/DNP, HCTH/DNP, PW91/DNP and BLYP/TNP levels using HPA and MPA charges.	65
4.1	Calculated docking energies of NAD adduct with INH and PZA drug molecule.	79
4.2	Selected geometric parameters of INH drug molecule in various environments. Bond lengths are in Å, bond angles are in degree.	81
4.3	Selected geometric parameters of PZA drug molecule in various environments. Bond lengths are in Å, bond angles are in degree.	83
4.4	Calculated interaction energies of INH and PZA	85
5.1	Artemisinin (molecule 1) and other derivatives with various functional groups.	95
5.2	Comparison of selected geometric parameters of artemisinin optimized at different theoretical levels with experimental results. Bond lengths are in Å, bond angles and dihedral angles are in degree.	97

<b>5.3</b>	Comparison of the global reactivity descriptors, $\mu$ , $\eta$ , and $\omega$ of artemisinin and various derivatives calculated at BLYP/DNP theoretical levels.	99
<b>5.4</b>	Fukui function ( $f_k^+$ ), local philicity ( $\omega_k^+$ ) and relative electrophilicity ( $f_k^+/f_k^-$ ) values for O1 and O2 atoms of artemisinin and derivatives calculated at BLYP/DNP level using HPA and MPA charges.	102
<b>5.5</b>	Parameters used to build the QSAR models along with the jackknife results for the selected set of artemisinin derivatives.	104
<b>5.6</b>	Experimental and calculated logRA values of artemisinin and derivatives from BLYP/DNP level.	105
<b>6.1</b>	Selected geometric parameters of artemisinin calculated using BLYP/DNP and VWN/DNP levels. Some data from reference works are also indicated.	117
<b>6.2</b>	Mulliken and Hirschfeld atomic charge density for all the oxygen atoms of artemisinin calculated using BLYP/DNP and VWN/DNP level.	117
<b>6.3</b>	Calculated Fukui function ( $f_k^-, f_k^+$ ), relative nucleophilicity ( $f_k^-/f_k^+$ ) and relative electrophilicity ( $f_k^+/f_k^-$ ) values of all the oxygen atoms of artemisinin. These values are evaluated at BLYP/DNP, VWN/DNP levels using HPA and MPA charges.	119
<b>6.4</b>	Selected geometric parameters for heme group coordinated to a histidine residue, calculated at various spin states using BLYP/DNP and VWN/DNP levels. Some data from reference works are also indicated.	122
<b>6.5</b>	Atomic charges on selected atoms of the heme group calculated at BLYP/DNP and VWN/DNP levels.	123
<b>6.6</b>	Spin densities on selected atoms of the heme group calculated at BLYP/DNP and VWN/DNP levels.	124
<b>6.7</b>	Relative energies for heme group coordinated to a histidine residue calculated at BLYP/DNP and VWN/DNP levels of theory	125
<b>6.8</b>	Geometric parameters calculated using BLYP/DNP and VWN/DNP level for the optimized heme-artemisinin complexes	127
<b>6.9</b>	Interaction and relative interaction energies for heme-artemisinin complexes calculated at BLYP/DNP and VWN/DNP levels of theory	128

# 1

## INTRODUCTION

---

### Abstract

Tuberculosis (TB), malaria and AIDS are the three primary diseases of poverty<sup>1</sup> as identified by the World Health Organization (WHO). These three are the world's most devastating diseases that account for 10% of all deaths globally. They have a destructive impact particularly on the developing world.

TB is a common and often deadly infectious disease causing new infections at a rate of about one per second<sup>2</sup> and some 1000 deaths every day. Overall, one-third of the world's population is currently thought to be infected with TB.<sup>3</sup> Effective control of TB has not been successful mainly because of its lethal combination with AIDS, each speeding the other's progress and also because of the emergence of strains with multi drug resistance (MDR). So, the need for more efficient antitubercular agents to fight this disease is intensified.

Malaria, another infectious disease caused by the unicellular parasite *Plasmodium sp.*, remains one of the world's greatest public health challenges. Half of the world's population is at risk of malaria, and an estimated 243 million cases led to an estimated 863 000 deaths in 2008. Artemisinin, isolated from the plant *Artemisia annua*, and its synthetic derivatives have been increasingly used over the last two decades in the treatment of MDR malaria causes by *Plasmodium falciparum*.

An introduction of TB and malaria diseases as well as some of the important drug molecules used for their treatment is presented in this chapter. The importance of molecular modeling techniques in designing and developing new drug molecules and their utility in studying antitubercular and antimalarial drug molecules have also been briefly reviewed.

## 1.1 Tuberculosis

TB is an ancient disease that has co-evolved with humans for many thousands of years, and perhaps for several million years.<sup>4</sup> The oldest known human remains showing signs of TB infection are 9,000 years old.<sup>5</sup> The WHO estimates that in 2008, globally there were 139 cases of TB per 100,000 populations.<sup>6</sup> The distribution of tuberculosis is not uniform across the globe. The highest number of infections is found in the African countries followed by many Asian countries. TB is less common in developed countries. Most of the estimated number of cases in 2008 occurred in Asia (55%) and Africa (30%), with small proportions of cases in the Eastern Mediterranean Region (7%), the European Region (5%) and the Region of the Americas (3%). The five countries that rank first to fifth in terms of total numbers of cases are India (1.6–2.4 million), China (1.0–1.6 million), South Africa (0.38–0.57 million), Nigeria (0.37–0.55 million) and Indonesia (0.34–0.52 million). An estimated 35% of TB cases occur in India and China.

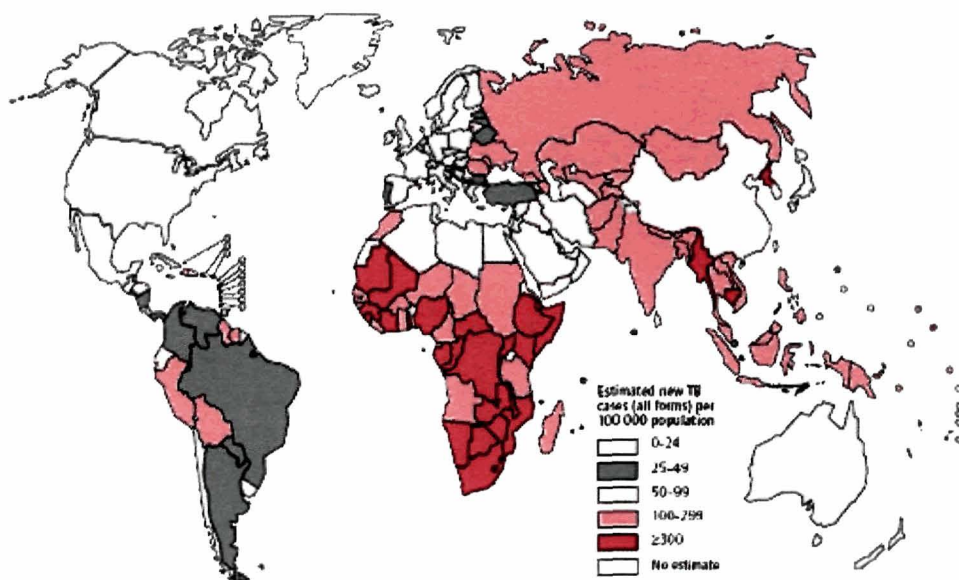


**Figure 1.1** Geographic distribution of TB in the world; Source:<http://www.cdc.gov/tb>

TB is a major public health problem in India that accounts for one-fifth of the global TB incident cases. Each year nearly 2 million people in India develop TB, of which around 0.87 million are infectious cases.<sup>7</sup> It is estimated that annually around 330,000 Indians die due to TB.

### 1.1.1 Symptoms and Transmission of TB

Tuberculosis is caused by mycobacteria, usually *Mycobacterium tuberculosis* in humans.<sup>8</sup> It was identified and described by Robert Koch in 1882. He was awarded the Nobel Prize in physiology or medicine in 1905 for this discovery.<sup>9</sup> The *M. tuberculosis* complex includes four other TB-causing mycobacteria: *M. bovis*, *M. africanum*, *M. canetti* and *M. microti*.<sup>10</sup> Unlike other bacteria which usually attack the lungs, *M. tuberculosis* can attack any part of the body such as the kidney, spine, and brain. If not treated properly, TB disease can be fatal.

TB is a disease basically of those with low immunity. There are a number of known factors that make people more susceptible to TB infection. The most important of these is Human immunodeficiency virus (HIV) that causes *acquired immunodeficiency syndrome* (AIDS), a condition in humans in which the immune system begins to fail, leading to life-threatening opportunistic infections. HIV and TB form a deadly combination. Due to the weak immune system, an HIV-positive person gets co-infected with TB and ultimately dies of it.

Along with population growth, poor nutrition has contribution to the strong link observed between tuberculosis and poverty.<sup>11</sup> The risk of developing active tuberculosis increases with severe malnutrition and its consequent damaging effects on the immune system, particularly in the developing world.<sup>12</sup> The main causes of TB in the people of the developed world are due to their weak immune systems compromised by immunosuppressive drugs or AIDS.

There are some other sources of causing TB. Smoking more than 20 cigarettes a day also increases the risk of TB by two to four times.<sup>13</sup> Diabetes mellitus is also an important risk factor for causing active TB in developing countries.<sup>14</sup> Persons exposed to possible indoor source of silica such as paint, concrete and Portland cement are vulnerable to silicosis and thereby become prone to the attack of TB.

TB is a highly infectious disease. A person with active but untreated tuberculosis can infect 10–15 other people per year.<sup>2</sup> When people suffering from active pulmonary TB, cough, sneeze, talk or spit, they expel infectious aerosol droplets of diameter 0.5 to 5  $\mu\text{m}$ , into the air. A single sneeze can release up to 40,000 such droplets.<sup>15</sup> Inhaling few of these droplets may transmit the disease,

since the infectious dose of tuberculosis is very low and a person needs only to inhale less than ten bacteria.<sup>16</sup> But people infected with TB bacilli do not necessarily become sick with the disease. In most people who breathe in TB bacteria and become infected, the body is able to fight the bacteria to stop them from growing. People with latent TB infection do not feel sick and do not have any symptoms. They are not infectious and cannot spread TB bacteria to others. However, TB bacteria become active if the immune system can't stop them from growing. Active TB bacteria can multiply in human body and make the person sick with TB disease. For persons whose immune systems are weak, especially those with HIV infection, the risk of developing TB disease is much higher than for persons with normal immune systems. Most infections in humans are latent infection, and about one in ten latent infections eventually progresses to active disease, which, if left untreated, kills more than half of its victims.

### **1.1.2 Prevention and control of TB**

WHO developed a Global Plan to stop tuberculosis that aims to save 14 million lives between 2006 and 2015.<sup>6</sup> Since the only host of *M. tuberculosis* is human, eradication would be possible by an effective vaccine.<sup>17</sup> Two parallel approaches are adopted to prevent and control TB. In the first, people with TB and their contacts are identified and then treated. Identification of infections often involves testing high-risk groups for TB. The second approach is vaccination where children are usually protected from TB by it.

#### **1.1.2.1 Vaccination**

Although TB incidences were reduced in 1950s by the introduction of antimycobacterial chemotherapy and the widespread use of BCG vaccine,<sup>18</sup> TB still remains a major international health problem which is likely to become even more alarming in the coming years due partly to TB deaths in HIV-infected patients and partly to the emergence of multidrug resistant strains of the *M. tuberculosis*.<sup>7</sup>

The first genuine success in immunizing against tuberculosis was developed by Albert Calmette and Camille Guérin in 1906 called "BCG" (Bacillus Calmette-Guérin). BCG is the widely accepted vaccine by many of the countries



as part of their TB control programs, especially for infants. According to the WHO, this is the most often used vaccine worldwide, with 85% of infants in 172 countries immunized in 1993.<sup>6</sup> However, BCG vaccination cannot be given to persons who are immunosuppressed (e.g., persons who are HIV infected) or who are likely to become immunocompromised (e.g., persons who are candidates for organ transplant). Although BCG provides some protection against severe forms of pediatric TB, no vaccine is available till date for providing reliable protection for adults.

Several new vaccines to prevent TB infection are being developed. The first recombinant tuberculosis vaccine rBCG30, entered clinical trials in the United States in 2004, sponsored by the National Institute of Allergy and Infectious Diseases (NIAID).<sup>19</sup> Another promising TB vaccine, MVA85A, based on a genetically modified vaccinia virus is currently in phase II trials in South Africa by a group led by Oxford University.<sup>20</sup> Many other strategies are also being used to develop novel vaccines.<sup>21</sup> In order to encourage further discovery, researchers and policymakers are promoting new economic models of vaccine development including prizes, tax incentives and advance market commitments.<sup>22</sup>

### 1.1.2.2 Treatment of TB

Treatment for TB uses antibiotics to kill the bacteria. Effective TB treatment is difficult, due to the unusual structure and chemical composition of the mycobacterial cell wall, which makes many antibiotics ineffective and hinders the entry of drugs.<sup>23</sup> At present, the accepted treatment of tuberculosis is achieved by drugs involving a combination of the first-line anti-TB agents such as isoniazid (INH), rifampicin (RIF), ethambutol (EMB) and pyrazinamide (PZA). There are three main properties of antitubercular drugs: bactericidal activity, sterilizing activity and the ability to prevent resistance. The essential antituberculosis drugs possess these properties to different extents. INH and RIF are the most commonly used powerful bactericidal drugs active against all populations of TB bacilli.<sup>6,24</sup> However, INH is never used alone to treat active tuberculosis because of quick development of resistance. PZA is only used in combination with other drugs such as INH and RIF in the treatment of *M. tuberculosis*. PZA in conjunction with RIF is a preferred treatment for latent tuberculosis.<sup>25</sup>

Unlike treating other bacterial infections, TB requires much longer periods of treatment (around 6 to 24 months) to entirely eliminate mycobacterium from the body.<sup>26</sup> Latent TB treatment usually uses a single antibiotic, while active TB disease is best treated with combinations of several antibiotics, to reduce the risk of the bacteria developing antibiotic resistance.<sup>27</sup> HIV-infected persons with either latent TB infection or active TB disease can be effectively treated with INH, PZA, and EMB.

The Directly Observed Treatment Short-course (DOTS) strategy of global TB eradication program recommended by WHO was based on clinical trials carried out in the 1970s by Tuberculosis Research Centre, Chennai, India. Treatment with properly implemented DOTS has a success rate exceeding 95% and prevents the emergence of further multi-drug resistant strains of tuberculosis. Another program, called "DOTS-Plus"<sup>28</sup>, included the treatment of MDR-TB and was introduced by the WHO in 1998.

Drug-resistant TB is a public health issue in many developing countries, as treatment is longer and requires more expensive drugs. Inconsistent or partial treatment of TB, when patients do not take all their medicines regularly for the required period because they start to feel better, because doctors and health workers prescribe the wrong treatment regimens, or because the drug supply is unreliable, is the main cause of Drug-resistant TB.

Multidrug-resistant TB (MDR TB) is TB that is resistant to at least two of the best first-line anti-TB drugs, INH and RIF. The rise in HIV infections and the neglect of TB control programs have enabled a resurgence of tuberculosis<sup>29</sup> resulting in the declaration of a global health emergency by the WHO in 1993.<sup>6</sup> Every year, nearly half a million new cases of multidrug-resistant tuberculosis (MDR-TB) are estimated to occur worldwide.<sup>6</sup> Extensively drug-resistant TB (XDR TB) is a relatively rare type of MDR TB where TB becomes resistant not only to first line drug but also to three or more of the six classes of second-line drugs.<sup>30</sup> Patients with XDR-TB are left with treatment options that are less effective and more expensive leaving the poor people in the developing world with no or limited access to these treatments.<sup>31</sup>

### 1.1.3 Theoretical efforts in development of new antitubercular drug

INH (isonicotinic acid hydrazide) is the most widely used antitubercular drug.<sup>24,32</sup> In particular, it has been extensively used in the prevention of tuberculosis among both HIV-infected adults and children.<sup>33,34</sup> Interestingly, the antitubercular activity of INH was recognized only in 1951<sup>35</sup> though it was first synthesized in 1912.<sup>36</sup> Since then no alternative novel anti-tubercular chemotherapeutic agents of INH could be introduced. Much effort has been directed at unraveling the genome of *M. tuberculosis* to identify new therapeutic targets. Thus cheap and effective chemotherapeutic agents with low toxicity are the needs of the hours. The lack of priority in the development of novel agents is in part due to a poor financial return on investment available from drugs primarily targeted for a disease which is considered as a 'Third World' problem.

Understanding the mode of action is very important in developing a drug. Molecular modeling studies can be of primary importance to elucidate the mechanism of action of INH and to understand the INH dependent resistances. The information obtained can be useful in designing new drug molecules with better antitubercular activity.

INH is a prodrug and needs activation by a bacterial catalase-peroxidase enzyme called KatG<sup>37</sup> that couples the isonicotinic acyl with NADH to form isonicotinic acyl-NADH complex. This complex binds tightly to ketoenoylreductase known as InhA, thereby blocking the natural enoyl-AcpM substrate and the action of fatty acid synthase. This process inhibits the synthesis of mycolic acid, required for the mycobacterial cell wall. A range of radicals are produced by KatG activation of INH, including nitric oxide<sup>38</sup> which has also been shown to be important in the action of another antimycobacterial prodrug PA-824.<sup>39</sup> On the other hand, PZA is largely bacteriostatic, but can be bacteriocidal on actively replicating TB bacteria. PZA is a prodrug that stops the growth of *M. tuberculosis*.

Considering the pharmacological relevance, worldwide uses of INH and the interest to further understand the details of reactivity, the molecular structure of INH have been investigated theoretically<sup>40-42</sup> by several groups of scientists. Recently, Borba *et al.*<sup>43</sup> studied the structure, spectroscopy, and photochemistry of INH by low-temperature infrared spectroscopy and quantum chemistry

calculations using density functional theory. The theoretical results were then used to interpret the IR spectra of the compound obtained under various experimental conditions.

Favila *et al.*<sup>42</sup> used a new DFT model called CHIH-DFT (Chihuahua-Heterocycles-Density Functional Theory) to calculate the molecular structure, infrared, UV spectra, chemical reactivity and electronic properties of few antitubercular compounds including INH and PZA. Cunha *et al.*<sup>44</sup> carried out a computational study to locate the most energetically-favorable INH–KatG interaction modes. The analysis of the complex formed by KatG and INH during docking simulations was evaluated at *ab initio* level with QM/MM techniques.

Several molecular modeling techniques such as docking and QSAR are utilized to study INH and analogues. Bonnac *et al.*<sup>45</sup> carried out comparative docking experiments with INH-NAD adducts. In a recent article, Amos *et al.*<sup>46</sup> reported their experiment supported by investigation using computational techniques to study the formation of an acyl radical as the active species from the oxidation of isoniazid. In a very recent article Merz, Jr.<sup>47</sup> presented the computation of protein–ligand interaction energies. Apart from those, Pasqualoto *et al.*<sup>48</sup> developed a 3D pharmacophore model of INH analogues hydrazides from a 4D-QSAR analysis. Subsequently, another 3D-QSAR model<sup>49</sup> was generated using the resulting hypothesized active conformations.

## 1.2 Malaria

The word malaria originates from the Italian word mal' aria which means 'bad air'. Malaria is caused by infection with protozoan parasites belonging to the genus *Plasmodium* transmitted by female Anopheles species mosquitoes. Malaria is widespread in tropical and subtropical regions, including parts of the Americas, Asia, and Africa. Transmission of malaria depends mainly on climatic factors such as temperature, humidity, and rainfall. In such climatic conditions anopheles mosquitoes can survive and multiply and help malaria parasites to complete their growth cycle in the mosquitoes.

Malaria is commonly associated with poverty, but is also a cause of poverty<sup>50</sup> and a major hindrance to economic development. Because malaria causes so much illness and death, the disease is a great drain on many national

economies. Since many countries with malaria are already among the poorer nations, the disease maintains a vicious cycle of disease and poverty.

Resistance to anti-malarial drugs and insecticides, the decay of public health infrastructure, population movements, political unrest, and environmental changes such as global warming are contributing to the spread of malaria.<sup>51</sup> Recent studies suggest that the number of malaria cases may double in next 20 years if new methods of control are not devised and implemented.<sup>52</sup>

### 1.2.1 History of Malaria

Malaria has been known since ancient times. Man and Malaria seem to have evolved together. Malaria has infected humans for over 50,000 years.<sup>53</sup> In many of the ancient Roman, Chinese, Indian and Egyptian manuscripts, malaria was mentioned. The symptoms of malaria were described in ancient Chinese medical writings of 2700 BC.<sup>54</sup> Malaria may have contributed to the decline of the Roman Empire,<sup>55</sup> and was so pervasive in Rome that once it was known as the "Roman fever".<sup>56</sup> Malaria appeared in the writings of the Greeks from around 500 BC. Hippocrates, "The Father of Medicine" and probably the first malariologist, described the various malaria fevers of man by 400BC. Malaria became widely recognized in Greece by the 4th century BC, and it was responsible for the decline populations in many cities. *Charaka Samhita*, one of the ancient Indian texts on Ayurvedic medicine which was written in approximately 300 BC, and the *Susruta Samhita*, written about 100 BC, the symptoms of malarial fever were described and attributed to the bites of certain insects. Malaria was the most important health hazard encountered by U.S. troops in the South Pacific during World War II, where about 500,000 men were infected.<sup>57</sup> Sixty thousand American soldiers died of malaria during the North African and South Pacific campaigns.<sup>58</sup>

Scientific studies on malaria made their first significant advance in 1880 with the discovery of the parasites in the blood of malaria patients by Alphonse Laveran. He identified and proposed this organism to be responsible for causing malaria.<sup>9</sup> The malarial parasite was named as *Plasmodium*. Laveran was awarded Nobel Prize for Physiology or Medicine in 1907 for this and related discoveries. Later, it was established that mosquitoes were transmitting disease to and from humans.<sup>59</sup> In 1898, Sir Ronald Ross working in the Presidency General Hospital in

Calcutta finally proved that malaria is transmitted by mosquitoes and for this work Ross received the 1902 Nobel Prize in Medicine.<sup>9</sup> In fact, four Nobel prizes have been awarded for work associated with malaria: to Sir Ronald Ross (1902), Charles Louis Alphonse Laveran (1907), Julius Wagner-Jauregg (1927), and Paul Hermann Muller (1948). The main historical events of discovery of malaria parasites and their vectors have been thoroughly discussed by Cox<sup>60</sup> in a recent review.

### 1.2.2 Global Scenario of Malaria

According to the WHO, nowadays malaria is a tropical and parasitic disease that causes more deaths and socioeconomic problems in the world than AIDS. Each year, there are approximately 350–500 million cases of malaria,<sup>61</sup> killing between one and three million people, the majority of whom are young children in Sub-Saharan Africa.<sup>62</sup> According to the World Health Organization's World Malaria Report 2009 and the Global Malaria Action Plan 3.3 billion people (half the world's population) is at the risk of malaria in 109 countries and territories. Ninety eight percent of global malaria deaths occur in 35 countries (30 in sub-Saharan Africa and 5 in Asia). The geographical distribution of malaria in the world is presented in Figure 1.2.

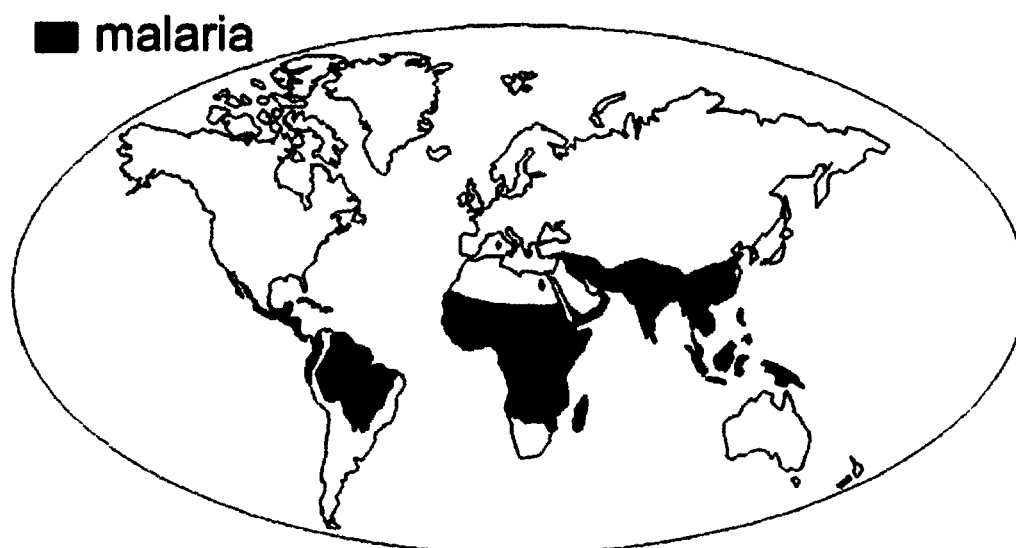


**Figure 1.2** Geographic distribution of malaria in the world

Source: <http://www.cdc.gov/malaria>.

### 1.2.3 Causes of Malaria

There are four members of the *Plasmodium* genus that infect humans. *Plasmodium vivax*, *Plasmodium ovale* and *Plasmodium malariae* cause mild forms of malaria by destroying red blood cells in peripheral capillaries and thus causing anaemia that is not generally fatal. The parasite responsible for the vast majority of fatal malaria infections, *Plasmodium falciparum*, leads to severe infections and if not promptly treated, may kill patients in a matter of hours. The fifth species, *Plasmodium knowlesi*, that causes malaria in macaques in Southeast Asia, can also infect humans, causing malaria that is transmitted from animal to human ("zoonotic" malaria).<sup>63</sup> Malaria is transmitted by inoculation of sporozoites during a bite of an infected female mosquito, *Anopheles*.<sup>64</sup> When a mosquito bites an infected person, a small amount of blood is taken, which contains malaria parasites. The parasite invades and develops within hepatocytes to release merozoites, which quickly invade erythrocytes to grow from "rings" to mature trophozoites, then to schizonts, and finally to release merozoites that invade more erythrocytes, repeating the cycle.<sup>65</sup> Thus the parasite develops within the mosquito. About one week later, when the mosquito takes its next blood meal, these parasites mix with the mosquito's saliva and are injected into the person being bitten. Sometimes, transmission occurs by blood transfusion, organ transplantation, needle sharing, or congenitally from mother to fetus. After a period of between 2 weeks and several months (occasionally years) spent in the liver, the malaria parasites start to multiply within red blood cells, causing symptoms that include fever and headache. In severe cases the disease worsens leading to coma, and death.

### 1.2.4 Control and treatment of malaria

Despite more than a century of efforts to eradicate or control malaria, the disease remains a major and growing threat to the public health and economic development of countries in the tropical and subtropical regions of the world. Control of malaria is a difficult task as it involves three living beings: Man (the host), *Plasmodia* (the agent), and *Anopheles* mosquito (the vector).

The international efforts on malaria control started in the 1950s were initially successful in the late 50's and early 60's. But later the program failed

globally because of various reasons such as the resistance of mosquitoes to insecticides used to kill them, the resistance of malaria parasites to drugs used to treat them, and administrative issues. Although malaria has been eliminated from many developed countries with temperate climates it is still a major health problem in many developing countries, in tropical and subtropical parts of the world.

#### 1.2.4.1 Vaccination

A safe and effective vaccine would have been the easiest way to control this disease, but even after decades of search, that vaccine is still indefinable. The malaria parasite is a complex organism with a complicated life cycle and its antigens are constantly changing. Developing a vaccine to prevent malaria has not become a reality because of the complex life cycle of the parasite involving human and vector mosquitoes as well as its allelic diversity and antigenic variations. However, many scientists all over the world are working on developing an effective malaria vaccine and clinical trials with possible vaccines are currently happening. But the challenging task of producing a widely available vaccine that provides a high level of protection for a sustained period is yet to be met<sup>66</sup> and as such a completely effective vaccine is not still available. The first promising studies demonstrating the potential for a malaria vaccine were performed in 1967 by immunizing mice.<sup>67</sup> Since the 1970s, there has been a considerable effort to develop similar vaccination strategies within humans. It was determined that an individual can be protected from a *P. falciparum* infection if they receive over 1,000 bites from infected, irradiated mosquitoes.<sup>68</sup> In fact, the first malaria vaccine that has undergone field trials is the SPf66, developed by Manuel Elkin Patarroyo in 1987. During phase I trials a 75% efficacy rate was demonstrated and the vaccine appeared to be well tolerated by subjects and immunogenic. The phase IIb and III trials were less promising, with the efficacy falling to between 38.8% and 60.2%. However, the efficacy of Patarroyo's vaccine has been disputed with some US scientists concluding in *The Lancet* (1997) that "the vaccine was not effective and should be dropped" while the Colombian accused them of "arrogance" putting down their assertions to the fact that he came from a developing country.

Among the malaria vaccines being developed, the RTS,S/AS02A vaccine is the candidate furthest along in vaccine trials.<sup>69</sup> This is the first of the current



generation of malaria vaccines that has reached upto Phase III testing.<sup>70</sup> The vaccine has a promising safety profile with more than 50% efficacy in reducing episodes of clinical malaria in children 5 to 17 months old in earlier testing, and can be administered together with the package of vaccinations routinely given to African children. However, further research will delay this vaccine from commercial release until around 2011.<sup>71</sup> A Phase III trial of the world's most clinically advanced malaria vaccine candidate was launched in Kisumu, Kenya, in July 2009.<sup>61</sup>

Notwithstanding serious efforts, a successful malaria vaccine is yet to be found, although one is in advanced clinical trials.<sup>72</sup> Therefore, development of new antimalarials is crucial to the control and management of the disease. An international effort<sup>73</sup> was launched in 1996 to sequence the *P. falciparum* genome with the expectation that the genome sequence would open new avenues for research. The sequencing *P. falciparum* genome was completed in 2002,<sup>74</sup> and hopefully, this knowledge will provide targets for new drugs or vaccines.

#### 1.2.4.2 Treatment of Malaria

Malaria has traditionally been treated with quinolines such as chloroquine, quinine, mefloquine, and primaquine and with antifolates such as Fansidar (sulfadoxinepyrimethamine). Chloroquine is the prototype anti malarial drug, most widely used to treat all types of malarial infections. It is also the cheapest, time tested and safe anti malarial agent. Most of the drugs for the treatment of malaria are derivatives of quinoline and acridine.

As early as 16th century, natural products gained wide acceptance in treatment of malaria, when the therapeutic action of the bark of cinchona tree was observed by indigenous people from South America. The active compound quinine isolated in 1820 was mainly used for malaria until other synthetic antimalarials were developed. Two of the important antimalarial drugs were derived from plants: quinine from the cinchona tree and artemisinin from the Qinghao plant. It is interesting to know that some of the important antimalarial drugs were developed under the influences of wars. Chloroquine resulted from the World War II. Mefloquin resulted from the Vietnam War on the American side, as a result of research into newer anti malarials, to protect the American soldiers from

the multi drug resistant falciparum malaria. Artemisinin also resulted from the Vietnam War as a result of large-scale research launched by the Chinese Government. However, resistance to antimalarial drugs is proving to be a challenging problem in malaria control in most parts of the world. The incidence of malaria is dramatically increasing since many *P. falciparum* strains are now resistant to widely-used drugs like chloroquine.<sup>75</sup> Since early 60s the sensitivity of the parasites to chloroquine, the best and most widely used drug for treating malaria, has been on the decline. Most of the strains of *P. falciparum* have become resistant to chloroquine and other traditional antimalarials,<sup>76</sup> and this demands further research works to be carried for the discovery of new drug molecules. The appearance of resistant strains of falciparum to some of those drugs has made it necessary to perform further investigation of new classes of compounds which might have effective action against them.<sup>77,78</sup> Newer antimalarials were discovered in an effort to tackle this problem, but all these drugs are either expensive or have undesirable side effects. Moreover, after a variable length of time, the parasites, especially the *falciparum* species, show resistance to these drugs.

Artemisinin, isolated from *Artemisia annua*, have been used in traditional Chinese herbal medicine.<sup>79</sup> The crystalline active principle component artemisinin (qinghaosu) was isolated in 1972<sup>80</sup> and it was found to be far superior to any available alternatives at that time. In particular, they have the ability to rapidly kill a broad range of asexual parasite stages at safe concentrations. The risk of resistance was thought to be low because of their very short half-life. These discoveries coincided with the appearance and spread of resistance to all the other major classes of antimalarials. As a result, artemisinin was picked up as the first-line antimalarial treatment worldwide. Nowadays, artemisinin, as well as some of its derivatives are the most promising class of compounds and rapidly acting antimalarial drugs at hand<sup>81</sup> for the treatment of drug-resistant malaria.

Artemisinin and its derivatives are the only group of compounds that are still effective against drug-resistant strains of malaria and thus the development of new antimalarial drugs is essentially based on these compounds. Artemisinin compounds have a different mode of action compared to other antimalarial drugs as a consequence of their unusual structures. This may be the possible reason why artemisinin compounds are still effective, while the others are not. Artemisinin is a

sesquiterpene lactone with an endoperoxide group, and their unusual 1,2,4-trioxane ring system has been proven to be critical for the antimalarial activity.<sup>82</sup> This unusual compound has a sesquiterpene lactone peroxide, unlike most other antimalarials, lacks nitrogen-containing heterocyclic ring systems and was found to be a superior plasmocidal and blood schizontocidal agent to conventional antimalarial drugs without obvious adverse effects in patients.<sup>80,83</sup>

### 1.2.5 New Antimalarials and Artemisinin

Artemisinin is obtained from *Artemisia annua*, with a maximum yield of 0.1%. Most of the active compound is found in the leaves and flowering tops of the plant, the highest yield being obtained just before flowering. The plant can be grown in many places but it shows peculiar behavior as all the plants may not yield artemisinin. Special agricultural conditions must be maintained for the plant to synthesize the product. Plantations in North Vietnam, mainly in the vicinity of Hanoi give best results with the highest content of artemisinin. Studies on artemisinin production requirements conducted in China, India, Europe and USA indicate that yields vary between 0.01 and 0.17% (w/w), depending on plant variety, cultivation conditions, harvest season and locality. In India, artemisinin is reported to have been isolated to the extent of 0.17% (w/w) from *Artemisia annua* plantation around Lucknow.<sup>84</sup> Total synthesis and biochemical synthesis of artemisinin have also been demonstrated, but these routes are economically unattractive being very complicated with low yield, and, therefore, are not viable as the mainstream source of artemisinin.<sup>85</sup>

The combination of outstanding biological activity, an interesting chemical structure (having promising prospects as a lead compound) and low yields of artemisinin from natural sources prompted scientists all over the world to search for new synthetic routes for artemisinin and related compounds.<sup>86</sup> However, the practical values of artemisinin as an antimalarial drug, nevertheless, are impaired by its poor solubility either in oil or water; the high rate of parasite recrudescence after treatment, and its poor oral activity.<sup>87</sup> The search for more effective and soluble drugs is still going on and a number of derivatives of the present drug have been prepared. Reduction of artemisinin to dihydroartemisinin (DHA) has in turn led to the preparation of a series of semisynthetic first-generation analogues which

include artemether, arteether, water soluble sodium artesunate and sodium artelinate. These semisynthetic derivatives are more active than artemisinin and are currently the drugs of choice for the treatment of malaria caused by multidrug-resistant *P. falciparum*.<sup>88</sup> The current developments of artemisinin and its derivatives including its dimers, trimers and tetramers, as potential 'leads' for anti-malarial and anticancer drugs have been reviewed very recently.<sup>89</sup>

To minimize the risk of artemisinin resistance the WHO recommended to use this in combination with other antimalarials as artemisinin combination therapies (ACTs).<sup>90</sup> ACTs are the first-line treatments for uncomplicated *P. falciparum* malaria in most malaria-endemic countries. Recently, partial artemisinin-resistant *P. falciparum* malaria has emerged on the Cambodia–Thailand border. Exposure of the parasite population to artemisinin monotherapies in sub-therapeutic doses for over 30 years, and the availability of substandard artemisinins, have probably been the main driving force in the selection of the resistant phenotype in the region. The current status of artemisinin resistance has been reviewed recently by Dondorp *et al.*<sup>91</sup> If this resistance were to spread, it would be devastating for malaria control efforts worldwide. The enormous challenge for the international community is how to avert this catastrophe and preserve the effectiveness of this antimalarial.<sup>92</sup>

The emergence of drug resistance to most of the available antimalarials has worsened the global malaria situation, which necessitates search for novel antimalarial drugs. Only a few compounds belonging to a new class of antimalarial drugs, including aminoalcohols (mefloquine, halofantrine, lumefantrine), sesquiterpene trioxanes (artemisinin derivatives), and naphthoquinones (atovaquone) have been developed for clinical usage<sup>93</sup> in the past two decades. Many approaches to antimalarial drug discovery currently being deployed cover optimization of therapy with available drugs including combination therapy, developing analogs of the existing drugs, evaluation of potent agents from natural products especially plants, use of compounds originally developed against other diseases, and evaluation of drug-resistance reversers (chemosensitizers) as well as new chemotherapeutic targets.<sup>94</sup> Recently through rational drug design approach, single hybrid molecules with dual functionality and/or targets have been developed as novel antimalarial drugs possessing no or minimum toxicity.<sup>95,96</sup> But

none of these hybrid molecules have reached clinical application so far.<sup>97</sup> One of the challenges of future malarial chemotherapy is to develop compounds that are innovative with respect to the chemical scaffold and molecular target.<sup>98</sup>

Quinine from Cinchona trees provided the lead for the discovery and development of synthetic aminoquinolines.<sup>96,99</sup> Likewise, the discovery of artemisinin from the Chinese herb *Artemisia annua* has served as a template for development of semi-synthetic artemisinins including artesunate and artemether, which are being used extensively in ACT against drug-resistant malaria.<sup>92</sup> The commercial availability of artemisinin (and hence its semi-synthetic derivatives) is limited by the fact that it is a natural product from *Artemisia annua*. Today, no fully synthetic peroxidic antimalarial drug has been made available for clinical application, which is unfortunate because of limitations associated with artemisinin semi-synthetics. The limitations include chemical (availability, purity, and cost), bio-pharmaceutical (poor bioavailability and limiting pharmacokinetics), and treatment (non-compliance with repeated regimens and recrudescence) issues that limit their therapeutic potential.<sup>100</sup> As a result, extensive research into synthetic endoperoxide antimalarials drugs has been undertaken in the last 15 years to produce molecules that are structurally simpler and synthetically accessible with a projected low cost of goods.<sup>101</sup>

Parallel to the experimental research, theoretical methods have also contributed significantly in understanding the properties of these molecules and the mechanism of actions. In the following section the theoretical works carried out on some of these molecules have been briefly highlighted.

### 1.2.6 Theoretical efforts in development of new antimalarial

The artemisinin family of molecules has been extensively studied to elucidate its mechanism of action as an antimalarial and to develop more potent and selective antimalarial agents.<sup>102,103</sup> The detailed mechanism of artemisinin action is still not clear.<sup>104</sup> An essential feature of artemisinin (and analogous molecules) activity is hypothesized to be the presence of a peroxide bridge, which forms a bond with a high valence non-heme iron molecule, leading to generation of free radicals.<sup>102</sup> Theoretical investigations dealing with the mechanism of trioxanes artemisinin were initiated by Gu *et al.*,<sup>82,105</sup> followed soon by several

other quantum-chemical studies.<sup>106-109</sup> Pereira *et al.*<sup>110</sup> performed DFT calculations at B3LYP/6-31G\*\* level to investigate probable mechanisms of decomposition of artemisinin. The results of DFT calculations have been correlated to antimalarial, anticancer, antiangiogenic and neurotoxicity activities of artemisinin and to its thermal, electrochemical, photochemical and spectroscopic properties.

Computational and QSAR studies of drugs molecules provide insights in unraveling their mechanisms of action and guidelines for the syntheses of new derivatives with improved efficiency. A number of QSAR studies have been reported for prescreening of prospective artemisinin analogs for antimalarial activity.<sup>77,111-114</sup>

In the following chapter, we have presented a brief introduction to computational methods namely molecular mechanics, Hartree-Fock, density functional theory and QM/MM methods used in this thesis. We also discuss how DFT based reactivity descriptors can be utilized in deriving efficient QSAR equations.

## References

1. [http://www.wpro.who.int/media\\_centre/press\\_releases/pr\\_20020916.htm](http://www.wpro.who.int/media_centre/press_releases/pr_20020916.htm), *Poverty Issues Dominate WHO Regional Meeting*. (2010)
2. World Health Organization. <http://who.int/mediacentre/factsheets/fs104> (2009)
3. Jasmer, R. M.; Nahid, P.; Hopewell, P. C. Latent Tuberculosis Infection, *N. Engl. J. Med.* **347**, 1860–1866 (2002)
4. Gutierrez, M. C. *et al.* Ancient origin and gene mosaicism of the progenitor of *Mycobacterium tuberculosis*, *PLoS Pathog.* **1**, e5 (2005)
5. Hershkovitz, I. *et al.* Detection and Molecular Characterization of 9000- Year-Old *Mycobacterium tuberculosis* from a Neolithic Settlement in the Eastern Mediterranean, *PLoS ONE* **3**, e3426 (2008)
6. <http://www.who.int>. (2010)
7. World Health Organization "Epidemiology". *Global tuberculosis control: epidemiology, strategy, financing*. 6–33, (2009)
8. Kumar, V.; Abbas, A. K.; Fausto, N.; Mitchell, R. N. *Robbins Basic Pathology* (8th ed.) Saunders Elsevier 516–522 (2007)
9. [http://nobelprize.org/nobel\\_prizes](http://nobelprize.org/nobel_prizes). (2010)

10. van Soolingen *et al.* A novel pathogenic taxon of the Mycobacterium tuberculosis complex, Canetti: characterization of an exceptional isolate from Africa. *Int. J. Syst. Bacteriol.* **47**, 1236–1245 (1997)
11. Davies, P. D. The world-wide increase in tuberculosis: how demographic changes, HIV infection and increasing numbers in poverty are increasing tuberculosis, *Annals of medicine* **35**, 235–243 (2003)
12. Schaible, U. E.; Kaufmann, S. H. Malnutrition and infection: complex mechanisms and global impacts, *PloS Med.* **4**, e115 (2007)
13. Jha, P.; Jacob, B.; Gajalakshmi, V. A nationally representative case–control study of smoking and death in India, *N. Engl. J. Med.* **358**, 1137–1147 (2008)
14. Restrepo, B. I. Convergence of the tuberculosis and diabetes epidemics: renewal of old acquaintances, *Clin. Infect. Dis.* **45**, 436–438 (2007)
15. Cole, E.; Cook, C. Characterization of infectious aerosols in health care facilities: An aid to effective engineering controls and preventive strategies, *Am. J. Infect. Control* **26**, 453–464, (1998)
16. Behr, M. A. Transmission of *Mycobacterium tuberculosis* from patients smear-negative for acid-fast bacilli, *Lancet* **353**, 444–449 (1999)
17. Martin, C. Tuberculosis vaccines: past, present and future, *Curr. Opin. Pulm. Med.* **12**, 186–191 (2006)
18. Chew C.H. , Hu P.Y *Singapore Medical Journal* **15**, 241-245 (1974).
19. <http://www.nih.gov/news/pr/jan2004/niaid-26.htm> (2009)
20. Ibanga, H. *et al.* Early clinical trials with a new tuberculosis vaccine, MVA85A, in tuberculosis-endemic countries: issues in study design, *Lancet Infect. Dis.* **6**, 522–528 (2006)
21. Doherty, T. M.; Andersen, P. Vaccines for Tuberculosis: Novel Concepts and Recent Progress, *Clinical Microbiol.Rev.* **18**, 687–702 (2005)
22. Barder, O.; Kremer, M.; Williams, H. Advance Market Commitments: A Policy to Stimulate Investment in Vaccines for Neglected Diseases, *The Economists' Voice* **3**, (2006)
23. Brennan, P. J.; Nikaido, H. The envelope of mycobacteria, *Annu. Rev. Biochem.* **64**, 29–63 (1995)

24. Silva, F. P. *et al.* Experimental and Theoretical Structure Characterization of Two Isoniazid Derivatives: 2,4-Difluoro-*N'*-isonicotinoylbenzohydrazide and 2,4-Dichloro-*N'*-isonicotinoylbenzohydrazide Hydrochloride, *J. Mol. Struct.* **788**, 63–71 (2006)
25. Centers for Disease Control and Prevention (CDC) "Targeted tuberculin testing and treatment of latent tuberculosis infection". *MMWR* **49** (No. RR-6): 31–32.
26. CDC, Division of Tuberculosis Elimination. *Core Curriculum on Tuberculosis: What the Clinician Should Know*, 4th ed. (2000)
27. O'Brien, R. Drug-resistant tuberculosis: etiology, management and prevention, *Semin. Respir. Infect.* **9**, 104–112 (1994)
28. Iseman, M. D. MDR-TB and the developing world a problem no longer to be ignored: the WHO announces 'DOTS Plus' strategy, *Int. J. Tuberc. Lung Dis.* **2**, 867 (1998)
29. Iademarco, M.F.; Castro, K. G. Epidemiology of tuberculosis, *Semin. Respir. Infect.* **18**, 225–240 (2003)
30. CDC, *MMWR Morb Mortal Wkly Rep.* **55**, 301–305 (2006)
31. Farmer, P. The major infectious diseases in the world--to treat or not to treat?, *N. Engl. J. Med.* **345**, 208–210 (2001)
32. Klopman, G.; Fercu, D.; Jacob, J. Computer-aided study of the relationship between structure and antituberculosis activity of a series of isoniazid derivatives, *Chem. Phys.* **204**, 181–193 (1996)
33. Szakacs, T. A *et al.* Adherence with isoniazid for prevention of tuberculosis among HIV-infected adults in South Africa *Bmc Infect. Dis.* **6**, 97–103 (2006)
34. Gray, D. M.; Zar, H.; Cotton, M. Impact of tuberculosis preventive therapy on tuberculosis and mortality in HIV-infected children, *Cochrane Database Syst. Rev.* **115**, CD006418 (2009)
35. Domagk, G.; Offe, H. A.; Siefken, W. Ein weiterer Beitrag zur experimentellen Chemotherapie der Tuberkulose (Neoteben), *Dtsch. Med. Wochenschr.* **77**, 573–578 (1952)



36. Meyer, H.; Mally, J. Hydrazine derivatives of pyridine-carboxylic acids, *Monatsh. Chem.* **33**, 393–414 (1912)
37. Suarez, J. An Oxyferrous Heme/Protein-based Radical Intermediate Is Catalytically Competent in the Catalase Reaction of Mycobacterium tuberculosis Catalase-Peroxidase (KatG), *J. Biol. Chem.* **284**, 7017–7029 (2009)
38. Timmins, G. S.; Master, S.; Rusnak, F.; Deretic, V. Nitric Oxide Generated from Isoniazid Activation by KatG: Source of Nitric Oxide and Activity against *Mycobacterium tuberculosis*, *Antimicrob. Agents Chemother.* **48**, 3006–3009 (2004)
39. Singh, R. *et al.* PA-824 Kills Nonreplicating Mycobacterium tuberculosis by Intracellular NO Release, *Science* **322**, 1392–1395 (2008)
40. Akalin, E.; Akyuz, S. Vibrational Structure of Free and Hydrogen Bonded Complexes of Isoniazid: FT-IR, FT-Raman and DFT Study, *J. Mol. Struct.* **834**, 492–497 (2007)
41. Yilmaz, A.; Bolukbasi, C.; Bakiler, M. An Experimental and Theoretical Vibrational Spectra of Isoniazide, *J. Mol. Struct.* **872**, 182–189 (2008)
42. Favila, A.; Gallo, M.; Glossman-Mitnik, D. CHIH-DFT Determination of the Molecular Structure Infrared Spectra, UV Spectra and Chemical Reactivity of Three Antitubercular Compounds: Rifampicin, Isoniazid and Pyrazinamide, *J. Mol. Model.* **13**, 505–518 (2007)
43. Borba, A.; Gomez, A. Z.; Fausto, R. Molecular Structure, Infrared Spectra, and Photochemistry of Isoniazid under Cryogenic Conditions, *J. Phys. Chem. A*, **113**, 9220–9230 (2009)
44. Cunha, E. F. F. D.; Ramalho, T. C.; Alencastro R. B. DE; Maia, E. R. Docking simulations and QM/MM studies between isoniazid prodrug, catalase-peroxidase (KatG) and S315T mutant from Mycobacterium Tuberculosis, *Comput. Math. Methods in Med.* **8**, 113–124 (2007)
45. Bonnac, L. *et al.* Synthesis of 4-phenoxybenzamide adenine dinucleotide as NAD analogue with inhibitory activity against enoyl-ACP reductase (InhA) of Mycobacterium tuberculosis, *Bioorg. Med. Chem. Lett.* **17**, 4588–4591 (2007)

46. Amos, R. I. J.; Gourlay, B. S.; Schiesser, C. H.; Smith, J. A.; Yates, B. F. A mechanistic study on the oxidation of hydrazides: application to the tuberculosis drug isoniazid *Chem. Commun.* **14**, 1695–1697 (2008)
47. Merz Jr., K. M. Limits of Free Energy Computation for Protein–Ligand Interactions, *J. Chem. Theory Comput.*, **6**, 1769–1776 (2010)
48. Pasqualoto, K. F. M.; Ferreira, E. I.; Santos-Filho, O. A.; Hopfinger, A. J. Rational design of new antituberculosis agents: receptor-independent four-dimensional quantitative structure-activity relationship analysis of a set of isoniazid derivatives, *J. Med. Chem.* **47**, 3755–3764 (2004)
49. Pasqualoto, K. F. M.; Ferreira, M. M. C.; Santos-Filho, O. A.; Hopfinger, A. J. Molecular dynamics simulations of a set of isoniazid derivatives bound to InhA, the enoyl-acyl reductase from *Mycobacterium tuberculosis*, *Int. J. Quant. Chem.* **106**, 2689–2699 (2006)
50. <http://ftp.iza.org/dp2997.pdf>. (2008)
51. Greenwood, B.; Mutabingwa, T. Malaria in 2002, *Nature* **415**, 670–672 (2002)
52. Breman, J. G. The ears of the hippopotamus: manifestations, determinants, and estimates of the malaria burden, *Am. J. Trop. Med. Hyg.* **64**, 1–11 (2001)
53. Joy, D. Early origin and recent expansion of *Plasmodium falciparum*, *Science* **300**, 318–321 (2003)
54. Cox, F. History of human parasitology, *Clin. Microbiol. Rev.* **15**, 595–612 (2002)
55. DNA clues to malaria in ancient Rome. *BBC News*. February 20, (2001).
56. Sallares, R. "Malaria and Rome" *ABC.net.au*. (2003)
57. *Armies of Pestilence: the effects of Pandemics on History* (Clarke, J. & Co., Cambridge, 2004)
58. Byrne, J. P. *Encyclopedia of Pestilence, Pandemics, and Plagues* 383 (2008)
59. Tan, S. Y.; Sung, H. Carlos Juan Finlay (1833–1915): of mosquitoes and yellow fever, *Singapore Med. J.* **49**, 370–371 (2008)
60. Cox, F. E. G. History of the discovery of the malaria parasites and their vectors, *Parasites & Vectors*, **3**, 5 (2010)

61. CDC, <http://www.cdc.gov/malaria>. (2010)
62. Snow, R. W.; Guerra, C. A.; Noor, A. M.; Myint, H. Y. ; Hay, S. I. The global distribution of clinical episodes of *Plasmodium falciparum* malaria, *Nature* **434**, 214–217 (2005)
63. Singh, B. *et al.* A large focus of naturally acquired *Plasmodium knowlesi* infections in human beings, *Lancet* **363**, 1017–1024 (2004)
64. Bowman, S. *et al.* The Complete Nucleotide Sequence of Chromosome 3 of *Plasmodium falciparum*, *Nature* **400**, 532–538 (1999)
65. O'Neill, P. M.; Bray, P. G.; Hawley, S. R.; Ward, S. A.; Park, B. K. 4-Aminoquinolines - Past, Present, and Future: A Chemical Perspective, *Pharmacol. Ther.* **77**, 29–58 (1998)
66. Kilama, W.; Ntoumi, F. Malaria: a research agenda for the eradication era, *Lancet* **374**, 1480–1482 (2009)
67. Nussenzweig, R.; Vanderberg, J.; Most, H.; Orton, C. Protective immunity produced by the injection of x-irradiated sporozoites of *plasmodium berghei*, *Nature* **216**, 160–162 (1967)
68. Hoffman, S. L. *et al.* Protection of humans against malaria by immunization with radiation-attenuated *Plasmodium falciparum* sporozoites, *J. Infect. Dis.* **185**, 1155–1164 (2002)
69. Heppner, D. G. *et al.* Towards an RTS,S-based, multi-stage, multi-antigen vaccine against *falciparum* malaria: progress at the Walter Reed Army Institute of Research, *Vaccine* **23**, 2243–2250 (2005)
70. Aponte, J. J. *et al.* 'Safety of the RTS,S/AS02D candidate malaria vaccine in infants living in a highly endemic area of Mozambique: a double blind randomised controlled phase I/IIb trial, *Lancet* **370**, 1543–1551 (2007)
71. Africa: Malaria-Vaccine Expected in 2011 *Accra Mail* (2007)
72. Maher, B. Malaria: The end of the beginning, *Nature* **451**, 1042–1046 (2008)
73. Hoffman, S. L. *et al.* Funding from malaria genome sequencing, *Nature* **387**, 647 (1997)
74. Gardner, M. J. *et al.* Genome sequence of the human malaria parasite *Plasmodium falciparum*, *Nature*, **419**, 498–511 (2002)

75. Delhaes, L. *et al.* Novel ferrocenic artemisinin derivatives: synthesis, in vitro antimalarial activity and affinity of binding with ferroprotoporphyrin IX, *Bioorg. Med. Chem.* **8**, 2739–2745 (2000)
76. O'Neill, P. M.; Posner, G. H. A medicinal chemistry perspective on artemisinin and related endoperoxides, *J. Med. Chem.* **47**, 2945–2964 (2004)
77. Avery, M. A.; Gao, F.; Chong, W. K. M.; Methrotra, S.; Millhous, W. K. Structure-activity relationships of the antimalarial agent artemisinin. 1. Synthesis and comparative molecular field analysis of C-9 analogs of artemisinin and 10-deoxoartemisinin, *J. Med. Chem.* **36**, 4264–4275 (1993)
78. O'Neill, P. M. *et al.* Novel, potent, semisynthetic antimalarial carba analogues of the first-generation 1,2,4-trioxane artemether, *J. Med. Chem.* **42**, 5487–5493 (1999)
79. Li, Wu. The Distinguished Naturalist, *J. Trad. Chin. Med.*, **3**, 323–328 (1983)
80. Klayman, D. L. Qinghaosu (Artemisinin): an Antimalarial Drug from China, *Science* **228**, 1049–1055 (1985)
81. Haynes, R. K. *et al.* Highly Antimalarial-Active Artemisinin Derivatives: Biological Activity Does Not Correlate with Chemical Reactivity, *Angew. Chem., Int. Ed.* **43**, 1381–1385 (2004)
82. Gu, J.; Chen, K.; Jiang, H.; Leszczynski, J. The Radical Transformation in Artemisinin: A DFT Study, *J. Phys. Chem. A* **103**, 9364–9369 (1999)
83. Butter, A. R.; Wu, Y. L. Artemisinin (qinghaosu): a new type of antimalarial drug, *Chem. Soc. Rev.* **21**, 85–90 (1992)
84. TDR News (News from the WHO Special Programme for research & training in Tropical Diseases) 1 (1986)
85. Liu, C.; Guo, C.; Wang, Y.; Ouyang, F. Comparison of various bioreactors on growth and artemisinin biosynthesis of *Artemisia annua* L. shoot cultures, *Process Biochem.* **39**, 45–49 (2003)
86. Bez, G.; Kalita, B.; Sarmah, P.; Barua, N. C.; Dutta, D. K. Recent Developments with 1,2,4-Trioxane-Type Artemisinin Analogues, *Curr. Org. Chem.* **7**, 1231–1255 (2003)

87. China Co-operative research group on Qinghousuo and its derivative as anti-malarial, *J. Tradit. Chin. Med.* **2**, 45 (1982)
88. Singh, C.; Chaudhary, S.; Puri, S. K. New Orally Active Derivatives of Artemisinin with High Efficacy against Multidrug-Resistant Malaria in Mice, *J. Med. Chem.* **49**, 7227–7233 (2006)
89. Chaturvedi, D.; Goswami, A.; Saikia, P. P.; Barua, N. C.; Rao, P. G. Artemisinin and its derivatives: a novel class of anti-malarial and anti-cancer agents, *Chem. Soc. Rev.* **39**, 435–454 (2010)
90. World Health Organization, *Guidelines for the treatment of malaria* (2006).
91. Dondorp, A. M. *et al.* Artemisinin resistance: current status and scenarios for containment, *Nature Rev. Microbiol.* **8**, 272–280 (2010)
92. Maude, R. J.; Woodrow, C. J.; White, L. J. Artemisinin Antimalarials: Preserving the "Magic Bullet", *Drug. Dev. Res.* **71**, 12-19 (2010)
93. Basco, L. K. *et al.* In Vitro Activities of DU-1102, a New Trioxaquine Derivative, against Plasmodium falciparum Isolates, *Antimicrob. Agents Chemother.* **45**, 1886–1888 (2001)
94. Kouznetsov, V. V.; Go´mez-Barrio, A. ChemInform Abstract: Recent Developments in the Design and Synthesis of Hybrid Molecules Based on Aminoquinoline Ring and Their Antiplasmodial Evaluation, *Eur. J. Med. Chem.* **44**, 3091–3113 (2009)
95. Benoit-Vical, F. *et al.* Trioxaquinones Are New Antimalarial Agents Active on All Erythrocytic Forms, Including Gametocytes. *Antimicrob. Agents Chemother.* **51**, 1463–1472 (2007)
96. Cosle´dan, F. *et al.* Selection of a trioxaquine as an antimalarial drug candidate, *Proc. Natl. Acad. Sci. USA* **105**, 17579–17584 (2008)
97. Muregi, F. W.; Ishih, A. Next-generation antimalarial drugs: hybrid molecules as a new strategy in drug design, *Drug. Dev. Res.* **71**, 20-32 (2010)
98. Olliaro, P.; Wells, T. N. The global portfolio of new antimalarial medicines under development, *Clin. Pharmacol. Ther.* **85**, 584–595 (2009)

99. Wang, X. *et al.* Spiro- and dispiro-1,2-dioxolanes: contribution of iron(II)-mediated one-electron vs two-electron reduction to the activity of antimalarial peroxides, *J. Med. Chem.* **50**, 5840–5847 (2007)
100. Vennerstrom, J. L. *et al.* Identification of an antimalarial synthetic trioxolane drug development candidate, *Nature* **430**, 900–904 (2004)
101. Sabbani, S. *et al.* Piperidine dispiro-1,2,4-trioxane analogues, *Bioorg. Med. Chem. Lett.* **18**, 5804–5808 (2008)
102. Posner, G. *et al.* Evidence for the Importance of High-Valent Fe=O and of a Diketone in the Molecular Mechanism of Action of Antimalarial Trioxane Analogs of Artemisinin, *J. Am. Chem. Soc.* **118**, 3537–3538 (1996)
103. Robert, A.; Meunier, B. Is alkylation the main mechanism of action of the antimalarial drug artemisinin?, *Chem. Soc. Rev.* **27**, 273–274 (1998)
104. Fidock, D. A.; Rosenthal, P. J.; Croft, S. L.; Brun, R.; Nwaka, S. Antimalarial drug discovery: efficacy models for compound screening, *Nat. Rev.* **3**, 509–520 (2004)
105. Gu, J. D.; Chen, K. X.; Jiang, H. L.; Leszczynski, J. A Model Molecule Study of the O-Centered and the C-Centered Free Radical Intermediates of Artemisinin, *J. Mol. Struct. (Theochem)* **491**, 57–66 (1999)
106. Tonmunphean, S.; Parasuk, V.; Kokpol, S. Theoretical Investigations on Reaction Mechanisms of Artemisinin Compounds: Effect of Structure on Kinetic Energy Profile and Antimalarial Activity, *J. Mol. Struct. (Theochem)* **724**, 99–105 (2005)
107. Moles, P.; Oliva, M.; Safont, V. S. Modeling the Decomposition Mechanism of Artemisinin, *J. Phys. Chem. A* **110**, 7144–7158 (2006)
108. Drew, M. G. B.; Metcalfe, J.; Ismail, F. M. D. Antimalarial drugs based on artemisinin: DFT calculations on the principal reactions, *J. Mol. Struct. (Theochem)* **756**, 87–95 (2005)
109. Taranto, A. G.; Carneiro, J. W. M.; Araújo, M. T. DFT Study of the Reductive Decomposition of Artemisinin, *Bioorg. Med. Chem.* **14**, 1546–1557 (2006)

110. Pereira, M. S. C.; Kiralj, R.; Ferreira, M. M. C. Theoretical Study of Radical and Neutral Intermediates of Artemisinin Decomposition, *J. Chem. Inf. Model.* **48**, 85–98 (2008)
111. Avery, M. A. *et al.* Structure-Activity Relationships of the Antimalarial Agent Artemisinin. 6. The Development of Predictive In Vitro Potency Models Using CoMFA and HQSAR Methodologies, *J. Med. Chem.* **45**, 292–303 (2002)
112. Cheng, F. *et al.* Molecular docking and 3-D-QSAR studies on the possible antimalarial mechanism of artemisinin analogues *Bioorg. Med. Chem.* **10**, 2883–2891 (2002)
113. Girones, X.; Gallegos, A.; Carbo-Dorca, R. Modeling Antimalarial Activity: Application of Kinetic Energy Density Quantum Similarity Measures as Descriptors in QSAR, *J. Chem. Inf. Comput. Sci.* **40**, 1400–1407 (2000)
114. Tonmunphean, S.; Parasuk, V.; Kokpol, S. QSAR Study of Antimalarial Activity and Artemisinin-Heme Binding Properties Obtained from Docking Calculations, *Quant. Struct.-Act. Relat.* **19**, 475–483 (2000)

# 2

## THEORETICAL METHODS

---

### 2.1 Computational Chemistry

Computational chemistry is a branch of chemistry that uses mathematical methods for the calculation of molecular properties or simulation of molecular behavior.<sup>1</sup> The term *computational chemistry* is usually used when a sufficiently well developed mathematical method from theoretical chemistry is incorporated into efficient computer programs for representation of realistic molecular structures and associated physical and chemical properties that are difficult to acquire experimentally. Although very few aspects of chemistry can be computed exactly, most of them can be described either qualitatively or in an approximate quantitative way using computational chemistry and the results normally complement the information obtained by chemical experiments. The computational chemistry combines all numerical methods based on molecular mechanics (MM), molecular dynamics (MD), Monte Carlo (MC) and quantum mechanics (QM) employed for prediction of the structure, electronic and other properties of materials.<sup>2-8</sup>

With the rapid development of computer science, computational chemistry is being widely used in various fields. These include establishing correlations between chemical structures and properties, designing molecules that interact in specific ways with other molecules (e.g. drug design and catalysis) etc. Although the developments in experimental techniques have enabled us to obtain highly accurate information of drug molecules, most of the techniques are very expensive and it is difficult to make trials-and-errors in experiments for designing new drug molecules. Computational chemistry may play a significant role in tailoring and designing drug molecule in a “green chemistry” way.



The basic principle of these simulations is the accurate determination of the total energy of an investigated system. Molecules consist of nuclei and electrons. Computational chemistry often attempts to solve the non-relativistic Schrödinger equation, with added relativistic corrections. Solving the Schrödinger equation either in its time-dependent or time-independent form is practically possible only for very small systems. Therefore, to study large molecules, approximate methods are frequently adopted for lesser computational cost. Large molecules can be studied by semi-empirical approximate methods. Another popular approximate method used to treat molecules with moderate number of atoms is density functional theory (DFT).<sup>9</sup> Larger molecules like protein, DNA etc can be efficiently treated with the help of molecular mechanics (MM) method. In the hybrid QM/MM methods, the active site of a large chemical system is treated quantum mechanically (QM), and the rest of the environment is handled by MM method.

In this thesis we have used various computational methods such as molecular mechanics (MM), quantum mechanics (QM), density functional theory and hybrid quantum mechanics/molecular mechanics (QM/MM). These methods along with docking and quantitative structure activity relationship (QSAR) techniques that have been extensively used in the thesis are discussed briefly in the following sections.

### **2.1.1 Molecular Mechanics**

Molecular mechanics can be used to compute the energy of systems containing a large number of atoms, such as molecules or complex systems of biochemical and biomedical interest. In contrast to quantum mechanics, molecular mechanics, which is based on Newtonian mechanics, simply ignore the motion of the electrons and compute the energy of a system only as a function of the nuclear positions. However, the electronic components of the system are included implicitly by adequate parameterization of the potential energy function. The set of equations and parameters which define the potential surface of a molecule is called force field.

Molecular mechanics considers a molecule to be a collection of masses interacting one with each other through harmonic forces. Thus, the atoms in molecules are treated as ball of different sizes joined together by springs of variable strength and equilibrium distances (bonds). This simplification allows to use molecular mechanics as a fast computational model applicable to molecules of any size.

The main advantage of MM is its inexpensive computational requirements: both in computation time and memory. Hence, small molecules as well as large bio-molecules with many thousands of atoms can be studied with MM. The main limitation of MM is its dependence on the parameterization for accuracy: the method is applicable only for a limited class of molecules for which the force field is parameterized. Secondly, molecular mechanics methods cannot be applied for the systems where electronic effects are prominent. For example, the process involving bond formation or bond breaking cannot be described by this method.

### 2.1.2 Quantum Chemical Methods

Quantum chemistry is based on the principles of quantum physics first developed in 1920's by pioneers of modern physics namely Heisenberg, Bohr, Sommerfeld, Born, Pauli, Schrödinger and Dirac. Quantum chemistry is concerned with finding the eigenfunctions and eigenvalues of the time independent Schrödinger equation.<sup>10</sup>

In Quantum mechanics, nuclei are arranged in the space and the corresponding electrons are spread all over the system in a continuous electronic density. One of the complications in solving Schrödinger equation is that the motion of the electrons and nuclear particles are coupled. Since the mass of a nucleus is thousands of times greater than that of an electron their relative motion can be approximately regarded as independent. The Born-Oppenheimer Approximation<sup>11,12</sup> separates the motion of electrons and nuclei by expanding the total molecular wave function as a product of electronic and nuclear wave functions.

The electronic structure and total electronic energy of atoms, molecules and crystals can be obtained by solving the time-independent, non-relativistic Schrödinger equation. The short-hand form for the time-independent, non-relativistic Schrödinger equation is:

$$\hat{H}\Psi_i = E_i\Psi_i \quad (2.1)$$

where  $\hat{H}$  is the molecular Hamiltonian operator,  $\Psi_i$  is the total wavefunction of the  $i$ -th electronic state and  $E_i$  is the corresponding energy eigenvalue of the system of interest.

The Hamiltonian ( $\hat{H}$ ) provides a complete representation of all interactions between the nuclei and electrons in a molecule. It can be expressed as:

$$\hat{H} = \frac{1}{2} \sum_i \nabla_i^2 - \sum_i \sum_A \frac{Z_A}{R_{Ai}} + \sum_{i < j} \frac{1}{r_{ij}} + \sum_{A < B} \frac{Z_A Z_B}{R_{AB}} \quad (2.2)$$

The first quantity on right hand side of equation (2.2) accounts for the kinetic energy of electron  $i$ , the other terms account for the potential energies, including attractions between electron  $i$  and nuclei  $A$  separated by a distance of  $R_{Ai}$ ; repulsions among electrons  $i$  and  $j$ ; repulsions among nuclei  $A$  and  $B$  of atomic numbers  $Z_A$  and  $Z_B$  separated by a distance of  $R_{AB}$ .

However, exact solution to the Schrödinger equation is not possible even for the smallest systems. The available solutions of the Schrödinger equation are approximate due to mathematical and computational complexities and the CPU time is exponential to a high power of the number of electrons.

Quantum chemical methods can be divided broadly into two classes: semi-empirical methods and non-empirical (*ab initio*, DFT etc.) methods. However, the goal of either method is to obtain the wave function of orbital  $\Phi(r)$  occupied by each electron, the eigenvalue (or orbital energy)  $\epsilon_i$  corresponding to that orbital, the total energy  $E_{tot}$  and the atomic force  $F$  on each atom by solving the Schrödinger wave equation. In Semi-empirical methods, only the outer or valence electron orbitals are calculated. The inner electrons are considered to be less importance for the chemical properties, and usually are parameterized empirically. Semi-empirical methods neglect many of the differential overlap approximations while the non-empirical methods evaluate all overlap integrals. Some of the most popular methods of this category are: complete neglect of differential overlap

(CNDO), intermediate neglect of differential overlap (INDO), modified intermediate neglect of differential overlap (MINDO), modified neglect of diatomic overlap (MNDO), Austin model 1 (AM1) and Parametric model 3 (PM3). *Ab initio* roughly translates in this context as "from first principles". The methods are based on the use of the full Schrödinger equation to treat all the electrons of a chemical system. Most of the *ab initio* calculations are based on the wave function based Hartree-Fock (HF)<sup>13</sup> method. In HF method, an approximate solution to the non relativistic time-independent electronic Schrödinger equation is obtained for the rigorous calculation of molecular electronic structure. It basically extends a Born-Oppenheimer type approximation to separately consider each wave function (Hartree's theory) but tries to account for average field of electron repulsion (Fock's integrals). Other commonly used methods, MP2 (second order Møller-Plesset perturbation theory), MP3, etc treat electron correlation more accurately.<sup>14</sup> Most of the *ab initio* methods produces better results but does so at a fairly high computational cost.<sup>15</sup> Therefore they are rendered impractical for the calculation with relatively large molecules.

### 2.1.2.1 Density Functional Theory

An alternative approach to the MPn methods is DFT. It is not strictly an *ab initio* method, since it includes a few empirically derived parameters. DFT can achieve quite accurate results with only a modest increase of computation time.<sup>16</sup>

The method was presented by Hohenberg, Kohn and Sham in two famous articles.<sup>17,18</sup> Although the theory was proposed in 1964, it had no large impact on the physics community and only in the last twenty years the method has really gained importance due to the development of new and accurate exchange-correlation potentials. The increase in computing power has revealed the full power and the range of applicability of the method and consequently in 1998 Walter Kohn was honored the Nobel Prize in chemistry for the development of density functional theory.

DFT provides an alternative way to solve the Schrödinger equation. The traditional quantum chemical methods are based on the wavefunctions. However, DFT is an entirely different approach that involves expressing the energy of a system as a functional of the electron density,  $\rho$ , rather than of a wavefunction,  $\Psi$ .

The electron density is the central quantity that allows to describe all ground state properties. As such, DFT provides a sound basis for the development of computational strategies for obtaining information about the energetics, structure, and properties of molecules (and atoms) at much lower costs than traditional *ab initio* wave function techniques.

The first Hohenberg-Kohn theorem<sup>17</sup> demonstrates that the electron density  $\rho(r)$  determines both the number of electrons and the external potential. As the number of electrons and the external potential determine the molecular Hamiltonian, and the Hamiltonian determines the energy of the system (via Schrödinger equation),  $\rho(r)$  ultimately determines the system's energy and all other molecular properties. The energy  $E$  can then be written as a functional of  $\rho(r)$ .

$$E = E[\rho(r)] \quad (2.3)$$

Thus, the ground state properties of a many-electron system can be uniquely determined by an electron density that depends on only 3 spatial coordinates. It lays the groundwork for reducing the many-body problem of  $N$  electrons with  $3N$  spatial coordinates to 3 spatial coordinates, through the use of functionals of the electron density. This theorem can be extended to the time-dependent domain to develop time-dependent density functional theory (TDDFT), which can be used to describe excited states.

The second H-K theorem defines an energy functional for the system and proves that the correct ground state electron density  $\rho(r)$  minimizes this energy functional  $E[\rho(r)]$ . It ensures that a variational principle for the energy functional can be applied for obtaining  $\rho(r)$ .

There exists a one-to-one correspondence between the electron density of a system and the energy. The ground-state density  $\rho(r)$  uniquely determines the external potential  $v(\mathbf{r})$  and also the ground-state wave function  $\Psi(\rho)$ . Consequently, every observable quantity of a quantum mechanical system is determined by the electron density alone. In other words, all observables of a many electron system are unique functionals of the electron density.

### 2.1.2.1.1 The Kohn-Sham Equations

The introduction of the electron density as the basic carrier of information, as opposed to the wave function in the conventional approach, was further developed by Kohn and Sham.<sup>18</sup> DFT calculations can be performed very conveniently in terms of single particle orbitals within the Kohn-Sham formalism.

The Kohn-Sham scheme expresses the ground state density of the interacting particles of a molecular system in terms of the orbitals of non-interacting particles moving in an effective external potential  $V_{ext}$ . The expression for  $E[\rho]$  can be divided in several parts:

$$E[\rho] = T_S[\rho] + E_{ext}[\rho] + E_C[\rho] + E_{XC}[\rho] \quad (2.4)$$

$T_S$  refers to the kinetic energy of the system of non-interacting electrons.  $E_{ext}$  is the classical Coulomb energy of the electrons moving in the external potential  $V_{ext}$ ,  $E_C$  the classical energy due to the mutual Coulomb interaction of the electrons and  $E_{XC}$  contains everything else that was not accounted for yet, that is exchange energy, correlation energy and the difference between the true kinetic energy and the kinetic energy of the system of non-interacting electrons. The search for a better and better exchange correlation potential turned the DFT method into an accurate and rapid method.

However, because the exact form of xc potential is not available in DFT, in order to solve the KS equations an approximation for the xc potential  $v_{xc}(\mathbf{r})$  is required. This xc potential should contain all the many-body effects. Currently, many different  $v_{xc}(\mathbf{r})$  functionals have been proposed for practical applications. The important approximations are the local density approximation (LDA),<sup>19</sup> in which it is assumed that, locally, the quantum system under study can be approximated by a homogeneous electron gas. Although this might not seem appropriate for real atoms and molecules, the LDA has been remarkably successful for some systems.

More recently, the generalized gradient approximations (GGA) have been developed.<sup>20</sup> Although the chemical consequences of gradient corrections for correlation are relatively small compared to their exchange counterparts,<sup>21</sup> the accurate estimation of correlation energy in GGA has also received considerable attention. Instead of taking only the electron density into account, as in the LDA,

the gradient of the density is also considered in GGA. This has led to important improvements in accuracy with respect to the LDA. The most popular correlation functionals are the LYP (Lee, Yang, and Parr), which includes both local and non-local terms,<sup>22</sup> the P86 (Perdew 1986) functional,<sup>23</sup> and the PW91 (Perdew and Wang 1991) functional.<sup>24</sup>

### 2.1.2.2 DFT based reactivity descriptors

Many of the chemical phenomena can be understood and predicted by some theoretical quantities that have a direct relationship with the characteristic sets of important chemical properties. These quantities are, in general, called descriptors. The reactivity descriptors are very much relevant to the reactivity of the molecular systems and are intended to provide a qualitative and semi-quantitative measure of the extent to which a particular site will be affected in a given condition. There are many such descriptors and all of them have their own merits and demerits. Here, we present the theoretical background of the DFT-based descriptors, such as chemical potential, hardness, softness, Fukui function and their derivatives.

The prime objectives for the formulation of these reactivity descriptors are essentially to quantify and analyze the conceptually important quantities such as chemical reactivity, selectivity and stability of the molecular systems from a general theoretical framework. There have been numerous works in this field bringing out the usefulness of these descriptors in generalizing the chemical reactivity problems within the framework of DFT.<sup>9,25-35</sup> In a very recent article, Roy *et al.*<sup>36</sup> have reviewed the use of DFT based reactivity descriptors to predict the regioselectivity of large biomolecular systems.

#### 2.1.2.2.1 Global reactivity descriptors

Density functional theory provides a framework to discuss reactions in terms of change in number of electrons ( $N$ ) or change in external potential  $v(r)$  due to nuclei. The first derivatives of  $E(\rho)$  with respect to the number of electron  $N$  under the constant external potential  $v(r)$  is defined as the chemical potential  $\mu$ .

$$\mu = \left( \frac{\delta E}{\delta N} \right)_{v(r)} = -\chi \quad (2.5)$$

The physical meaning of chemical potential in DFT is that it measures the escaping tendency of an electron cloud. It is constant in three dimensional spaces for the ground state of an atom, molecule or solid and equals the slope of E versus N curve at constant external potential.<sup>37</sup> It is important to note that chemical potential is exactly identical with the definition of one of the important concepts, electronegativity and  $\mu$  equals minus the electronegativity  $\chi$ .<sup>38</sup>

The corresponding second derivative of energy with respect to N, keeping the external potential or the nuclear charge fixed is called the Global hardness ( $\eta$ ).<sup>39</sup>

$$\eta = \frac{1}{2} \left( \frac{\delta^2 E}{\delta N^2} \right)_{v(r)} = \left( \frac{\delta \mu}{\delta N} \right)_{v(\bar{r})} \quad (2.6)$$

The global softness is the inverse of global hardness with a factor 1/2:

$$S = \frac{1}{2\eta} = \left( \frac{\delta^2 N}{\delta E^2} \right)_{v(\bar{r})} = \left( \frac{\delta N}{\delta \mu} \right)_{v(\bar{r})} \quad (2.7)$$

Thus, the parameter hardness is interpreted as the resistance of the chemical potential to change in the number of electrons or resistance to deformation or change. The minimum value of hardness is zero and it corresponds to the maximum softness. Chemical potential, hardness and softness are obtained by averaging over atomic or molecular space. Hence, these are called as global reactivity descriptors (GRD).

By applying finite difference approximation the global hardness and softness can be expressed in terms of the ionization potential and electron affinity.

$$\mu = \frac{-(IE + EA)}{2} \quad (2.8)$$

$$\eta = \frac{IE - EA}{2} \quad (2.9)$$

$$S = \frac{1}{IE - EA} \quad (2.10)$$

Using Koopmans' theorem IE and EA can be approximated as negative of  $E_{HOMO}$  and  $E_{LUMO}$ , respectively and thus,  $\mu$  and  $\eta$  can be written in terms of  $E_{HOMO}$  and  $E_{LUMO}$  as<sup>40</sup>:



$$\mu = \frac{E_{LUMO} + E_{HOMO}}{2} \quad (2.11)$$

$$\eta = \frac{E_{LUMO} - E_{HOMO}}{2} \quad (2.12)$$

Here it is essential to note that the hardness now represents half of the energy gap between HOMO and LUMO.

Parr *et al*<sup>41</sup> defined a specific quantity of a chemical species, electrophilicity index ( $\omega$ ), which is expressed as the square of the electronegativity divided by its chemical hardness. This quantity is found to be useful in predicting the extent of partial electron transfer that contributes to the lowering of the total binding energy by maximum flow of electrons.

$$\omega = \frac{\mu^2}{2\eta} = \frac{\chi^2}{2\eta} \quad (2.13)$$

#### 2.1.2.2.2 Local reactivity descriptors

Global reactivity descriptors can not identify the reactive part or site of a molecule that has the high tendency to undergo chemical reactions. For this purpose, appropriate local reactivity descriptors need to be defined. In particular, three local properties are of great interest, namely, the Fukui function  $f(r)$ , the local softness  $s(r)$  and the local hardness  $\eta(r)$ .

The Fukui function  $f(r)$  is formally defined by Parr and Yang<sup>42</sup> as the derivative of electron density with respect to the total number of electrons  $N$  in the system, at constant external potential  $v(r)$ ,

$$f(r) = \left( \frac{\delta^2 E}{\delta N \delta v(r)} \right) = \left[ \frac{\delta \mu}{\delta v(r)} \right]_N = \left( \frac{\delta \rho(r)}{\delta N} \right)_{v(r)} \quad (2.14)$$

where,  $\rho(r)$  is the electron density. Fukui function is a reactivity index for orbital controlled reactions, the larger the value of the Fukui function, the higher the reactivity. It reflects the component of chemical reactivity that is conveyed through the charge transfer between systems. Using left and right derivatives with respect to the number of electrons, electrophilic and nucleophilic Fukui functions can be defined. To describe site selectivity or reactivity of an atom in a molecule, it is necessary to condense the values of Fukui function around each atomic site into a single value. This can be achieved by electronic population analysis. Thus

for an atom  $k$  in a molecule, depending upon the type of electron transfer, we have three different types of condensed Fukui function  $(f_k^+)$ ,  $(f_k^-)$  and  $(f_k^0)$  which correspond to electrophilic, nucleophilic and free radical attack, respectively.

$$f_k^+ = \rho_k(N+1) - \rho_k(N) \quad (2.15)$$

$$f_k^- = \rho_k(N) - \rho_k(N-1) \quad (2.16)$$

$$f_k^0 = [\rho_k(N+1) - \rho_k(N-1)]/2 \quad (2.17)$$

Here,  $\rho_N(r)$ ,  $\rho_{N+1}(r)$  and  $\rho_{N-1}(r)$  are the electron densities of the  $N$ ,  $N+1$  and  $N-1$  electron systems, respectively.

The Fukui function  $(f_k^+)$ , represents the way the electron density,  $\rho(r)$ , changes as the number of electrons increases from  $N$  to  $N+1$  at constant external potential,  $\nu(r)$ . Likewise, the Fukui function  $(f_k^-)$ , represents the way the electron density changes as the number of electrons decreases from  $N$  to  $N-1$  at constant external potential.

At the point  $r$ ,  $(f_k^+)$  and  $(f_k^-)$  are direct measures of reactivity toward nucleophilic and electrophilic attack, respectively. That is, regions where  $(f_k^+)$  is large capably stabilize additional electron density and hence are especially reactive towards electron-rich reactants. Regions where  $(f_k^-)$  is large readily give up their electrons, and are thus reactive towards electron-poor reactants.

The local softness  $s(\vec{r})$  contains the same information as the Fukui function plus additional information about the total molecular softness. The local softness is defined by Yang and Parr<sup>43</sup> as:

$$s(\vec{r}) = \left( \frac{\partial \rho(\vec{r})}{\partial \mu} \right)_{\nu(\vec{r})} \quad (2.18)$$

The local softness is related to the Fukui function by the global molecular softness.

$$s(\vec{r}) = \left( \frac{\partial \rho(\vec{r})}{\partial \mu} \right)_{\nu(\vec{r})} = \left( \frac{\partial \rho(\vec{r})}{\partial N} \right)_{\nu(\vec{r})} \left( \frac{\partial N}{\partial \mu} \right)_{\nu(\vec{r})} = f(\vec{r})S \quad (2.19)$$

The predictive power for intermolecular reactivity sequences of the local softness clearly shows that  $f(r)$  and  $s(\vec{r})$  contain the same information on the relative site reactivity within a single molecule, but that  $s(r)$ , in view of the information about the total molecular softness, is more suited for intermolecular

reactivity sequences. Moreover, there is a major drawback with using the Fukui function as a reactivity descriptor. This quantity becomes increasingly diluted and spreads out around a molecule as the molecular size increases, because it has a fixed normalization. This implies that the local softness can correctly capture the fact that local reactivity does not necessarily decrease as molecular size increases, unlike the Fukui function. In practice, the softness is approximated in a condensed form completely equivalent to the condensed Fukui function equation, e.g., in the finite difference approach

The corresponding condensed local softnesses, can be also defined.

$$s_k^+ = [\rho_k(N_0 + 1) - \rho_k(N_0)]S \quad (\text{for nucleophilic attack on the system}) \quad (2.20)$$

$$s_k^- = [\rho_k(N_0) - \rho_k(N_0 - 1)]S \quad (\text{for electrophilic attack on the system}) \quad (2.21)$$

$$s_k^0 = \frac{1}{2}[\rho_k(N_0 + 1) - \rho_k(N_0 - 1)]S \quad (\text{for radical attack on the system}) \quad (2.22)$$

Local reactivity descriptors should reveal finer details about the behavior of a system. Although these indices were successful in generating the experimentally observed intra-molecular reactivity trends in several cases, the study by Roy *et al.* showed that the reactivity trends are not always very reliable.<sup>44</sup> Based on the condensed Fukui functions (or local softness), Roy *et al.*<sup>44</sup> introduced two different local reactivity descriptors, “relative electrophilicity” ( $s_k^+ / s_k^-$ ) and “relative nucleophilicity” ( $s_k^- / s_k^+$ ) of any particular atom  $k$ , to locate the preferable site for nucleophilic and electrophilic attack, respectively. The individual values of  $s_k^+$  and  $s_k^-$  are strongly influenced by the basis set or correlation effects. However, the ratio of  $s_k^+$  and  $s_k^-$ , involving two differences of electron densities of the same system differing by one in the number of electrons, at constant nuclear framework, are expected to be less sensitive to the basis set and correlation effects. These two reactivity descriptors are shown to generate improved intra molecular reactivity trends than those obtained from condensed Fukui function indices.

### 2.1.3 Hybrid QM/MM methods

In hybrid QM/MM (quantum mechanics/ molecular mechanics) method the strength of both QM (accuracy) and MM (speed) calculations are combined

together. The idea of studying the chemistry of a large molecule by uncoupled quantum mechanics with molecular mechanics was first introduced by Warshel and Bromberg in 1970.<sup>45</sup> The fundamental concept of the QM/MM method is to partition a system into two regions.

QM/MM total potential energy is obtained from three independent calculations and is expressed as:

$$E_{\text{tot}} = E_{\text{QM}} + E_{\text{MM}} + E_{\text{QM/MM}} \quad (2.24)$$

where  $E_{\text{QM}}$  is the total QM energy of the *I* region,  $E_{\text{MM}}$  is the potential energy of the *O* region and  $E_{\text{QM/MM}}$  is the QM/MM interaction energy. This makes it possible to compare energies of different conformers, perform geometry optimizations, and so forth, as long as the atomic composition of both subsystems remains unchanged.

The central "chemically active" portion of the chemical system (labeled *I*), is treated by quantum mechanical (QM) calculation. Remaining bulk outer region (labeled *O*), is described using forcefield (molecular mechanics: MM). The interactions at the boundary zone are handled with special care. Figure 2.1 gives a schematic representation of the calculation regions for a QM/MM treatment

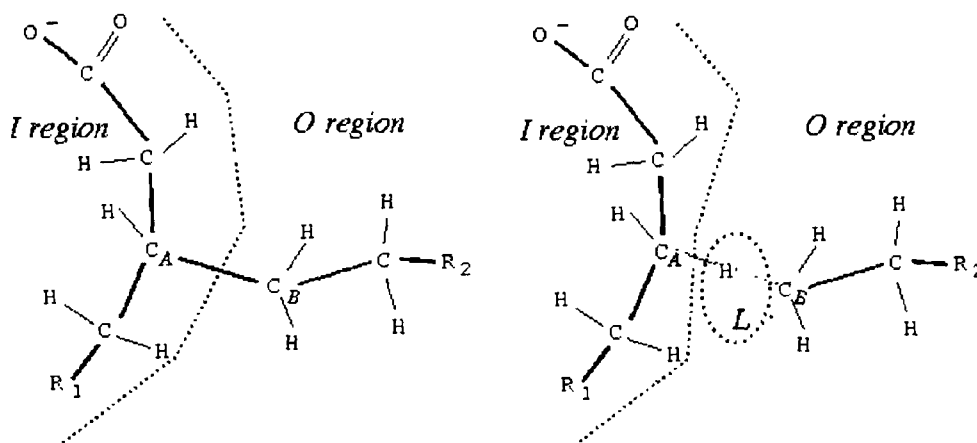


**Figure 2.1** Schematic representation of the calculation regions for a QM/MM treatment. Saturation of a dangling covalent bond between the QM (region *I*) and MM (region *O*) zones of an organic system by a hydrogen "link" (region *L*). The region used in the QM calculation is *C*, the union of *I* and *L*.

However, presence of covalent bonds between the quantum mechanical and molecular mechanics regions in the input structure makes the scenario different. Typically, the QM/MM bond is saturated by introducing a capping hydrogen "link" atom to the QM system. This is depicted in Figure 2.1, where *A* denotes one QM host atom of the QM region, *B* is the corresponding MM host atom of the MM region, and *L* is the region containing the link atom. Accordingly, it becomes necessary to make modifications of the QM and MM calculations.

Ideally, two types of situation arise. In case of subtractive scheme, the link atoms are added to the forcefield calculation on the *I* system of the QM/MM potential energy expressions. Here, the electrostatic (and van der Waals) interactions between *I* and *O* atoms are included. Three calculations are performed at each QM/MM step in order to obtain a consistent overall "subtractive" energy expression  $E_{\text{tot}}^{\text{sub}}$  as:

$$E_{\text{tot}}^{\text{sub}} = E_{\text{QM}}(C) + E_{\text{MM}}(S) - E_{\text{MM}}(C) \quad (2.25)$$

where  $E_{\text{QM}}(C)$  is the high level QM energy of the inner zone (*C*) [i.e., the QM atoms (*I*) plus possibly link atoms (*L*)];  $E_{\text{MM}}(S)$  is the energy of the whole system (*S*) performed using the low level (forcefield) method and finally,  $E_{\text{MM}}(C)$  is the low-level MM energy of the *C* zone, which will possibly include link atoms.

On the other hand, in additive scheme, the bonding forcefield terms are partially extended from the MM host atoms into the QM region to ensure that the covalent terms and the interactions between the QM and MM host atoms (*A* and *B*, respectively, in Figure 2.1) and their bonding neighbors are described correctly. Here, the forcefield calculation is performed only on the *O* region, including some cross-border bonding force field terms and the QM/MM van-der-Waals interactions and the calculation on region *C* is avoided. This makes these methods particularly attractive: no bonding forcefield parameters are needed for *I* atoms in the interior of that region. The final energy,  $E_{\text{tot}}^{\text{add}}$  is calculated as follows:

$$E_{\text{tot}}^{\text{add}} = E_{\text{QM}}(C) + E_{\text{MM}}(O+) + E_{\text{QM/MM}}(CO) \quad (2.26)$$

where  $E_{\text{MM}}(O+)$  is the MM energy and  $E_{\text{QM/MM}}(CO)$  denotes the interactions between *C* and *O*. In such calculations, the QM/MM electrostatic interaction energy  $E_{\text{QM/MM}}(CO)$  in Equation 2.26 is calculated at the classical level, by taking the point charge interactions of the QM atoms with the MM atoms.

A very important issue related to QM/MM calculations is the treatment of the QM/MM boundary region.<sup>46</sup> For solvent effects on organic molecules, the division in a QM and a MM system is straightforward and doesn't cause any problems. However, for a protein this no longer holds; in order to make a division in a QM and a MM system, one has to cut through covalent bonds. QM/MM schemes can be classified further on the basis of how the interaction between subsystems and the atoms in the boundary region are handled. The interaction between the QM and MM atoms is described by the term "embedding" which describes the way in which the interactions between the quantum mechanics, *I*, and molecular mechanics, *O*, regions are treated. The QM $\leftrightarrow$ MM interactions comprise the long-range Coulomb interactions between the *I* and *O* regions on one hand and the remaining short range secondary interactions of van der Waals type on the other hand. With the focus being set to the Coulomb forces, the QM/MM embedding can be classified as either mechanical or electronic.

In this thesis we use QMERA<sup>47</sup> to perform QM/MM calculations. Treating the complete protein by DFT is not feasible and also not required. If done so, valuable computer resources would be wasted by using a high-quality description for a large region that can be treated very well by classical interactions. Therefore, only the active site has been placed in the QM system, while the rest of the protein and the solvent have been put in the MM system. MS QMERA uses a hybrid QM/MM to combine DFT calculations done with DMol<sup>3</sup> and molecular mechanics with General Utility Lattice Program (GULP).<sup>48</sup> QMERA can perform virtual experiments, leading to a cost-effective approach to combining the accuracy of quantum mechanics with the speed of a force field calculation. This approach makes it possible to perform calculations on very large systems to yield results with accuracy that rivals that of pure DFT, but at a fraction of the computational cost.

#### 2.1.4 Quantitative Structure Activity Relationship (QSAR)

The quantitative structure activity relationship (QSAR) module is a comprehensive set of tools for creating statistical regression models between experimental information ("activity") and molecular level characteristics ("descriptors"). The International Union of Pure and Applied Chemistry (IUPAC)

have defined QSAR as “*The building of structure biological activity models by using regression analysis with physicochemical constants, indicator variables or theoretical calculations*”. QSAR studies are of great importance in modern chemistry and biochemistry. In general, QSAR are methods for estimating properties of a chemical from its molecular structure. The basic concept of QSAR is to transform searches for optimal compounds with the desired properties based on chemical intuition and experience into searches with a mathematically founded and computerized form. The method requires a training set of materials where the property of interest is known. Molecular descriptors can then be calculated and a mathematical regression linking the property to the descriptors can be generated. This mathematical model can then be used for prediction of materials with unknown activity.

QSAR methods have been applied widely in the pharmaceutical industry for drug discovery, lead optimization, risk assessment, toxicity prediction and regulatory decisions.<sup>49</sup> The multi-stage process of drug discovery needs improvement particularly in order to shorten the cycle time needed to identify compounds that possess the desired drug like properties. The challenging task of screening large libraries of molecules for biological activities can be attained with *in silico* prediction of biological activity based on the molecular structure. The main use of QSAR models is to find information on the potency of medicinally active compounds or drug molecules with reduced time, financial cost and without any animal testing. Thus, compounds that possess too many undesirable characteristics can be eliminated prior to investing time in synthesis, chemical analysis and testing.

Therefore, the IUPAC has redefined QSAR in drug design as *mathematical relationships linking chemical structure and pharmacological activity in a quantitative manner for a series of compounds*. Despite the specific definition, the use of QSAR is not restricted to drug design but is also used for regulatory goals of hazard assessment, risk assessment and the assessment of persistent, bio-accumulating and toxic products in the chemical industry.

The validity, predictive power, robustness and reliability of a QSAR model depend critically on the information used, encoded as appropriate molecular descriptors. Effective descriptor or variable selection is an integral part of the

QSAR modeling process.<sup>50</sup> Obtaining a good-quality QSAR model depends on many factors, such as the quality of biological data, the choice of descriptors and the statistical methods adopted. Any QSAR modeling should ultimately lead to statistically robust models capable of making accurate and reliable predictions of biological activities of compounds.

QSAR models are subdivided into three categories: 2-dimensional QSAR (2D-QSAR), 3-dimensional QSAR (3D-QSAR) and Quantum QSAR. The subdivision is based on the information used for building the QSAR model. 2D QSAR models are set up using global information. It correlates biological activities of drugs with physicochemical properties that encode certain structural features such as constitutional, geometrical, topological or quantum chemical. 3D QSAR models use local field information and Quantum QSAR is based on the continuous density vector.

#### **2.1.4.1 Model building**

Developing a QSAR model has three important stages: data generation, data analysis, and model validation. A key part of any QSAR analysis is the statistical methods which help to build models, estimate a model's predictive abilities, and find correlations among variables. Statistical analysis of the generated data is used to recombine data into different forms, and group observations into hierarchies. Regression methods are used to build a model in the form of an equation that gives one or more dependent variables (usually activity) in terms of independent variables ("descriptors"). This model can then be used for predicting properties or activity of new molecules in the form of screening a large group of molecules whose activities are not known. A model's ability to provide insight into the system is as important as its predictive ability. Finally, models thus developed are validated to establish their true predictive power on unseen data.

A wide variety of statistical techniques are available in QSAR analysis. Regression analysis is such a technique for modeling and analyzing several variables. Various regression methods such as simple linear regression, multiple linear regression (MLR), stepwise multiple linear regression, principal components regression (PCR), partial least squares (PLS), genetic function approximation (GFA), genetic partial least squares (G/PLS) are available. However, the type and



quality of data together with the type of property or activity to be investigated determines the particular techniques to be used. Basically, regression analysis describes the correlation between individual values of dependent and independent variables. In linear regression analysis, the relationship between two variables  $x$  and  $y$  are described by an equation:

$$y = mx + c \quad (2.27)$$

This equation predicts values of  $y$  from values of  $x$ . The constants  $m$  and  $c$  are chosen to give the smallest possible sum of least squares difference between the true  $y$  values and the  $y$  values predicted using this equation. The constant  $m$  indicates the slope of the graph, and  $c$  is the intercept.

Another commonly used QSAR technique is multiple regression analysis. It is an extension of linear regression to predict  $y$  values from multiple  $x$  variables. The analysis derives an equation of the form:

$$y = a_1x_1 + a_2x_2 + \dots + a_nx_n + c \quad (2.28)$$

where  $a_1$ ,  $a_2$  etc., and  $c$  are constants chosen to give the smallest possible sum of least squares difference between true  $y$  values and the  $y'$  values predicted using this equation. The  $a$  values are known as the regression coefficients of the  $x$  variables, and the constant  $c$  is the intercept with the  $y$  axis.

Although  $y$  can be predicted from a series of independent variables by this equation, the reliability of the regression model needs to be checked. The multiple correlation coefficient  $r^2$  helps in assessing the regression model. It can be expressed as:

$$r^2 = \frac{ESS}{TSS} = \frac{\sum_{i=1}^n (y'_i - \bar{y}_i)^2}{\sum_{i=1}^n (y_i - \bar{y}_i)^2} \quad (2.29)$$

where  $ESS$  is Explained Sum of Squares. It gives the variation in  $y$  explained by the regression equation and is expressed as the sum of the difference between the predicted  $y$  values ( $y'$ ) and the mean. Another term  $TSS$  (Total Sum of Squares) gives the total variation in  $y$  and is expressed as the sum of the difference between the observed  $y$  values and their mean. If the regression equation describes the data

perfectly, then  $r^2 = 1.0$ . If the  $r^2$  values are higher than 0.50 the model is a good one and if lower the model is a poor one.

#### 2.1.4.2 Model validation

Validation is a crucial aspect of any QSAR modeling. Before application, a QSAR model is validated for its predictive power i.e. the ability of the model to predict accurately the activity of compounds that were not used for model development. External validation evaluates how well the equation generalizes. The original data are divided into two groups, the training set and the external test set. The training set is used to derive a model, and the model is used to predict the activities of the test set members. It is generally considered to be the most rigorous validation procedure, because the compounds in the external test set do not affect the model development. An alternative method, called internal validation, uses the dataset from which the model is derived and checks for internal consistency. The procedure derives a new model using a reduced set of structural data. The new model is used to predict the activities of the molecules that were not included in the new-model set. This is repeated until all compounds have been deleted and predicted once. Internal validation is less rigorous than external validation.

Cross validation<sup>51</sup> provides an internal check on the models derived using multiple linear regression or partial least squares analysis method to estimate the true predictive power. The simplest cross validation procedure is the leave-one-out (LOO) technique, where each compound is removed, one at a time. This technique is particularly important as this deletion scheme is unique and the predictive ability of the different models can be compared accurately. However, the predictive ability obtained is often too optimistic, particularly with larger datasets, because the perturbation in the dataset is small and insignificant when only one compound is omitted. To obtain more realistic estimates of the predictive ability, it is necessary to remove more than one compound in each step. Leave-many-out (LMO) method is another cross-validation procedure where a block of predefined size is deleted from each model building.

In regression analysis applications, the data training set contains some cases that are outlying or extreme. The outlying cases often have a marked effect on the

fitted least squares regression function. The outlying cases are studied carefully<sup>52</sup> and separately from the remaining data.<sup>53</sup> Once these outlying cases are investigated and possibly eliminated, the chemical space occupied by the training data set becomes the basis for estimating the domain of applicability. The domain of applicability of a QSAR model is the response and chemical structure space in which the model makes predictions with a given reliability.

### 2.1.5 Docking

Docking studies are computational techniques for exploration of the possible binding modes of a substrate to a given receptor, enzyme or other binding site.<sup>54</sup> In docking, computational simulation is performed to predict the preferred orientation of a ligand that binds to a particular protein of interest to form a stable complex<sup>55</sup> so that the free energy of the overall system is minimized. The strength of binding affinity between two molecules can be predicted from the knowledge of the preferred orientation. Molecular docking resembles with the problem of “*lock-and-key*”, where the correct relative orientation of the “*key*” to open up the “*lock*” is searched. Here, the protein can be thought of as the “*lock*” and the ligand can be thought of as a “*key*”. Since both the ligand and the protein are flexible, Jorgensen suggested the analogy “*hand-in-glove*” to be more appropriate than “*lock-and-key*”.<sup>56</sup> Docking has biological and pharmaceutical significance and thus plays an important role in rational drug design.<sup>57</sup>

#### 2.1.5.1 Docking approaches

The first requirement for docking is the structure of the protein of interest. Usually the structure is determined using a biophysical technique such as X-ray crystallography or NMR spectroscopy. This protein structure and a database of potential ligands serve as inputs to a docking program. There are two popular approaches for molecular docking. In the first approach, a matching technique is used that describes the protein and the ligand as complementary surfaces.<sup>58,59</sup> The receptor’s molecular surface is described in terms of its solvent accessible surface area and the ligand’s molecular surface is described in terms of its matching surface description.

The second approach simulates the actual docking process in which the interaction energies of ligand-protein pair are calculated.<sup>60</sup> Here, the protein and the ligand are separated by some physical distance, and the ligand finds its position into the protein's active site after a certain number of "moves" in its conformational space. The moves incorporate rigid body transformations such as translations and rotations, as well as internal changes to the ligand's structure including torsion angle rotations. The simulation method is more amenable to incorporate ligand flexibility into its modeling whereas shape complementarity techniques have to use some ingenious methods to incorporate flexibility in ligands. Another advantage of this method is that the process is physically closer to what happens in reality, when the protein and ligand approach each other after molecular recognition. But this technique takes longer time to evaluate the optimal pose of binding since they have to explore a large energy landscape. However, grid-based techniques as well as fast optimization methods have significantly overcome these problems.

In the present thesis we have utilized several molecular modeling techniques to investigate structure, properties and mode of action of two categories of organic bio-active molecules having antitubercular and antimalarial activities. DFT calculations have been performed to study chemical reactivity and site selectivity of the molecules. The mode of interaction of antitubercular drug molecules has been studied with docking and hybrid QM/MM approaches. QSAR method is used to investigate the antimalarial activities of artemisinin and some of its synthetic derivatives. We also studied the mode of interaction of heme-artemisinin complexes. The results of these studies are summarized in the following chapters.

## References

1. van de Waterbeemd, H. *et al.* Willett, P. *Glossary of Terms Used in Computational Drug Design* (Academic Press, San Diego, 1998)
2. Wang, L. L.; Perera, A.; Cheng, H. P. Molecular dynamics simulation of potential energy sputtering on LiF surface by slow highly charged ions, *Phys. Rev. B* **68**, 115409–115422 (2003)

3. Boese, A. D.; Chandra, A.; Martin, J. M. L.; Marx, D. From ab initio quantum chemistry to molecular dynamics: the delicate case of hydrogen bonding in ammonia, *J. Chem. Phys.* **119**, 5965–5980 (2003)
4. Penna, G. L.; Mitsutake, A.; Masuya, M.; Okamoto, Y. Molecular dynamics of C-peptide of ribonuclease A studied by replica-exchange Monte Carlo method and diffusion theory, *Chem. Phys. Lett.* **380**, 609–619 (2003)
5. Vink, R. L. C.; Barkema, G. T. Large well-relaxed models of vitreous silica, coordination numbers, and entropy, *Phys. Rev. B* **67**, 245201–245208 (2003)
6. Polak, W.; Patrykiewicz, A. Monte Carlo simulations Local structures in medium-sized Lennard-Jones clusters, *Phys. Rev. B* **67**, 115402–115413 (2003)
7. Aussenac, F.; Laguerre, M.; Schmitter, J. M.; Dufourc, E. J. Detailed structure and dynamics of bicelle phospholipids using selectively and per-deuterated labels: A  $^2\text{H}$ -NMR and molecular mechanics study, *Langmuir* **19**, 10468–10479 (2003)
8. Rockenbauer, A. et al. Large Phosphorus Hyperfine Coupling as a Sensitive Tool for Studying Molecular Dynamics: ESR and Molecular Mechanics Studies of Ring Interconversion in the cis-2,5-Diphosphoryl-2,5-dimethyl-pyrrolidinoxyl Radical, *J. Phys. Chem. A* **107**, 3851–3857 (2003)
9. Parr, R. G; Yang, W. *Density Functional Theory of Atoms and Molecules* (Oxford University Press, New York, 1989)
10. Schrödinger, E. Quantisierung als Eigenwertproblem (Erste Mitteilung) *Ann. Physik* **79**, 361–376 (1926)
11. Born, M.; Oppenheimer, J. R. Zur Quantentheorie der Moleküle, *Ann. Physik* **84**, 457–484 (1927)
12. Hurley, A. C. *Introduction to the Electron Theory of Small Molecules* (Academic Press, London, 1976)
13. Roothaan, C. C. New Developments in Molecular Orbital Theory, *J. Rev. Modern Phys.* **23**, 69–87 (1951)
14. Møller, C.; Plesset, M. S. Note on an Approximation Treatment for Many-Electron Systems, *Phys. Rev.* **46**, 618–622 (1934)

15. Foresman, J. B.; Frisch, Æ. *Exploring Chemistry Electronic Structure Methods* (Gaussian, Pittsburg, PA, 1996)
16. Becke, A. D. Exploring the limits of gradient corrections in density functional theory, *J. Comp. Chem.* **20**, 63–69 (1999)
17. Hohenberg, P.; Kohn, W. Inhomogeneous electron gas, *Phys. Rev. B* **136**, 864–871 (1964)
18. Kohn, W.; Sham, L. Self-consistent equations including exchange and correlation effects, *J. Phys. Rev. A* **140**, 1133–1138 (1965)
19. Slater, J. C. *The self-consistent Filed of Molecular and Solids in Quantum Theory of Molecular and Solids, Vol. 4*, (McGraw-Hill, New York, 1974)
20. Leeuwen, R. V.; Baerends, E. J. Exchange-correlation potential with correct asymptotic behavior, *Phys. Rev. A* **49**, 2421–2431 (1994)
21. Becke, A. Density-functional thermochemistry I. The effect of the exchange-only gradient correction, *J. Chem. Phys.* **96**, 2155–2160 (1992)
22. Lee, C.; Yang, W.; Parr, R. G. Development of the Colle-Salvetti correlation-energy formula into a functional of the electron density, *Phys. Rev. B* **37**, 785–789 (1988)
23. Perdew, J. P.; Wang, Y. Accurate and simple density functional for the electronic exchange energy: Generalized gradient approximation, *Phys. Rev. B* **33**, 8800–8802 (1986)
24. Perdew, J. P.; Wang, Y. Accurate and Simple Analytic Representation of the Electron-Gas Correlation Energy, *Phys. Rev. B* **45**, 13244–13249 (1992)
25. Sen, K. D. *Chemical Hardness, Structure and Bonding*, Vol.80, (Springer-Verlag, Berlin, 1993)
26. Nalewajski R. F. *Density Functional Theory, Topics in Current Chemistry*, Vol. 1-4, (Springer, Berlin, 1996)
27. Chandra, A. K.; Nguyen, M. T. Use of DFT-based reactivity descriptors for rationalizing radical addition reactions: applicability and difficulties, *Faraday Discuss.* **135**, 191–201 (2007)
28. Pearson, R. G. *Chemical Hardness: Applications from Molecules to Solids*; (Wiley-VCH Verlag GMBH, Weinheim, 1997)

29. De Proft, F.; Geerlings, P. Conceptual and Computational DFT in the Study of Aromaticity, *Chem. Rev.* **101**, 1451–1464 (2001)
30. Ayers, P. W.; Parr, R. G. Variational Principles for Describing Chemical Reactions: The Fukui Function and Chemical Hardness Revisited, *J. Am. Chem. Soc.* **122**, 2010–2018 (2000)
31. Mondal, P.; Hazarika, K.; Deka, R. C. Reactivity of  $\alpha,\beta$ -unsaturated carbonyl compounds towards nucleophilic addition reaction: a local hard-soft acid-base approach, *Phys. Chem. Commun.* **6**, 24–27 (2003)
32. Mondal, P.; Arunabhiram, C.; Hazarika, K. K.; Deka, R. C. Quantum chemical studies on acidity of isomorphously substituted ZSM-5 zeolite, *Bull. Catal. Soc. Ind.* **3**, 82–93 (2008)
33. Hazarika, K. K.; Barua, N. C.; Deka, R. C. Molecular Structure and Reactivity of Anti-tuberculosis Drug Molecules Isoniazid, Pyrazinamide and 2-Methylheptylisonicotinate: a Density Functional Approach, *Struct. Chem.* **20**, 1079–1085 (2009)
34. Sarmah, P.; Deka, R. C. Anticancer activity of nucleoside analogues: A density functional theory based QSAR study, *J. Mol. Model.* **16**, 411–418 (2010).
35. Mondal, P.; Hazarika, K. K.; Deka, A.; Deka, R. C. Density functional studies on Lewis acidity of alkaline earth metal exchanged faujasite zeolite, *Mol. Simul.* **34**, 1121–1121 (2008)
36. Roy, R. K.; Saha, S. Studies of Regioselectivity of Large Molecular Systems using DFT Based Reactivity Descriptors, *Annu. Rep. Prog. Chem., Sect. C: Phys. Chem.* **106**, 118–162 (2010)
37. Parr, R. G.; Donnelly, R. A.; Levy, M.; Palke, W. E. Electronegativity: The density functional viewpoint, *J. Chem. Phys.* **68**, 3801–3807 (1978)
38. Iczkowski, R. P.; Margrave, J. L. Electronegativity, *J. Am. Chem. Soc.* **83**, 3547–3551 (1961)
39. Parr, R. G.; Pearson, R. G. Absolute hardness: companion parameter to absolute electronegativity, *J. Am. Chem. Soc.* **105**, 7512–7516 (1983)

40. Koopmans, T. A. The distribution of wave function and characteristic value among the individual electrons of an atom, *Physica* **1**, 104–113 (1933)
41. Parr, R. G.; Szentpály, L. V.; Liu, S. Electrophilicity Index, *J. Am. Chem. Soc.* **121**, 1922–1924 (1999)
42. Parr, R. G.; Yang, W. Density functional approach to the frontier-electron theory of chemical reactivity, *J. Am. Chem. Soc.* **106**, 4049–4050 (1984)
43. Yang, W.; Parr, R. G. Hardness, softness, and the Fukui function in the electron theory of metals and catalysis, *Proc. Natl. Acad. Sci. U.S.A.* **82**, 6723–6726 (1985)
44. Roy, R. K.; Krishnamurthy, S.; Geerlings, P.; Pal, S. Local softness and hardness based reactivity descriptors for predicting intra- and intermolecular reactivity sequences: carbonyl compounds, *J. Phys. Chem. A* **102**, 3746–3755 (1998)
45. Warshel, A.; Bromberg, A. Oxidation of 4a,4b-dihydrophenanthrenes. III. A theoretical study of the large kinetic isotope effect of deuterium in the initiation step of the thermal reaction with oxygen, *J. Chem. Phys.* **52**, 1262–1269 (1970)
46. Gao, J.; Thompson, M. A. Eds. *Combined Quantum Mechanical and Molecular Mechanical Methods*, Series 712 (ACS Symposium, 1998)
47. Sherwood, P. *et al.* QUASI: A general purpose implementation of the QM/MM approach and its application to problems in catalysis, *Theochem-J. Mol. Struct.* **632**, 1–28 (2003)
48. Gale J. D.; Kristallogr, Z. GULP: Capabilities and Prospects, *Z. Kristallogr.*, **220**, 552–554 (2005)
49. Tong, W. *et al.* Assessing QSAR Limitations - A Regulatory Perspective, *Curr. Comp.-Aided Drug Design* **1**, 195–205 (2005)
50. Ghafourian, T. ; Cronin, M. T. D. The Impact of Variable Selection on the Modeling of Oestrogenicity, *SAR QSAR Environ. Res.* **16**, 171–190 (2005)
51. Hawkins, D. M.; Basak, S. C.; Mills, D. Assessing model fit by cross-validation, *J. Chem. Inf. Comput. Sci.* **43**, 579–586 (2003)



52. Tetko, I. V.; Bruneau, P.; Mewes, H. W.; Rohrer, D. C.; Poda, G. I. Can we estimate the accuracy of ADME-Tox predictions? *Drug Discovery Today* **11**, 700–707 (2006)
53. Jaworska, J.; Nikolova-Jeliazkova, N.; Aldenberg, T. QSAR applicability domain estimation by projection of the training set descriptor space: a review, *Altern. Lab. Anim.* **33**, 445–459 (2005)
54. Nic, M.; Jirat, J.; Kosata, B. *IUPAC Compendium of Chemical Terminology - the Gold Book*, <http://goldbook.iupac.org>. (2010)
55. Lengauer, T; Rarey, M. Computational methods for biomolecular docking, *Curr. Opin. Struct. Biol.* **6**, 402–406 (1996)
56. Jorgensen, W. L. Rusting of the lock and key model for protein-ligand binding, *Science* **254**, 954–955 (1991)
57. Kitchen, D. B.; Decornez, H.; Furr, J. R.; Bajorath, J. Docking and scoring in virtual screening for drug discovery: methods and applications, *Nat. rev. Drug discovery* **3**, 935–949 (2004)
58. Meng, E. C.; Shoichet, B. K.; Kuntz, I. Automated docking with grid-based energy evaluation, *J. Comput. Chem.* **13**, 505–524 (2004)
59. Morris, G. M. *et al.* Automated docking using a Lamarckian genetic algorithm and an empirical binding free energy function, *J. Comput. Chem.* **19**, 1639–1662 (1998)
60. Feig, M *et al.* Performance comparison of generalized Born and Poisson methods in the calculation of electrostatic solvation energies for protein structures, *J. Comput. Chem.* **25**, 265–284 (2004)

# 3

## **Molecular Structure and Reactivity of Anti-tuberculosis Drug Molecules Isoniazid, Pyrazinamide and 2-Methylheptylisonicotinate: a Density Functional Approach**

### **Abstract**

Density functional theory calculations have been performed to determine structure and reactivity of two of the most commonly used antitubercular drug molecules, isoniazid and pyrazinamide. Having found good agreement with the available experimental data for these two molecules, we extended DFT calculation to predict the properties of 2-methylheptylisonicotinate which is a novel natural analogue of Isoniazid. The chemical reactivity of these compounds was compared using density functional based descriptors such as global softness, global electrophilicity, Fukui function and philicity. The experimental better reactivity of 2-methylheptylisonicotinate with respect to the well known anti-tuberculosis drug molecule, isoniazid has been successfully established.

### 3.1 Introduction

Tuberculosis is a common and often deadly infectious disease causing a death of about 2 million lives every year out of approximately 8 million people getting infected by it. Moreover, 70–90% of AIDS-stricken patients die because of tuberculosis<sup>1</sup> and newly emergent drug resistant strains of *Mycobacterium tuberculosis* is mainly responsible for this life toll. The reasons for the increased success of the pathogen include synergy with AIDS, war and famine-mediated disruption of control regimes, lack of compliance, inappropriate monotherapy and multi-drug resistance (MDR-TB).<sup>2-4</sup>

The patients suffering from tuberculosis are usually treated with chemotherapy. But new drug resistant strains have hindered the effect of this treatment. The mostly used agents against drug-resistant tuberculosis are: isoniazid (INH), rifampicin (RIF), and pyrazinamide (PZA).<sup>5</sup> Drug molecules effective against tuberculosis can be divided into two categories: broad spectrum agents and narrow spectrum agents.<sup>6</sup> INH and PZA are narrow spectrum agents employed against *Mycobacterium tuberculosis*. Their combination with another broad spectrum agent Rifampicin, shortens the treatment period from 12-18 months to 6 months, and these three drugs together constitute the widely used short therapy “DOTS” (directly observed therapy, short course) employed by the WHO (World Health Organization).<sup>7</sup> Some success has been gained by the employment of DOTS.

Isoniazid, also known as isonicotinic acid hydrazide, INH, is an organic compound that is the first-line antituberculosis medication in prevention and treatment. Interestingly, INH was synthesized for the first time by Meyer and Mally in 1912,<sup>8</sup> but its antituberculous activity was recognized only in 1951.<sup>9</sup> It has been widely used as an effective drug for the treatment of tuberculosis for over half a century since no alternative novel anti-tubercular chemotherapeutic agents of INH could be introduced. With the introduction of isoniazid, cure for tuberculosis was first considered reasonable. However it is found to be ineffective against newly emergent strains of *Mycobacterium tuberculosis*.<sup>10</sup> Isoniazid is never used on its own to treat active tuberculosis because of quick development of resistance. In particular, it has been receiving extensive use in the prevention of tuberculosis among both HIV-infected adults and children.<sup>11,12</sup> The lack of priority in the

development of novel agents is in part due to poor financial return on investment available from drugs primarily targeted at a disease which is perceived as a 'Third World' problem. Still, much effort has been given to identify new effective chemotherapeutic agents with low toxicity.

The alarming spread of tuberculosis especially in developing and underdeveloped countries due to HIV infection has focused the attention on the need to understand the pathogenesis of this disease. The frequencies and types of life threatening fungal infections have increased dramatically among the immunocompromised patients.<sup>13,14</sup> Moreover, secondary fungal infections that appear towards the later part of medication, among the TB patients, aggravate the situation.<sup>15</sup> Hence the need for novel anti-TB drug with antifungal activity is highly felt. 2-Methylheptylisonicotinate (MHI), a natural analogue of INH, is a novel bioactive microbial metabolite isolated from the soil microbe of North East India.<sup>16-18</sup> The molecule is found to have both antibacterial and antifungal properties. Thus, MHI and its derivatives hold a lot of promises towards developing new and better drug molecules with optimum activity.

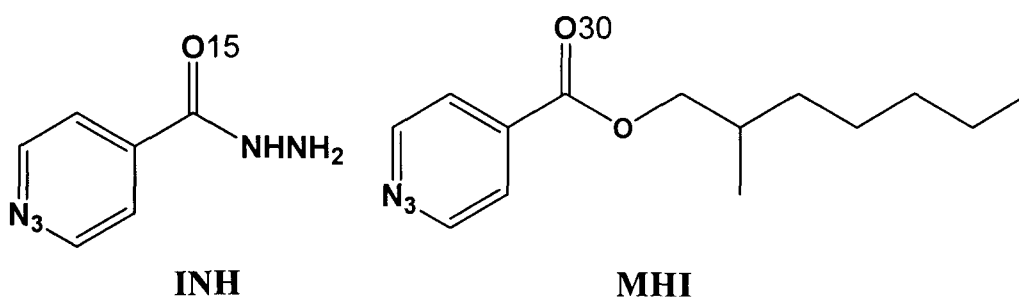


**Figure 3.1** Schematic Representation of the Molecule of INH and MHI with Adopted Atom Numbering

### 3.2 Theoretical background

DFT based reactivity descriptors have been found to be quite successful in predicting structure-property relationship of organic and inorganic compounds.<sup>19</sup> The detailed description on the reactivity descriptors, (GRD and LRD) has already been presented in the pervious chapter. However, a brief outline of the reactivity descriptors would be helpful before we go into the details of the present chapter. The global descriptors like softness (S), chemical potential ( $\mu$ ) and electrophilicity index ( $\omega$ ) reflect the reactivity of entire molecule while the reactivity of atoms in a molecule is characterized by local descriptors. Chattaraj and co-workers<sup>20</sup> have used electrophilicity index as a possible biological activity descriptor. Recently, various aspects of electrophilicity index and philicity have been critically reviewed by Chattaraj *et al.*<sup>21,22</sup> The objective of the present work is to perform a detailed DFT calculation on the molecular structures of the antitubercular agents INH, PZA and MHI. We also demonstrate the power of density functional based descriptors in predicting chemically active sites of the molecules and in comparing their reactivity.

### 3.3 Methodology and Computational Details

Geometries of all the molecules were optimized by DMol<sup>3</sup> program<sup>23</sup> using double numerical with polarization (DNP) and Triple Numerical plus polarization (TNP) basis sets<sup>24</sup> and generalized gradient approximation (GGA) exchange-correlation functionals like HCTH, BLYP, BOP and PW91.<sup>25-28</sup> The electronic populations are calculated using both Mulliken Population Analysis<sup>29</sup> (MPA) and Hirshfeld Population Analysis<sup>30</sup> (HPA). The size of DNP basis set is comparable to the 6-31G\*\* basis set.<sup>31</sup> However, they are believed to be much more accurate than a Gaussian basis set of the same size.<sup>32</sup> TNP basis set is like DNP including additional polarization functions on all atoms giving higher accuracy.

Möller-Plesset second order (MP2) quantum chemical calculation has also been performed on INH and PZA drug molecules at MP2/6-31G\*\* level of theory to validate the accuracy of various functionals used in this study. The MP2 calculations were carried out using the GAMESS program<sup>33</sup>.

### 3.4 Results and Discussion

#### 3.4.1 Geometry optimization

The optimized structures of INH, PZA and MHI at BLYP/DNP level are shown in Figure 3.2. It is seen from the figure that INH has a planar structure, with the exception of the NH<sub>2</sub> group, located slightly out of the plane.

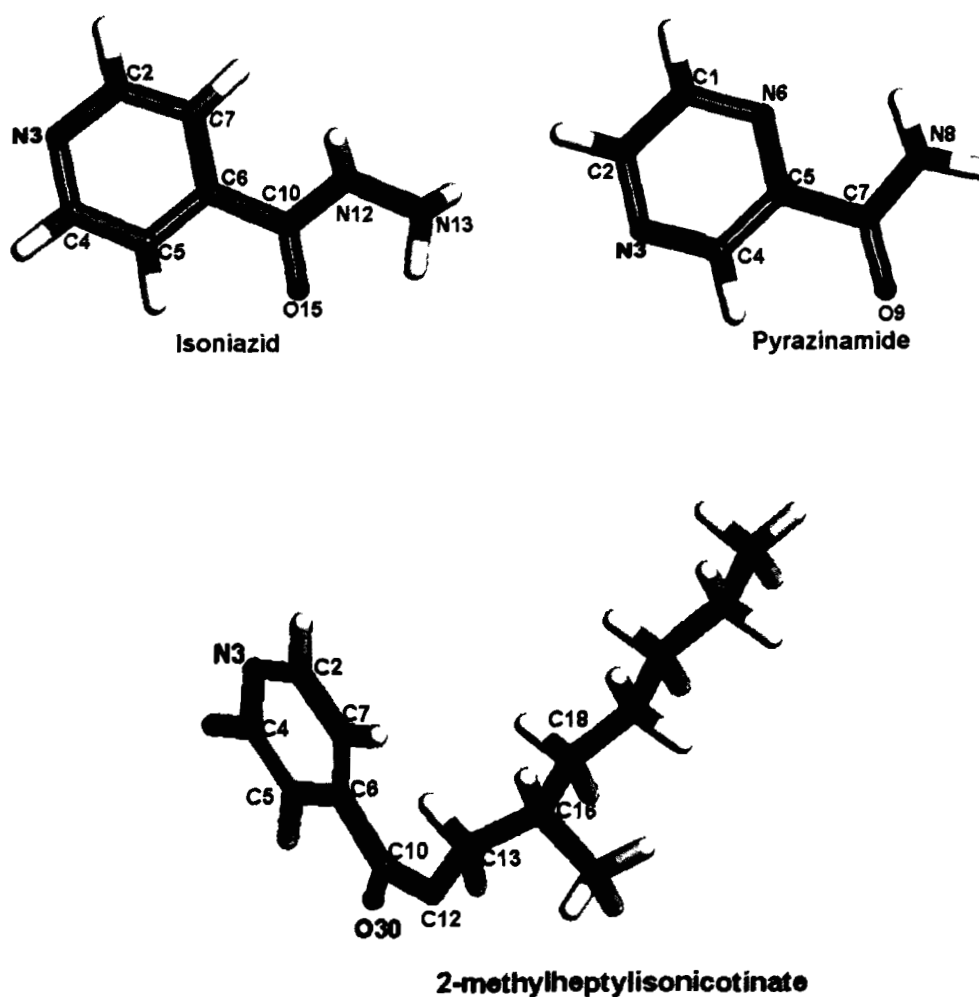


**Figure 3.2** Isoniazid, Pyrazinamide and 2-methylheptylisonicotinate molecules optimized at BLYP/DNP level.

In Table 3.1 we present the geometric parameters of INH calculated using various DFT functionals and they are compared with the experimental X-ray crystallographic structure.<sup>34</sup> From Table 3.1 it is observed that the C-C, C-N and C-O bonds are in very good agreement with the experimental values at all levels of calculations. Moreover, all calculated bond angles are nearly close to that of experimental values.

**Table 3.1** Calculated and experimental geometric parameters of Isoniazid drug molecule. Bond lengths are in Å, bond angles are in degree.

Geometry	Experimental	Theoretical			
		BLYP	BOP	HCTH	PW91
<b>Bond length</b>					
C2-C7	1.394	1.40	1.40	1.40	1.40
C2-N3	1.334	1.35	1.35	1.33	1.34
N3-C4	1.334	1.35	1.35	1.33	1.34
C4-C5	1.385	1.40	1.40	1.39	1.39
C5-C6	1.403	1.40	1.41	1.40	1.40
C6-C7	1.388	1.41	1.41	1.40	1.40
C6-C10	1.485	1.51	1.52	1.51	1.50
C10-O15	1.234	1.24	1.24	1.23	1.23
C10-N12	1.332	1.38	1.39	1.37	1.37
N12-N13	1.413	1.44	1.44	1.39	1.42
<b>Bond angle</b>					
C2-C7-C6	119.8	118.8	118.9	118.8	118.8
C7-C2-N3	123.6	123.7	123.8	123.9	123.8
C2-N3-C4	116.5	116.9	116.8	117.0	116.9
C4-C5-C6	119.4	119.0	119.0	118.8	118.9
N3-C4-C5	124.1	123.7	123.8	123.9	123.8
C5-C6-C7	116.5	117.8	117.7	117.6	117.9
C7-C6-C10	125.2	124.0	123.6	123.8	123.5
C5-C6-C10	118.3	118.2	118.6	118.6	118.6
C6-C10-O15	122.2	122.3	122.3	122.4	122.4
C6-C10-N12	115.5	115.8	115.5	115.3	115.5
O15-C10-N12	122.0	122.0	122.2	122.3	122.1
C10-N12-N13	120.7	119.4	120.2	121.7	120.6

PZA is also a planar molecule. The calculated and the experimental X-ray crystallographic structure<sup>35,36</sup> of PZA are given in Table 3.2. The interatomic bond distances and bond angles are in favor of the experimental values. The calculated geometric parameters of MHI are given in Table 3.3.

**Table 3.2** Calculated and experimental geometric parameters of pyrazinamide drug molecule. Bond lengths are in Å, bond angles are in degree.

Geometry	Experimental	Theoretical			
		BLYP	BOP	HCTH	PW91
<b>Bond length</b>					
C4-C5	1.383	1.41	1.41	1.40	1.40
N3-C4	1.329	1.35	1.35	1.33	1.34
N6-C5	1.344	1.35	1.35	1.34	1.34
C1-N6	1.354	1.35	1.35	1.33	1.34
C1-C2	1.375	1.40	1.40	1.40	1.40
N3-C2	1.353	1.35	1.35	1.33	1.34
C7-O9	1.241	1.24	1.24	1.23	1.23
C7-N8	1.309	1.37	1.37	1.36	1.36
<b>Bond angle</b>					
C5-C4-N3	122.6	121.9	122.0	121.8	121.9
C4-C5-N6	121.9	121.5	121.4	121.5	121.6
C4-C5-C7	120.9	119.8	119.9	119.2	119.8
N6-C5-C7	117.2	118.7	118.7	119.3	118.6
C5-N6-C1	115.4	116.6	116.6	116.7	116.5
N6-C1-C2	122.4	121.6	121.7	121.5	121.6
C1-C2-N3	121.4	122.1	122.2	122.3	122.2
C2-N3-C4	116.0	116.3	116.2	116.2	116.1
C5-C7-O9	119.1	121.4	121.5	121.2	121.5
C5-C7-N8	117.5	114.2	114.4	114.6	113.7
O9-C7-N8	123.2	124.4	124.2	124.2	124.9



**Table 3.3** Geometric parameters of MHI molecule calculated using various functionals with DNP basis set. Bond lengths are in Å, bond angles are in degree.

Geometry	Theoretical			
	BLYP	BOP	HCTH	PW91
<b>Bond length</b>				
N3-C4	1.35	1.35	1.33	1.34
C4-C5	1.40	1.40	1.40	1.40
C5-C6	1.40	1.41	1.40	1.40
C6-C7	1.41	1.41	1.40	1.40
C2-C7	1.40	1.40	1.40	1.40
C2-N3	1.35	1.34	1.33	1.34
C6-C10	1.51	1.52	1.51	1.50
C10-O30	1.22	1.22	1.21	1.21
C10-O12	1.37	1.37	1.35	1.36
O12-C13	1.48	1.48	1.45	1.46
C13-C16	1.54	1.54	1.53	1.53
C16-C18	1.55	1.56	1.54	1.54
C16-C31	1.54	1.55	1.53	1.53
C18-C21	1.54	1.55	1.53	1.53
C21-C24	1.54	1.55	1.53	1.53
C24-C27	1.54	1.55	1.53	1.53
C27-C35	1.54	1.54	1.53	1.53
<b>Bond angle</b>				
N3-C2-C7	123.8	123.9	123.9	123.8
C2-N3-C4	116.9	116.7	117.1	116.9
N3-C4-C5	123.7	123.9	123.9	123.8
C2-C7-C6	118.7	118.7	118.6	118.7
C4-C5-C6	118.8	118.8	118.6	118.7
C5-C6-C7	117.9	117.9	117.9	117.9
C5-C6-C10	119.9	120.1	120.2	119.9
C7-C6-C10	121.9	121.9	121.8	121.9
C6-C10-O30	121.2	121.1	120.9	121.2
C6-C10-O12	119.2	119.4	119.3	118.9
O30-C10-O12	119.5	119.4	119.7	119.8
C10-O12-C13	122.2	122.9	122.8	121.3
O12-C13-C16	111.6	111.4	112.1	111.7

### 3.4.2 Experimental reactivity

Experimental comparison of MHI and INH with respect to bio activity against various bacterial strains (such as *Bacillus subtilis*, *E. Coli*, *Shigella sp.*, *Klebsiella sp.* and *Proteus mirabilis*) showed that MHI is 3-5 times more active than INH. Antifungal activity of MHI when tested against dominant fungal

pathogen (such as *Fusarium moniliforme*, *F. senmitectum*, *F. solani*, *F. oxysporum* and *Rhizoctonia solani*) is found to be about 5-15 times more than that of INH.

### 3.4.3 Global Descriptors

Global reactivity parameters such as global softness, chemical potential, global hardness and global electrophilicity of INH, PZA and MHI have been calculated from the optimized geometry using BLYP/DNP, BOP/DNP, HCTH/DNP, PW91/DNP and TNP/BLYP levels and they are presented in Table 3.4. The calculated global reactivity descriptors for INH and PZA at MP2/6-31G\*\* level are given in Table 3.4.

#### 3.4.3.1 Global Softness/Hardness/Chemical potential

According to the maximum hardness principle (MHP),<sup>37</sup> at constant external potential, stability of a molecule increases with hardness and with the increase in stability, the reactivity decreases. Softness is just the reciprocal of hardness, so higher the softness lower is the stability i.e higher is the reactivity. It is seen from Table 3.4 that the global softness values do not vary much in going from INH to MHI. Thus it is difficult to derive the experimental order of reactivity of these molecules from global softness and global hardness values. It is also observed that global softness and global hardness values are sensitive to functional used. However, the BLYP/DNP and HCTH/DNP derived reactivity parameters are for all three molecules are in good agreement with the higher level calculation, BLYP/TNP. Moreover, these values for INH and PZA are in consistent with the MP2/6-31G\*\* level calculations. The other global reactivity parameter, chemical potential also does not vary much in going from INH to MHI.

#### 3.4.3.2 Electrophilicity Index

The electrophilicity index is considered as a measure of electrophilic power of a molecular system towards a nucleophile. Larger the electrophilic power of a chemical system, higher is its reactivity as an electrophile. Conversely, lower is the electrophilic power of a chemical system, higher is its reactivity as a nucleophile. It can be seen from Table 3.4 that the electrophilicity index calculated with BLYP/DNP, BOP/DNP, HCTH/DNP, PW91/DNP and BLYP/TNP levels

decreases in the order: PZA > INH > MHI. Therefore, from the values of electrophilicity index the observed order of reactivity as a nucleophile is PZA<INH<MHI. Like other global descriptors, electrophilicity index is also sensitive to the functionals. The MP2 results also follow the trend for PZA and INH.

The electrophilicity index values revealed that the reactivity of MHI as a nucleophile is maximum and that of PZA is minimum. However, other global descriptors, global hardness, global softness and chemical potential are observed to be less significant to predict the reactivity of the molecules correctly. Hence, there is a need for more reliable parameters to describe reactivity of these molecules. In order to derive the trend of reactivity of these three compounds we present the local reactivity descriptors of ring nitrogen atom, N3, (Figure 1) of the molecules.

**Table 3.4** Global reactivity descriptors for INH, PZA and MHI (in atomic units). The quantities are calculated at BLYP/DNP, BOP/DNP, HCTH/DNP, PW91/DNP, BLYP/TNP and MP2/6-31G\*\* levels.

Molecule	Functional/ Basis set	Global softness (S)	Chemical potential ( $\mu$ )	Chemical hardness ( $\eta$ )	Electrophilicity index ( $\omega$ )
INH	BLYP/DNP	3.273	-0.159	0.153	0.083
	BOP/DNP	0.763	-0.155	0.656	0.018
	HCTH/DNP	3.189	-0.169	0.157	0.091
	PW91/DNP	0.785	-0.163	0.637	0.021
	BLYP/TNP	3.253	-0.152	0.154	0.076
	MP2/6-31G**	2.778	-0.136	0.180	0.052
PZA	BLYP/DNP	3.285	-0.165	0.152	0.090
	BOP/DNP	0.802	-0.161	0.624	0.021
	HCTH/DNP	3.261	-0.175	0.153	0.099
	PW91/DNP	0.802	-0.171	0.623	0.023
	BLYP/TNP	3.274	-0.158	0.153	0.082
	MP2/6-31G**	2.943	-0.137	0.170	0.055
MHI	BLYP/DNP	3.281	-0.154	0.152	0.078
	BOP/DNP	0.535	-0.148	0.935	0.012
	HCTH/DNP	3.217	-0.163	0.155	0.086
	PW91/DNP	0.549	-0.176	0.912	0.017
	BLYP/TNP	3.246	-0.147	0.154	0.071

### 3.4.4 Local Descriptors

Local reactivity parameters describe the relative reactivity and site selectivity of atoms in a molecule. The nucleophilic attack at a particular site of a system represents the sites with maximum values of Fukui function, ( $f_k^+$ ) and/or local philicity,  $\omega_k^+$ . Similarly, electrophilic attack at a particular site of a system represents the sites with maximum values of Fukui function,  $f_k^-$  and/or local philicity,  $\omega_k^-$ .

Philicity and local softness, respectively, would be better intermolecular reactivity indices (because they are products of global and local indices) than the Fukui function for analyzing electrophile–nucleophile interactions and hard–soft interactions. Recently, some of these aspects have been numerically verified.<sup>38</sup> Philicity and local softness essentially provide the same information that is provided by the Fukui function regarding intramolecular reactivity trends except for the intramolecular processes where  $\omega$  and/or  $S$  also changes along with  $f(r^-)$ . However, for analyzing the intermolecular reactivity,  $f_k^\pm$  would be inadequate and  $s_k^\pm$  (or  $\omega_k^\pm$ ) should be used to compare the hard–soft (electrophilic–nucleophilic) behavior of a given atomic site in one molecule with that of another atomic site in another molecule. For the same molecule,  $f_k^\pm$  is adequate.

The local electrophilicity is a more reliable descriptor than its global counterpart.<sup>39</sup> However, it is recommended that both global and local descriptors, other charge-based descriptors, and, if possible, other effects, such as steric, solvent, and entropy effects, need to be considered in order to have better insights into the chemical reactivity and selectivity although, a few of them will dominate over the rest and some will be dependent on the others.<sup>21</sup>

We calculated fukui function for all the atoms of INH, PZA and MHI to derive the most reactive atoms of each of the molecules. From the fukui function values it was found that the N3 atom shown in Figure 1 is the most reactive atom in each of the molecule. Therefore, we considered Fukui function, local softness, local philicity and relative nucleophilicity values only for N3 atom of INH, PZA and MHI to derive the reactivity order.

### 3.4.4.1 Fukui function, ( $f_k^-$ )

Fukui function values ( $f_k^-$ ) of N3 atom of INH, PZA and MHI derived from MPA and HPA schemes using BLYP/DNP, BOP/DNP, HCTH/DNP, PW91/DNP and BLYP/TNP levels are listed in Table 3.5. It is seen from Table 3.5 that  $f_k^-$  values of the N3 atom calculated with MPA and HPA schemes increase in the order PZA<INH<MHI. Therefore, from  $f_k^-$  values of N3 atom, we can report that the reactivity of these molecules towards electrophilic attack increases in the order: PZA<INH<MHI.

**Table 3.5** Calculated Fukui function ( $f_k^-$ ), local softness ( $s_k^-$ ), local philicity ( $\omega_k^-$ ) and relative nucleophilicity ( $f_k^-/f_k^+$ ) values for N3 atom of INH, PZA and MHI. These values are evaluated using BLYP/DNP, BOP/DNP, HCTH/DNP, PW91/DNP and BLYP/TNP levels using HPA and MPA charges.

Molecule	Functional/ Basis set	HPA				MPA			
		$f_k^-$	$s_k^-$	$\omega_k^-$	$f_k^-/f_k^+$	$f_k^-$	$s_k^-$	$\omega_k^-$	$f_k^-/f_k^+$
INH	BLYP/DNP	0.137	0.448	0.011	1.142	0.104	0.340	0.009	1.010
	BOP/DNP	0.153	0.117	0.003	1.254	0.116	0.089	0.002	1.105
	HCTH/DNP	0.163	0.520	0.015	1.347	0.129	0.411	0.012	1.229
	PW91/DNP	0.169	0.133	0.004	1.374	0.132	0.104	0.003	1.222
	BLYP/TNP	0.160	0.520	0.012	1.333	0.077	0.250	0.006	0.939
PZA	BLYP/DNP	0.125	0.411	0.011	0.969	0.101	0.332	0.009	0.935
	BOP/DNP	0.123	0.099	0.003	0.953	0.100	0.080	0.002	0.917
	HCTH/DNP	0.129	0.421	0.013	1.040	0.110	0.359	0.011	1.058
	PW91/DNP	0.125	0.100	0.003	0.969	0.105	0.084	0.002	0.938
	BLYP/TNP	0.131	0.429	0.011	1.031	0.082	0.268	0.007	0.911
MHI	BLYP/DNP	0.197	0.646	0.015	1.589	0.146	0.479	0.011	1.390
	BOP/DNP	0.192	0.103	0.002	1.524	0.144	0.077	0.002	1.333
	HCTH/DNP	0.198	0.637	0.017	1.597	0.156	0.502	0.013	1.472
	PW91/DNP	0.198	0.109	0.003	1.623	0.153	0.084	0.003	1.430
	BLYP/TNP	0.213	0.691	0.015	1.732	0.096	0.312	0.007	1.171

#### 3.4.4.2 Local softness and philicity ( $s_k^-$ and $\omega_k^-$ )

Local softness and philicity are considered as better intermolecular reactivity indices (because they are products of global and local indices) than the Fukui function for analyzing electrophile-nucleophile interactions and hard-soft interactions. Local softness ( $s_k^-$ ) and philicity ( $\omega_k^-$ ) values of N3 atom of INH, PZA and MHI derived from MPA and HPA schemes using BLYP/DNP, BOP/DNP, HCTH/DNP, PW91/DNP and BLYP/TNP levels are presented in Table 3.5. From Table 3.5 it is distinct that local softness values for N3 atom is higher in case of MHI compared to INH and PZA. However, philicity is observed to be less significant to predict the reactivity of the molecules correctly except for the most accurate DFT calculation with TNP basis set. It is also observed that individual values of ( $s_k^-$ ) and ( $\omega_k^-$ ) are strongly influenced by the functional.

#### 3.4.4.3 Relative nucleophilicity, ( $f_k^-/f_k^+$ )

The relative nucleophilicity, ( $f_k^-/f_k^+$ ) values of N3 atom of PZA, INH and MHI derived from MPA and HPA schemes at BLYP/DNP, BOP/DNP, HCTH/DNP, PW91/DNP and BLYP/TNP levels are reported in Table 3.5. It is noticed from Table 3.5 that  $f_k^-/f_k^+$  values of N3 atom increase in the order: PZA<INH<MHI. Therefore, reactivity of PZA, INH and MHI towards a nucleophile increases in the order: PZA<INH<MHI. This sequence is in perfect agreement with experimental results for MHI and INH.<sup>40</sup>

Thus, based on local reactivity descriptors, MHI is predicted to be more reactive than INH and PZA which is in good agreement with the available experimental results. Based on our DFT calculations the relative nucleophilicity is found to be a better descriptor to reproduce experimental reactivity sequence.

### 3.5 Conclusions

The molecular structures for three anti-tubercular agents were calculated using density functional theory. Comparison with experimental X-ray crystallographic structure data indicates that the optimized geometries of INH and PZA are in consistent with experimental values. DFT based global reactivity descriptor, electrophilicity index, calculated for three antitubercular drug

molecules PZA, INH and MHI revealed that MHI is the most reactive molecule among these three molecules and PZA is the least reactive one. However, other global descriptors like global hardness, global softness and chemical potential are observed to be less significant to predict the reactivity of the molecules correctly and they are sensitive to functionals used. Calculated local descriptors for N3 atom of each of the molecule show a reactivity order of: PZA < INH < MHI. However, Fukui function, local softness and philicity values are sensitive to the functional used. The relative nucleophilicity is a better reactivity descriptor to reproduce experimental reactivity sequence and it does not seem to vary with the functional and basis sets.

The importance of predicting chemically active sites can help experimentalist to better understand the mechanism of action of these antitubercular compounds. Understanding the mode of action may help to design further molecules with better reactivity. This necessitates the study of mechanism of action of this type of antitubercular drug molecules to have better insight of the whole phenomena.

### References

1. Dessen, A.; Quernard, A.; Blanchard, J. S.; Jacobs, Jr W. R. ; Sacchetti, J. C. Crystal structure and function of the isoniazid target of Mycobacterium tuberculosis, *Science* **267**, 1638–1641 (1995)
2. Young, D. B. Blueprint for the White Plague, *Nature* **393**, 515–516 (1998).
3. Ahmed, Y. *et al.* A study of maternal mortality at the University Teaching Hospital, Lusaka, Zambia: the emergence of tuberculosis as a major non-obstetric cause of maternal death, *Int. J. Tuberc. Lung Dis.* **3**, 675–680 (1999)
4. Petrini, B.; Hoffner, S. Drug-resistant and multidrug-resistant tubercle bacilli, *Int. J. Anti Agents* **13**, 93–97 (1999)
5. Sociedad Argentina de Pediatría. Criterios de diagnóstico y tratamiento de la tuberculosis infantil, *Arch. Argent Pediatr* **100**, 159–178 (2002)
6. Chopra, I.; Brennan, P. Molecular action of antimycobacterial agents, *Tuberc. Lung Dis.* **78**, 89–98 (1998)

7. World Health Organization. <http://who.int/mediacentre/factsheets/fs104> (2009).
8. Meyer, H.; Mally, J. Hydrazine derivatives of pyridine-carboxylic acids, *Monatsh. Chem.* **33**, 393–414 (1912)
9. Domagk, G.; Offe, H. A.; Siefken, W. Ein weiterer beitrag zur experimentellen chemotherapie der tuberkulose (neoteben), *Dtsch. Med. Wochenschr.* **77**, 573–578 (1952)
10. Hans, L. Riede. Fourth-generation fluoroquinolones in tuberculosis, *Lancet* **373**, 1148–1149 (2009)
11. Szakacs, T. A. *et al.* Adherence with Isoniazid for Prevention of Tuberculosis among HIV-Infected Adults in South Africa, *Bmc Infect. Dis.* **6**, 97–103 (2006)
12. Gray, D. M.; Zar, H.; Cotton, M. Impact of Tuberculosis Preventive Therapy on Tuberculosis and Mortality in HIV-Infected Children, *Cochrane Database Syst. Rev.* **115** (2009)
13. Anaissie, E. J. Opportunistic mycoses in the immunocompromised host: experience at a cancer center and review, *Clin. Infect. Dis.* **14** (Suppl. 1), 43–53 (1992)
14. Richardson, M. D. Opportunistic and pathogenic fungi, *J. Antimicrob. Chemother Suppl. A* **26**, 1–11 (1991)
15. Georgopapadakou, N. H.; Walsh, T. J. Antifungal agents: chemotherapeutic targets and immunologic strategies, *Antimicrob. Agents Chemother.* **40**, 279–291 (1996)
16. Bordoloi, G. *et al.* Isolation and structure elucidation of a new antifungal and antibacterial antibiotic produced by *Streptomyces* sp. 201, *Biosci. Biotechnol. Biochem.* **65**, 1856–1858 (2001)
17. Bordoloi, G. N. *et al.* Potential of a novel antibiotic, 2-methylheptyl isonicotinate, as a biocontrol agent against fusarial wilt of crucifers, *Pest Manag. Sci.* **58**, 297–302 (2002)
18. Bordoloi, G.; Kumari, B.; Bordoloi, M.; Roy, M. K.; Bora, T. C. US patent No. US 6,998,411 B2 Feb 14, (2006)



19. (a) Geerlings, P.; Proft, F. D.; Langenaeker, W. Conceptual Density Functional Theory, *Chem. Rev.* **103**, 1793–1874 (2003) (b) Bartolotti, L. J.; Ayers, P. W. An Example Where Orbital Relaxation Is an Important Contribution to the Fukui Function, *J. Phys. Chem. A* **109**, 1146–1151 (2005) (c) Parthasarathi, R.; Padmanabhan, J.; Subramanian, V.; Maiti, B.; Chattaraj, P. K. Chemical Reactivity Profiles of Two Selected Polychlorinated Biphenyls, *J Phys Chem A* **107**, 10346–10352 (2003)
20. Parthasarathi, R.; Subramanian, V.; Roy, D. R.; Chattaraj, P. K. Electrophilicity index as a possible descriptor of biological activity, *Bioorg. Med. Chem.* **12**, 5533–5543 (2004)
21. Chattaraj, P. K.; Sarkar, U.; Roy, D. R. Electrophilicity Index, *Chem. Rev.*, **106**, 2065–2091 (2006)
22. Roy, D. R. Careful Scrutiny of the Philicity Concept, *J. Phys. Chem. A* **110**, 1084–1093 (2006)
23. DMol3, Accelrys, San Diego, CA.
24. Delley, B. J. An all-electron numerical method for solving the local density functional for polyatomic molecules, *J. Chem. Phys.* **92**, 508–517 (1990)
25. Becke, A. D. Density-functional exchange-energy approximation with correct asymptotic behavior, *Phys. Rev. A* **38**, 3098–3100 (1988)
26. Lee, C.; Yang, W.; Parr, R. G. Development of the Colle-Salvetti correlation-energy formula into a functional of the electron density, *Phys. Rev. B* **37**, 785–789 (1988)
27. Tsuneda, T.; Suzumura, T.; Hirao, K. A new one-parameter progressive Colle-Salvetti-type correlation functional, *J. Chem. Phys.* **110**, 10664–10678 (1999)
28. Hamprecht, F. A.; Cohen, A. J.; Tozer, D. J.; Handy, N. C. Development and assessment of new exchange–correlation functionals, *J. Chem. Phys.* **109**, 6264–6271 (1998)
29. Mulliken, R. S. Electronic population analysis on LCAO-MO [linear combination of atomic orbital-molecular orbital] molecular wave functions, *J. Chem. Phys.* **23**, 1833–1840 (1955)

30. Hirshfeld, F. L. Bonded-atom fragments for describing molecular charge densities, *Theor. Chim. Acta* **44**, 129–138 (1977)
31. Hehre, W. J.; Ditchfield, R.; Pople, J. A. Self Consistent Molecular Orbital Methods. Further Extensions of Gaussian Type Basis Sets for Use in Molecular Orbital Studies of Organic Molecules, *J. Chem. Phys.* **56**, 2257–2261 (1972)
32. Delley, B. From molecules to solids with the DMol3 approach, *J. Chem. Phys.* **113**, 7756–7764 (2000)
33. Schmidt, M. W. *et al.* General Atomic and Molecular Electronic Structure System, *J. Comput. Chem.* **14**, 1347–1363 (1993)
34. Jensen, L. H. The Crystal Structure of Isonicotinic Acid Hydrazide, *J. Am. Chem. Soc.* **76**, 4663–4667 (1954)
35. Takaki, Y.; Sasada, Y.; Watanabe, T. The crystal structure of 2-pyrazinamide, *Acta Crystallogr.* **13**, 693–702 (1960)
36. Chis, V. Experimental and DFT study of pyrazinamide, *Chem. Phys.* **316**, 153–163 (2005)
37. Pearson, R. G. Recent advances in the concept of hard and soft acids and bases, *J. Chem. Educ.* **64**, 561–567 (1987)
38. Roy, R. K.; Usha, V.; Paulovìè, J.; Hirao, K. Are the Local Electrophilicity Descriptors Reliable Indicator of Global Electrophilicity Trends? *J. Phys. Chem. A* **109**, 4601–4606 (2005)
39. Roy, R. K. On the Reliability of Global and Local Reactivity Descriptor, *J. Phys. Chem. A* **108**, 4934–4939 (2004)
40. Boruwa, J.; Kalita, B.; Barua, N. C. Synthesis, absolute stereochemistry and molecular design of the new antifungal and antibacterial antibiotic produced by *Streptomyces* sp. 201, *Bioorg. Med. Chem. Lett.* **14**, 3571–3574 (2004)

# 4

---

## Mode of interaction of anti TB drug molecules using docking and hybrid (QM/MM) methods

### Abstract

The front-line antituberculosis drug isoniazid (INH) inhibits InhA, the NADH-dependent fatty acid biosynthesis enoyl ACP-reductase from *Mycobacterium tuberculosis*, via formation of covalent adducts with NAD (INH-NAD adducts). The predictions of ligand–protein interactions at the molecular level can be of primary importance in elucidating the mechanisms of action of INH and pyrazinamide (PZA). This may help in identifying the effective mycobactericidal entities and in the design of a new generation of antitubercular drugs. In this chapter, we present our study to explore the modes of interaction and binding energy of INH and another structurally similar antituberculosis drug molecule PZA placed in the active site of InhA with the help of various molecular modeling techniques.

#### 4.1 Introduction

Isoniazid (isonicotinic acid hydrazide, INH, Figure 4.1) is one of the most common and efficient drugs used in the treatment of tuberculosis.<sup>1-3</sup> Even after some 50 years of its discovery this potent and highly selective agent is still an attraction of therapy.<sup>4-6</sup> Currently, there are ten drugs in use approved by the U.S. Food and Drug Administration (FDA) for treating TB out of which the first-line anti-TB agents include isoniazid (INH), rifampin (RIF), ethambutol (EMB) and pyrazinamide (PZA). Instead of these, searching new antimycobacterial agents still has relevance because of the serious side effects of these anti-TB drugs, drug resistance, and the lack of efficacy in immunodepressed patients.<sup>7</sup>

The mechanism of action of INH is not yet fully understood. It was well established that isoniazid itself is not the true drug. It gets oxidized to an active species and then acts as a drug. Electron spin resonance (ESR) studies have identified radicals as intermediates in the activation.<sup>8</sup> Sacchetti *et al.* reported the crystal structure of isonicotinic acyl-NADH in the active site of the enzyme InhA (part of the FASII pathway involved in building the bacterial cell wall) on the basis of which it was confirmed that a reactive intermediate from isoniazid and nicotinamide adenine dinucleotide, NAD<sup>+</sup> combined to give the true inhibitor of the bacterium (Figure 4.1).<sup>9</sup> Several mechanisms of action of INH were reported. Timmins and co-worker<sup>10</sup> reviewed a range of potent mechanisms that explain the exceptional and highly selective potency of INH against *M. tuberculosis*.

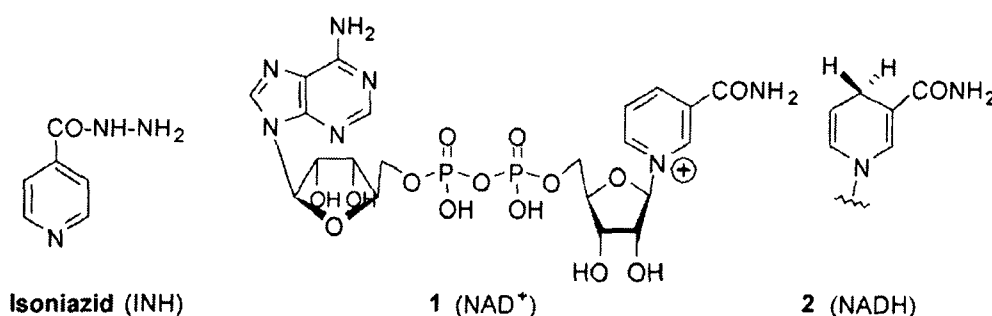


**Figure 4.1** Structures of isoniazid and of the two redox cofactors NAD<sup>+</sup> and NADH.

INH itself is not toxic to the bacterial cell, but acts as a prodrug. The mechanism of this *in vivo* activation is still unknown but it is clear that a functional form of KatG is necessary.<sup>11,12</sup> INH enters the mycobacterial cell by passive diffusion.<sup>13</sup> A catalase/oxidase KatG is required for isoniazid activation. *Mycobacterium tuberculosis* KatG is a catalase-oxidase consisting of two 82 kDa subunits. It has been hypothesized that KatG is responsible for converting INH into an activated form.<sup>11,12,14-17</sup> INH is oxidatively activated *in vivo* by the mycobacterial enzyme KatG,<sup>18</sup> a multifunctional catalase-oxidase to generate an isonicotinoyl radical. This highly reactive species then reacts non-enzymatically with the cellular pyridine nucleotide coenzymes, NAD<sup>+</sup> and NADP<sup>+</sup>,<sup>19</sup> to generate several adducts of isonicotinoyl-NAD(P) to inhibit the *inhA*-encoded enoyl-ACP reductase.<sup>9,20,21</sup> Recent work suggests that activated INH acts as an inhibitor of enzymes involved in mycolic acid.

The identification of novel targets needs the identification of specific biochemical pathways. Many unique metabolic processes occur during the biosynthesis of mycobacterial cell wall components.<sup>22</sup> Mycolic acids being the major components of the cell wall of *M. tuberculosis*,<sup>23</sup> is one of these attractive targets for the rational design of new antituberculosis agents. Mycolic acids are high molecular weight  $\alpha$ -alkyl,  $\beta$ -hydroxy fatty acids covalently linked to arabinogalactan.<sup>23-25</sup> Differences in mycolic acid structure may affect the fluidity and permeability of an asymmetric lipid bilayer that would explain the different sensitivity levels of various mycobacterial species to lipophilic inhibitors.<sup>26</sup> The fatty acid synthase (FAS) are the enzymes that involve in the formation of fatty acids. Since the molecular organization of FAS is found to be different in most bacteria and mammals,<sup>25,27,28</sup> it becomes the ideal targets for designing new antibacterial agents.

After activation by the catalase-oxidase KatG,<sup>18,29,30,31</sup> it inhibits enoyl-acyl carrier protein reductase InhA, an enzyme involved in the fatty acid biosynthesis (FAS II system), which is an essential process to elaborate important cellular components of *Mycobacterium tuberculosis*.<sup>32,33</sup>

Experimentally, the mechanism of the inhibition of INH was studied by X-ray crystallography,<sup>9</sup> mass spectrometry<sup>34</sup> and isotopic experiments.<sup>35</sup> These studies reveal that the process involves a covalent attachment of the activated form

of the drug (isonicotinoyl radical) to the nicotinamide ring of NAD(H). This ultimately modifies the nature of the coenzyme and its interaction with the target enzyme, InhA.

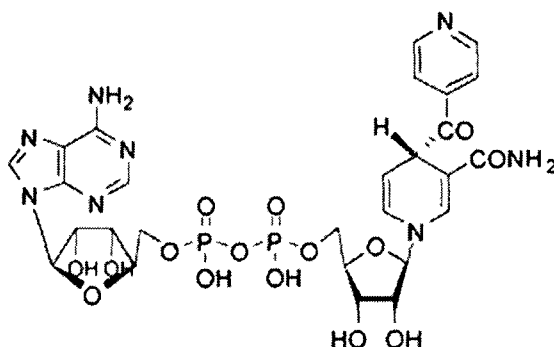


**Figure 4.2** Structures of INH-NAD adduct.

Recent studies have suggested that the 1,4-dihydropyridine INH-NAD adduct exhibits the keto-carboxamide<sup>9</sup> (Figure 4.2). The key structural factors involved in the ring-chain tautomerism equilibrium has been discussed on a series of simplified analogues of isoniazid-NAD adducts.<sup>36</sup> Rawat *et al.*<sup>20</sup> have reported that the analogue of INH-NAD adduct derived from metabolic activation of benzoylhydrazine structure, also behaves as a potent inhibitor of InhA. Subsequently, Broussy *et al.*<sup>37</sup> showed the existence of the adducts in two epimeric ring structures. Recently, it was suggested that the difference between bactericidal (FAS I and FAS II systems) and mammalian (FAS I system) fatty acid biosynthesis makes InhA an attractive molecular target whose selective inhibition is sought in the development of antibiotics with new mechanism of action. In addition, it was observed that the high prevalence of resistances to INH was mainly due to KatG mutants that could not activate isoniazid. Hence, direct inhibitors of InhA, not KatG-dependent, have been considered as promising antitubercular agents.

Computer-aided drug design approaches are powerful tools for better knowledge of the biological effects of molecules. These approaches are widely used to develop direct inhibitors of InhA based on the understanding of isoniazid mechanism.<sup>37-39</sup> In a recent article,<sup>40</sup> Bonnac *et al.* carried out comparative docking experiments of chain INH-NAD adducts and the 4-phenoxybenzamide adenine dinucleotide analogue in interaction with InhA. Amos *et al.*<sup>41</sup> reported

their experiment supported by investigation using computational techniques to study the formation of an acyl radical as the active species from the oxidation of isoniazid.

Apart from those, Pasqualoto *et al.*<sup>42</sup> performed a 4D-QSAR analysis of a set of INH analogues hydrazides, which led the authors to develop a 3D pharmacophore model. Subsequently, in a recent study, the resulting hypothesized active conformations were then used as point of departure in molecular dynamics simulations to generate a 3D-QSAR model,<sup>43</sup> which allowed them to identify the critical thermodynamic descriptors. In this work, we compute the molecular interactions associated with the binding of INH-NAD and PZA-NAD adducts with InhA. These studies can be of primary importance to elucidate the mechanism of action of isoniazid and to better understand the isoniazid-dependent resistances. They can also prove useful in the design of a new generation of antitubercular drugs.

## 4.2 Computational Details

Up to now, only limited data at the molecular level is available on the interactions of INH-NAD(P) adducts with the proposed isoniazid target proteins. The main reports concern the early crystallographic study of the InhA:INH-NAD adduct complex<sup>9</sup> and, recently, description of the crystallized InhA:INH-NADP adduct complex.<sup>44</sup> Based on the X-ray structure of InhA:INH-NAD complex, very few modeling studies were performed, mainly to select relevant descriptors of the biological activity and for structure-based design of new antituberculosis agents.<sup>40,43,42</sup>

The crystal structure of the *M. tuberculosis* enoyl-acyl reductase, named InhA, in complex with cofactor NADH and the inhibitor isoniazid (INH) was isolated by Rozwarski and co-workers (1998) (PDB entry code 1zid). They showed that the drug mechanism of action in *M. tuberculosis* involves a covalent attachment of the activated form of the drug (isonicotinic acyl anion or radical) to the carbon at position 4 of the nicotinamide ring of NADH bound within the active site of InhA, resulting in the formation of an INH-NAD adduct.<sup>9</sup> The crystal structure of the complex between INH-NAD adduct and InhA provides a basis for the design of agents that inhibit InhA without needing a KatG drug activation.<sup>9,45</sup>

#### 4.2.1 Protein and ligands structures

The coordinates of INH-NAD adduct complexed to InhA were taken from the RCSB Protein Data Bank (PDB code 1ZID)<sup>9</sup> and is presented in Figure 4.3. The adduct, highlighted with yellow color, was extracted from the PDB file and hydrogen atoms were added to the protein. Similarly, hydrogen atoms were added on the crystal structure of INH-NAD adduct and energy-minimized using the AMMP<sup>46</sup> force field implemented on the VEGA ZZ<sup>47</sup> molecular modeling package. Subsequently, we modified the structure of INH to PZA in INH-NAD adduct so as to obtain the coordinates of PZA-NAD adduct.



**Figure 4.3** INH-NAD adduct complexed to InhA taken from the Brookhaven Protein Data Bank (PDB code 1ZID)



### 4.2.2 Docking studies

The docking studies were performed with the program Autodock Vina<sup>48</sup> (version 1.0 beta 02). The crystallographic structures of INH-NAD inhibitor obtained by X-Ray diffraction of the enzyme InhA with INH-NAD inhibitor bound in the active site was used as starting point for the docking studies (PDB 1ZID).<sup>9</sup> Water molecules were discarded, except those surrounding the binding site (i.e. water molecules 403, 404, 424, 429, 436, 437, 453 and 455). The Autodock graphical interface AutoDockTools<sup>49,50</sup> was used to keep polar hydrogens and add partial charges for protein. Before attempting any docking simulations, all partial atomic charges and all of the ligand's rotatable bonds were assigned using AutoDock Tools. Missing residues and hydrogen atoms were similarly built back into the model with the same software. Flexible torsions in the ligands were assigned with Autotors, an auxiliary module of AutoDockTools. The crystallographic structure was used without geometry optimization. The atomic charges were calculated from a single-point calculation. After forming the .pdbqt files with the calculated charges, using a Python script, the receptor molecules were put into final form (i.e., adding the salvation parameters) for use with AutoDock to generate the potential energy maps. The grid for these maps was so chosen as to place the ligand molecule at the bottom of the grid. It is also important to note that the dimensions of the box are sufficiently large to accommodate all poses of the ligand molecules. A GRID-based procedure was employed to prepare the structural input and to define the binding sites [24]. A rectangular lattice ( $126 \times 126 \times 126 \text{ \AA}^3$ ) with points separated by  $0.375 \text{ \AA}$  was superimposed upon the entire protein structure. The automated docking was performed using a simulated annealing Monte Carlo simulation in combination with a rapid grid-based energy evaluation method. Lamarckian genetic algorithm (LGA) was selected for ligand conformational searching. Default parameters were used, except for the number of energy evaluations and docking runs, which were set to 2,000,000 and 200, respectively.

The resulting docked conformations with root-mean-square-deviation (rmsd) clustering tolerance values of less than  $1 \text{ \AA}$  were clustered into families of similar conformations. The lowest docking-energy configuration was selected as a representative for each group. Our attention was focused on the group with the

highest number of members, referred to as “the most occurring configuration”. Thus, it is most probable that this configuration represents the real system.

The more relevant docked conformations were then used to compute the interaction energy between the ligands and the InhA cavity.

### 4.2.3 Hybrid QM/MM studies

The hybrid quantum mechanical and molecular mechanical methodologies (QM/MM) use different levels of method for different parts of a molecule. They treat a localized region, e.g. the active site of the enzyme, with QM methods and include the influence of the surroundings, e.g. the protein environment at the MM level. Since treating a large region like the complete protein using a high-quality description such as DFT is not feasible, QM/MM method is an effective tool to study these complex structures.

In this work, we used QMERA<sup>51</sup> to perform QM/MM calculations. QMERA uses a hybrid QM/MM to combine the accuracy of quantum mechanics with the speed of molecular mechanics while performed on very large systems. In QMERA, DFT calculations are performed with DMol<sup>3</sup> and molecular mechanics with GULP to yield results with the accuracy of pure DFT at a lesser computational cost. The model system (i.e. the adduct) was fully optimized at the GGA/DNP level while the rest of the system was treated with GULP. The QM/MM interaction was treated by mechanical embedding.

## 4.3 Results and discussion

### 4.3.1 Docking calculations

Using docking method it is possible to predict the structure of receptor ligand complexes where the receptor is usually a protein and the ligand is either a small molecule or another protein.

First, INH, MHI and PZA were docked onto InhA protein. Next, NADH was placed within the protein binding site. Subsequently, docking studies were then performed with INH-NAD and PZA-NAD adducts. The results of docking of receptor protein InhA with individual drug molecules, drug-NAD adduct and NADH are presented in Table 4.1.

**Table 4.1** Calculated docking energies of NAD adduct with INH and PZA drug molecule.

<b>Ligands (Molecules)</b>	<b>Energy (kcal/mol)</b>	<b>Ligands (Adduct)</b>	<b>Energy (kcal/mol)</b>
INH	-5.0	INH-NAD	-10.8
MHI	-6.0	NADH	-6.5
PZA	-4.1	PZA-NAD	-9.4

It is seen from Table 4.1 that in case of docking with individual molecules the most favorable docking is with molecule MHI followed by INH and PZA. This is in excellent agreement with our theoretical studies for three antitubercular drug molecules, PZA, INH and MHI. These studies, as presented in the previous chapter, utilize several DFT based reactivity descriptors to reveal that MHI is the most reactive among these three molecules and PZA is the least reactive one. The order of reactivity is: PZA < INH < MHI.

While compared all the six docking experiences, it is observed that the docking with adduct are energetically more favorable than docking with drug molecules. The calculated docking energy for the docking of NADH is -6.5 kcal/mol. The INH-NAD and PZA-NAD adducts, docked in the same conditions as NADH, exhibited energies of -10.8 and -9.4 kcal/mol, respectively (Table 4.1). According to these results, affinity for the InhA target is in the increasing order: NADH < PZA-NAD < INH-NAD.

Thus, NAD-INH shows the best docking with lowest energy of the complex. The docked complexes were visualized using the Pymol viewer.<sup>52</sup> The best docked view of INH-NAD adduct bound to protein receptor InhA is shown in Figure 4.4. Hydrogen bonds with existing solvent and the protein can be distinguished in the closer view. Both the INH-NAD and PZA-NAD were found docked in almost the same place where INH-NAD was present as predicted by earlier X-ray crystallographic studies. However, some changes of ligand conformation and the ligand–protein interactions were evident.

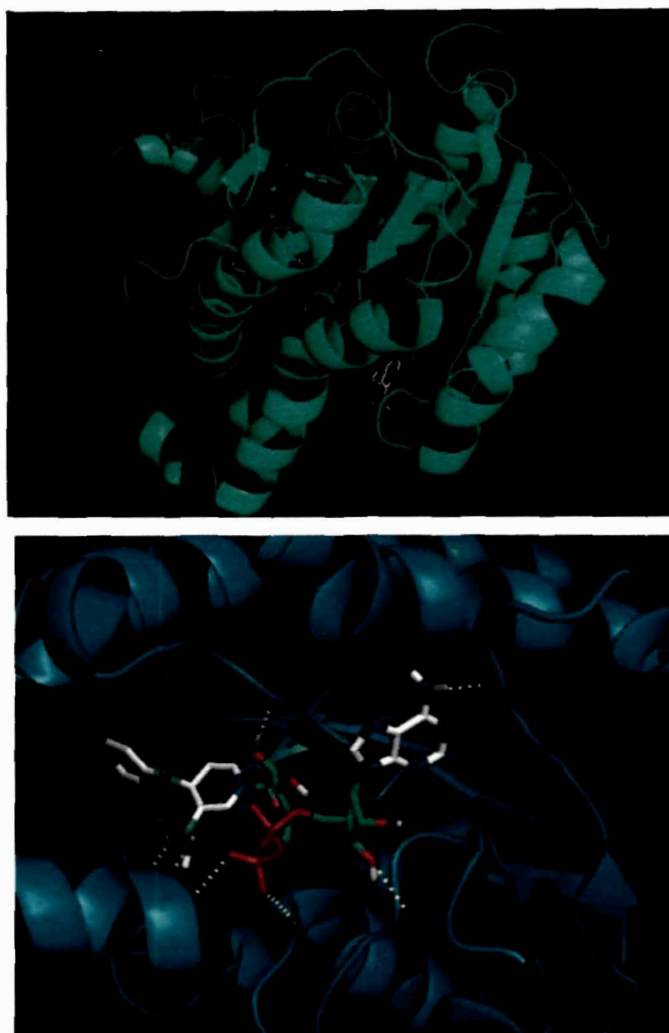


**Figure 4.4** Docked view of ligand (INH-NAD adduct) bound to protein receptor InhA. Hydrogen bonds with existing solvent and the protein are shown.

#### 4.3.2 Hybrid QM/MM

Hybrid QM/MM methods simplifies the energy calculation by treating the active region with a high-level quantum mechanical (*ab initio* or density functional) approach and rest of the environment with a less expensive molecular mechanics force field method. We performed QM/MM calculations with INH-NAD and PZA-NAD adducts in presence of protein. Instead of taking the whole protein, a large portion of the protein in the vicinity of the adduct were selected for carrying out QM/MM calculations. We only considered the amino acid residues, which encompass ligands at the level of the reactive cavity of InhA and in which the relaxed ligand was inserted.

The quantum chemically calculated important geometric parameters such as bond length, bond angle and torsion angle of isolated INH along with experimental values are presented in Table 4.2. Apart from those, theoretically (QM) calculated geometry of INH in INH-NAD adduct; QM/MM calculated and experimentally observed geometry for INH in INH-NAD adduct in protein environment are also presented in the table. It is seen from Table 4.2 that the experimentally found geometric parameters of INH are matching well with the values obtained from quantum chemical calculation. The C10-C19 bond length (which is actually C10-N12 in isolated INH) seems to increase in theoretical calculations.

**Table 4.2** Selected geometric parameters of INH drug molecule in various environments. Bond lengths are in Å, bond angles are in degree.

Geometry of INH	INH in isolation		NAD Adduct	NAD Adduct with protein	
	Expt.	QM	QM	QM/MM	Expt.
<b>Bond length</b>					
C2-C7	1.394	1.40	1.43	1.47	1.47
C2-N3	1.334	1.35	1.39	1.43	1.43
N3-C4	1.334	1.35	1.39	1.42	1.43
C4-C5	1.385	1.40	1.43	1.48	1.47
C5-C6	1.403	1.40	1.45	1.46	1.48
C6-C7	1.388	1.41	1.45	1.48	1.48
C6-C10	1.485	1.51	1.51	1.49	1.49
C10-O15	1.234	1.24	1.21	1.23	1.23
C10-C19	1.332	1.38	1.55	1.53	1.53
<b>Bond angle</b>					
C2-C7-C6	119.8	118.8	119.2	119.7	119.7
C7-C2-N3	123.6	123.7	122.0	120.3	120.3
C2-N3-C4	116.5	116.9	119.4	121.3	121.4
C4-C5-C6	119.4	119.0	119.0	120.4	119.9
N3-C4-C5	124.1	123.7	121.9	119.8	120.1
C5-C6-C7	116.5	117.8	118.3	118.3	118.5
C7-C6-C10	125.2	124.0	122.0	121.2	121.1
C5-C6-C10	118.3	118.2	119.2	119.9	119.9
C6-C10-O15	122.2	122.3	118.1	116.9	116.8
C6-C10-C19	115.5	115.8	120.8	121.8	121.9
<b>Torsion angle</b>					
C5-C6-C10-O15	122.0	122.0	36.50	35.6	36.8
C7-C6-C10-O15	120.7	119.4	135.5	135.8	135.8

On the other hand, in presence of protein environment, the geometric parameters of INH in INH-NAD adduct are found to be similar. It is observed that both QM/MM calculated and experimentally observed values of various bond length and bond angles match well.

However, in the adduct, all the C-C and C-N bond lengths are observed to get elongated except the C10-C15 bond, which rather shortens. Drastic increase in C10-C19 bond length is obvious because it is the C10-N12 bond in isolated INH. The nitrogen containing part vanishes in the INH-NAD adduct.

On the other hand, INH of INH-NAD adduct in protein environment shows increase in all the C-C and C-N bond lengths compared to both isolated INH as well as INH-NAD adduct. The exception is the C10-C15 bond, which rather decreases.

While comparing the bond angles, the C2-N3-C4 bond angle increases in the adduct while the adjacent angles of N3 i.e. the N3-C4-C5 bond angle decreases slightly compared to that in isolated INH. The C2-N3-C4 bond angle of INH of INH-NAD adduct in protein environment increases further where the N3-C4-C5 bond angle decreases. In contrast, the bond angle involving O15, (C6-C10-O15), is observed to decrease significantly in both the environment.

Regarding the planarity of the molecule, it is observed from the torsion angles that the planarity of the side chain changes drastically in going from the isolated molecule to the adduct. The change of torsion angle of INH of INH-NAD adduct in protein environment is also drastic compared to isolated INH but almost similar to those of INH-NAD adduct without protein environment.

All the theoretically calculated values are in good agreement with available experimental values. The compatibility of hybrid QM/MM derived values with experimental values establishes the accuracy of the method.

Experimentally observed and theoretically calculated selected geometric parameters of isolated PZA molecule, PZA in PZA-NAD adduct and PZA-NAD adduct in protein environment are presented in Table 4.3. As in case of INH, it is seen from Table 4.3 that the experimentally found geometric parameters of PZA are in good agreement with the values obtained from theoretical calculation. All the C-C and C-N bond lengths are observed to get elongated in the adduct except the C7-O9 bond which gets shortened slightly. The PZA-NAD adduct in protein

environment shows further increase in all the C-C and C-N bond lengths compared to both isolated PZA and PZA-NAD adduct.

**Table 4.3** Selected geometric parameters of PZA drug molecule in various environments. Bond lengths are in Å, bond angles are in degree.

Geometry	PZA in isolation		NAD Adduct	NAD Adduct with protein
	Expt.	QM	QM	QM/MM
<b>Bond length</b>				
C4-C5	1.383	1.406	1.45	1.46
N3-C4	1.329	1.346	1.42	1.48
N6-C5	1.344	1.350	1.43	1.48
C1-N6	1.354	1.345	1.42	1.47
C1-C2	1.375	1.401	1.43	1.43
N3-C2	1.353	1.347	1.40	1.43
C7-O9	1.241	1.235	1.22	1.23
C7-N8	1.309	1.368	1.52	1.53
C5-C7			1.55	1.49
<b>Bond angle</b>				
C5-C4-N3	122.6	121.9	119.6	120.7
C4-C5-N6	121.9	121.5	119.4	118.4
C4-C5-C7	120.9	119.8	119.4	119.9
N6-C5-C7	117.2	118.7	120.8	121.2
C5-N6-C1	115.4	116.6	119.6	119.6
N6-C1-C2	122.4	121.6	120.3	120.3
C1-C2-N3	121.4	122.1	120.5	121.3
C2-N3-C4	116.0	116.3	120.5	119.5
C5-C7-O9	119.1	121.4	116.1	116.9
C5-C7-N8	117.5	114.2	121.9	121.8
O9-C7-N8	123.2	124.4	122.0	121.3
<b>Torsion angle</b>				
C4-C5-C7-O9			36.8	35.6
N6-C5-C7-O9			-136.21	-135.8

Similarly, the bond angles are also observed to follow the same trend as in case of INH. The C2-N3-C4 bond angle increases in the adduct while the adjacent angle of N3 i.e. the C5-C4-N3 bond angle decreases slightly in going from isolated PZA to PZA-NAD adduct. The bond angle involving O9, (C5-C7-O9), is observed to decrease significantly in both the environments.

The optimized geometries of INH and PZA in various forms and environments are presented in figures 4.5, 4.6 and 4.7.

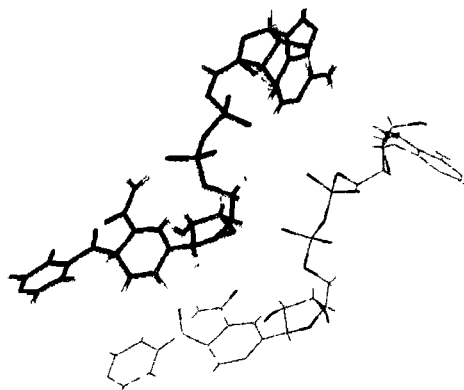


**Figure 4.5** Geometry of INH in INH-NAD adduct in presence of protein environment (bold stick) and in isolation (thin stick).

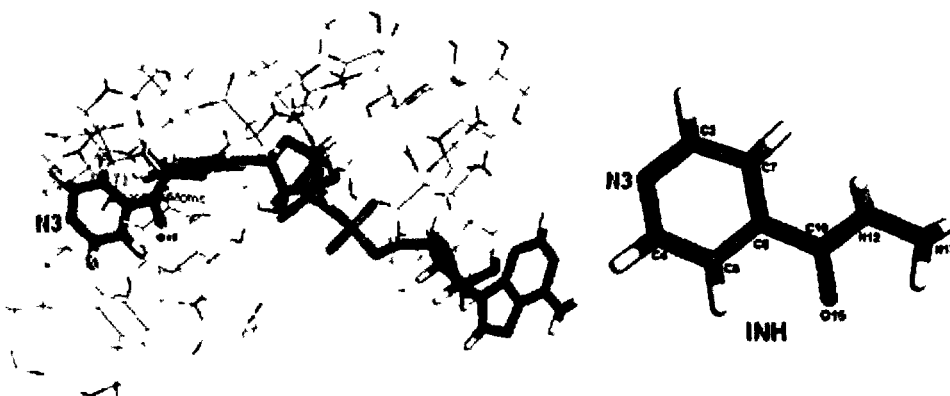


**Figure 4.6** Geometry of INH in presence of protein environment.

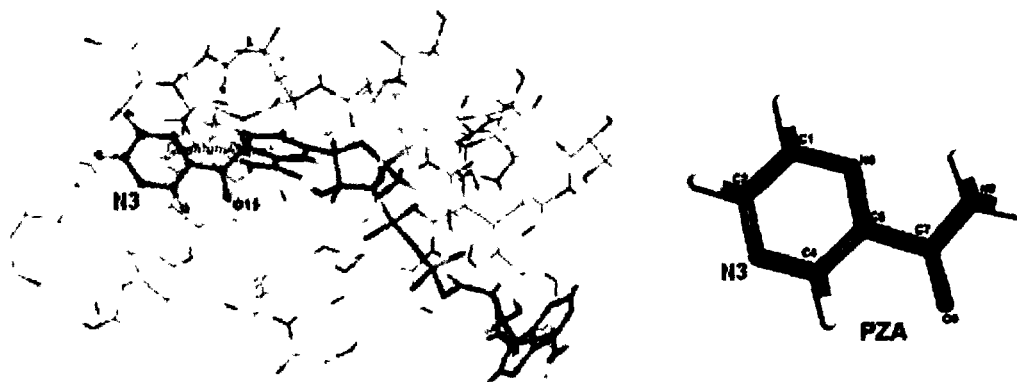


**Figure 4.7** Geometry of PZA in presence of protein environment.



The similar geometric parameters as well as changes in geometric parameters of INH and PZA in various forms and environments attribute similar types of interactions of the drug molecules with InhA.

#### 4.3.2.1 Interaction Energy

The energy values of drug-NAD adduct, protein and “drug-NAD adduct with protein” calculated separately for the drug molecules INH and PZA are presented in Table 4.4. The interaction energy for the two systems have also been calculated and presented in the same table.

It is seen from Table 4.4 that the energy of the drug protein environment involving INH is relatively higher than that involving PZA. The interaction energy calculated for INH is found to be slightly lower than that of PZA which indicated that the INH interaction with the protein environment is more favorable compared to PZA interaction.

**Table 4.4** Calculated interaction energies of INH and PZA

Drug Molecule	Energy (au)			Interaction Energy	
	Drug-NAD with protein (QM/MM)	Protein (MM)	Drug-NAD Adduct (QM)	(au)	(kcal/mol)
INH	-870.333231	-511.66292	-358.66025	-0.0101	-6.34
PZA	-886.306377	-511.66292	-374.63396	-0.0095	-5.96

#### 4.4 Conclusions

The geometrical parameters of both the molecules INH and PZA show a significant change in the geometry in various forms and environment. The theoretically calculated selected geometric parameters of INH and PZA are in good agreement with those of the available experimental values. Particularly, the values obtained from hybrid QM/MM calculations are compatible with experimental values and thereby establishes the accuracy of the method.

The geometric parameters for INH-NAD and PZA-NAD in protein environment are similar in nature. This supports the possibility of similar types of interactions for both the drug molecules.

The interaction energy values show that the interaction of INH is more favorable compared to PZA interaction. This supports further that INH is a better antitubercular drug in comparison to PZA.

## References

1. Bartmann, K.; Iwainsky, H.; Kleeberg, H.H.; Mison, P.; Offe, H.A.; Otten, H.; Tettenborn, D.; Trnka, L. *Antituberculosis Drugs*, Springer-Verlag, Berlin-Germany, (1988)
2. Blanchard, J. S. Molecular mechanisms of drug resistance in *Mycobacterium tuberculosis*, *Annu. Rev. Biochem.* **65**, 215–239 (1996)
3. Bloom, B. R.; Murray, C. J. Tuberculosis: Commentary on a Reemergent Killer, *Science* **257**, 1055–1064 (1992)
4. Youatt, J. An enzyme system of *Mycobacterium tuberculosis* that reacts specifically with isoniazid, *Am. Rev. Respir. Dis.* **99**, 729–749 (1969)
5. Deretic, V.; Pagan-Ramos, E.; Zhang, Y.; Dhandayuthapani, S.; Via, L. E. The extreme sensitivity of *Mycobacterium tuberculosis* to the front-line antituberculosis drug isoniazid, *Nat. Biotechnol.* **14**, 1557–1561 (1996)
6. Zhang, Y.; Dhandayuthapani, S.; Deretic, V. Molecular basis for the exquisite sensitivity of *Mycobacterium tuberculosis* to isoniazid, *Proc Natl. Acad. Sci. USA* **93**, 13212–13216 (1996)
7. Sensi, P.; Grass, I. G. Antimycobacterial Agents. In *Burger's Medicinal Chemistry and Drug Discovery*, 5th ed.; Burger, A., Wolff, M. E., Eds.; John Wiley & Sons: New York, **2**, 575–635 (1996)
8. Wengenack, N.; Rusnak, F. Evidence for isoniazid-dependent free radical generation catalyzed by *Mycobacterium tuberculosis* KatG and the isoniazid-resistant mutant KatG(S315T), *Biochemistry* **40**, 8990–8996 (2001)
9. Rozwarski, D. A.; Grant, G. A.; Barton, D. H.; Jacobs, W. R. Jr.; Sacchettini, J. C. Modification of the NADH of the isoniazid target (InhA) from *Mycobacterium tuberculosis*, *Science* **279**, 98–102 (1998)

10. Timmins, G. S.; Deretic, V. Mechanisms of action of isoniazid, *Mol. Microbiol.* **62**,1220–1227 (2006)
11. Wengenack, N. L.; Todorovic, S.; Yu, L.; Rusnak, F. Evidence for differential binding of isoniazid by *Mycobacterium tuberculosis* KatG and the isoniazid-resistant mutant KatG (S315T), *Biochemistry* **37**, 15825–15834 (1998)
12. Johnsson, K.; Schultz, P. G. Mechanistic Studies of the Oxidation of Isoniazid by the Catalase Peroxidase from *Mycobacterium tuberculosis*, *J. Am. Chem. Soc.* **116**, 7425–7426 (1994)
13. Bardou, F.; Raynaud, C.; Ramos, C.; Laneelle, M.A.; Laneelle, G. Mechanism of isoniazid uptake in *Mycobacterium tuberculosis*, *Microbiology* **144**, 2539–2544 (1998)
14. Zabinski, R. F.; Blanchard, J. S. The Requirement for Manganese and Oxygen in the Isoniazid-Dependent Inactivation of *Mycobacterium tuberculosis* Enoyl Reductase, *J. Am. Chem. Soc.* **119**, 2331–2332 (1997)
15. Magliozzo, R. S.; Marcinkeviciene, J. A. Evidence for Isoniazid Oxidation by Oxyferrous Mycobacterial Catalase–Peroxidase, *J. Am. Chem. Soc.* **118**, 11303–11304 (1996)
16. Wengenack, N. L.; Jensen, M. P.; Rusnak, F.; Stern, M. K. *Mycobacterium tuberculosis* KatG is a peroxynitritase, *Biochem. Biophys. Res. Commun.* **256**, 485–487 (1999)
17. Riley, L. W. In *Tuberculosis*; Rom, W. N., Garay, S., Eds.; Little, Brown & Co.: Boston, 763-771 (1996)
18. Zhang, Y.; Heym, B.; Allen, B.; Young, D.; Cole, S. The catalase-peroxidase gene and isoniazid resistance of *Mycobacterium tuberculosis*, *Nature*, **358**, 591–593 (1992)
19. Zhao, X. *et al.* Hydrogen Peroxide-Mediated Isoniazid Activation Catalyzed by *Mycobacterium tuberculosis* Catalase-Peroxidase (KatG) and Its S315T Mutant, *Biochemistry* **45**, 4131–4140 (2006)
20. Rawat, R.; Whitty, A.; Tonge, P. J. The isoniazid-NAD adduct is a slow, tight-binding inhibitor of InhA, the *Mycobacterium tuberculosis* enoyl reductase:

- Adduct affinity and drug resistance, *Proc. Natl. Acad. Sci. U. S. A* **100**, 13881–13886 (2003)
21. Nguyen, M.; Quemard, A.; Broussy, S.; Bernadou, J.; Meunier, B. Mn(III) pyrophosphate as an efficient tool for studying the mode of action of isoniazid on the InhA protein of *Mycobacterium tuberculosis*, *Antimicrob. Agents Chemother* **46**, 2137–2144 (2002)
  22. Barry, C. E. III. New horizons in the treatment of tuberculosis, *Biochem. Pharmacol.* **54**, 1165–1172 (1997)
  23. Pasqualoto, K. F. M.; Ferreira, E. I. An approach for the rational design of new antituberculosis agents, *Curr. Drug Targets* **2**, 427–437 (2001)
  24. Brennan, P. J.; Nikaido, H. The envelope of mycobacteria, *Annu. Rev. Biochem.* **64**, 29–63 (1995)
  25. Barry, C. E., III. *et al.* Mycolic acids: structure, biosynthesis and physiological functions, *Prog. Lipid Res.* **37**, 143–179 (1998)
  26. Liu, J.; Barry, C. E., III; Besra, G. S.; Nikaido, H. Mycolic acid structure determines the fluidity of the mycobacterial cell wall, *J. Biol. Chem.* **271**, 29545–29551 (1996)
  27. McCarthy, A. D.; Hardie, D. G. Fatty acid synthase: an example of protein evolution by gene fusion, *Trends Biochem. Sci.* **9**, 60–63 (1984)
  28. Magnuson, K.; Jackowski, S.; Rock, C. O.; Cronan, J. E., Jr. Regulation of fatty acid biosynthesis in *Escherichia coli*, *Microbiol. Rev.* **57**, 522–542 (1993)
  29. Marcinkeviciene, J. A.; Magliozzo, R. S.; Blanchard, J. S. Purification and characterization of the *Mycobacterium smegmatis* catalase-peroxidase involved in isoniazid activation, *J. Biol. Chem.* **270**, 22290–22295 (1995)
  30. Johnsson, K.; Froland, W.A.; Schultz, P.G. Overexpression, Purification, and Characterization of the Catalase-peroxidase KatG from *Mycobacterium tuberculosis*, *J. Biol. Chem* **272**, 2834–2840 (1997)
  31. Wang, J.-Y.; Burger, R. M.; Drlica, K. Role of Superoxide in Catalase-Peroxidase-Mediated Isoniazid Action against Mycobacteria, *Antimicrob. Agents Chemother.* **42**, 709–711 (1998)

32. Queard, A. *et al.* Binding of Catalase-Peroxidase-Activated Isoniazid to Wild-Type and Mutant *Mycobacterium tuberculosis* Enoyl-ACP Reductases, *J. Am. Chem. Soc.* **118**, 1561–1562 (1996)
33. Marrakchi, H.; Laneelle, G.; Queard, A. InhA, a target of the antituberculous drug isoniazid, is involved in a mycobacterial fatty acid elongation system, FAS-II, *Microbiology* **146**, 289–296 (2000)
34. Lei, B.; Wie, C.-J.; Tu, S.-C. Action Mechanism of Antitubercular Isoniazid. Activation by *Mycobacterium tuberculosis* KatG, isolation, and characterization of InhA inhibitor, *J. Biol. Chem.* **275**, 2520–2526 (2000)
35. Nguyen, M.; Claparols, C.; Bernadou, J.; Meunier, B. Is the isonicotinoyl radical generated during activation of isoniazid by Mn-III-pyrophosphate? *Comptes. Rendue. Chimie* **5**, 325–330 (2002)
36. Delaine, T. *et al.* Ring-chain tautomerism of simplified analogues of isoniazid-NAD(P) adducts: an experimental and theoretical study, *Eur. J. Org. Chem.* 1624–1630 (2007)
37. Broussy, S. *et al.* <sup>1</sup>H and <sup>13</sup>C NMR characterization of pyridinium-type isoniazid-NAD adducts as possible inhibitors of InhA reductase of *Mycobacterium tuberculosis*, *Org. Biomol. Chem.* **3**, 670–673 (2005)
38. Broussy, S. *et al.* The First Chemical Synthesis of the Core Structure of the Benzoylhydrazine–NAD Adduct, a Competitive Inhibitor of the *Mycobacterium tuberculosis* Enoyl Reductase, *J. Org. Chem.* **70**, 10502–10510 (2005)
39. Delaine, T. ; Génisson, V. B. ; Meunier, B.; Bernadou, J. Synthesis of the Isonicotinoylnicotinamide Scaffolds of the Naturally Occurring Isoniazid–NAD(P) Adducts, *J. Org. Chem.* **72**, 675–678 (2007)
40. Bonnac, L. *et al.* Synthesis of 4-phenoxybenzamide adenine dinucleotide as NAD analogue with inhibitory activity against enoyl-ACP reductase (InhA) of *Mycobacterium tuberculosis*, *Bioorg. Med. Chem. Lett.* **17**, 4588–4591 (2007)
41. Amos, R. I. J.; Gourlay, B. S.; Schiesser, C. H.; Smith, J. A.; Yates, B. F. A mechanistic study on the oxidation of hydrazides: application to the tuberculosis drug isoniazid, *Chem. Commun.* **14**, 1695–1697 (2008)

42. Pasqualoto, K. F. M.; Ferreira, E. I.; Santos-Filho, O. A.; Hopfinger, A. J. Rational Design of New Antituberculosis Agents: Receptor-Independent Four-Dimensional Quantitative Structure-Activity Relationship Analysis of a Set of Isoniazid Derivatives, *J. Med. Chem.* **47**, 3755–3764 (2004)
43. Pasqualoto, K. F. M.; Ferreira, M. M. C.; Santos-Filho, O. A.; Hopfinger, A. J. Molecular dynamics simulations of a set of isoniazid derivatives bound to InhA, the enoyl-ACP reductase from *Mycobacterium tuberculosis*, *Int. J. Quantum Chem.* **106**, 2689–2699 (2006)
44. Argyrou, A.; Vetting, M. W.; Blanchard, J. S. New Insight into the Mechanism of Action of and Resistance to Isoniazid: Interaction of *Mycobacterium tuberculosis* enoyl-ACP Reductase with INH-NADP, *J. Am. Chem. Soc.* **129**, 9582–9583 (2007)
45. Pasqualoto, K. F. M.; Ferreira, E. I. An approach for the rational design of new antituberculosis agents, *Curr. Drug Targets* **2**, 427–437 (2001)
46. Harrison, R.W. Stiffness and energy conservation in molecular dynamics, *J. Comp. Chem.* **14**, 1112–1122 (1993)
47. Pedretti, A.; Villa, L.; Vistoli, G. VEGA: a versatile program to convert, handle and visualize molecular structure on windows-based PCs, *J. Mol. Graph.* **21**, 47–49 (2002)
48. Trott, O.; Olson, A. J. AutoDock Vina: improving the speed and accuracy of docking with a new scoring function, efficient optimization, and multithreading, *J. Comput. Chem.* **31**, 455–461 (2010)
49. Sanner, M. F.; Duncan, B. S.; Carillo, C. J.; Olson, A. J. Integrating Computation and Visualization for Biomolecular Analysis: An Example Using Python and AVS, *Pac. Sympos. Biocomput.* **4**, 401–412 (1999)
50. AutoDockTools. Molecular Graphics Laboratory, Scripps Research Institute, La Jolla, California. <http://www.scripps.edu/~sanner/python/> (2009)
51. Sherwood, P. *et al.* QUASI: A general purpose implementation of the QM/MM approach and its application to problems in catalysis, *Theochem-J. Mol. Struct.* **632**, 1–28 (2003)
52. <http://pymol.org> (2010).

# 5

## Density Functional Theory Studies on Reactivity of Artemisinin and Some of its Derivatives

---

### Abstract

A comparative study on the structure and chemical reactivity of antimalarial drug, artemisinin and some of its selected derivatives were performed using DFT. Calculated geometry of artemisinin is in good agreement with the available X-ray data. DFT based global reactivity descriptors such as global softness and global electrophilicity calculated at the optimized geometries are used to investigate the usefulness of these descriptors for understanding the reactive nature of the molecules. Local descriptors, Fukui function and philicity values successfully describe the reactive sites of the molecules. Antimalarial activities of artemisinin derivatives against the chloroquine-resistant, mefloquine-sensitive *Plasmodium falciparum* W-2 clone were investigated by QSAR analysis using DFT based descriptors as well as some molecular mechanics parameters.

## 5.1 Introduction

Malaria remains one of the world's greatest public health challenges. Half of world's population is at the risk of malaria. In 2008, 109 countries were recognized as endemic for malaria with 3.3 billion people at risk among which 45 countries were within the WHO African region. *Plasmodium falciparum* was among the leading causes of death worldwide in 2004 from a single infectious agent.<sup>1</sup> This parasite, responsible for the majority of fatal malaria infections, can kill patients in a matter of hours. Malaria continues to be a critical problem worldwide owing to the emergence of resistance strains of malarial parasites to almost all available antimalarial drugs.<sup>2</sup>

Artemisinin (Fig. 5.1), isolated from a Chinese medicinal herb, and some of its derivatives are still found to be a potent antimalarial drug against the resistant strains of *P. falciparum*. However, total synthesis and biochemical synthesis of artemisinin are not viable as the mainstream sources of artemisinin since these routes are not cost effective. Despite of serious efforts, a successful malaria vaccine has remained a distant dream and therefore development of new antimalarials based on artemisinin is crucial to control and cure the disease.

The effectiveness of artemisinin and its derivatives as antimalarial drugs for the treatment of multi-drug-resistant *P. falciparum* has received considerable attention in recent years.<sup>3,4</sup> The development of a new drug is a very long and expensive process. It is thus ideal to have a method that enables prediction of biological activity of new compounds in advance on the basis of chemical structure alone. For drug discovery and development, QSAR techniques<sup>5</sup> are often employed because using these techniques the bioactivity of new compounds can be predicted effectively with reduced efforts. Traditional QSAR<sup>6</sup> studies have been used since the early 1970s to predict activities of untested molecules. Development of a QSAR based pharmacophore model<sup>7</sup> may be of great help to find out a pharmaceutically acceptable and economically viable peroxide-based antimalarial. QSAR studies on artemisinin<sup>8-12</sup> have contributed a lot in understanding the behavior of artemisinin. Tonmunphean *et al.*<sup>5</sup> performed a QSAR study correlating antimalarial activities and artemisinin-heme binding properties obtained from docking calculations. Avery *et al.*<sup>11</sup> considered a dataset of 211 artemisinin analogs and used comparative molecular field analysis



(CoMFA)<sup>13</sup> as a tool to model the activity of artemisinin analogs in terms of active site binding. Subsequently, Cheng *et al.*<sup>14</sup> performed molecular docking and 3D-QSAR studies on the possible antimalarial mechanism of artemisinin analogues. Guha *et al.*<sup>15</sup> developed of QSAR models to predict and interpret the biological activity of 179 artemisinin analogues.

DFT based reactivity descriptors namely, global hardness ( $\eta$ ), electronegativity ( $\chi$ ), chemical potential ( $\mu$ ), electrophilicity index ( $\omega$ ), Fukui functions ( $f(r)$ ) and philicity ( $\omega_k^\pm$ ),<sup>16-19</sup> have attracted considerable interests to describe reactivity and site selectivity of various bio-molecules.<sup>20,21</sup> The electrophilicity and philicity indices have also been successfully used to predict the biological activity/toxicity/property of different organic molecules.<sup>22-24</sup> The performance of these descriptors has been quite substantially reviewed in recent times.<sup>25-27</sup>

Among different descriptors for describing the electronic properties of molecules, the quantum chemical descriptors based on DFT and semi-empirical methods have been found useful in several QSAR studies.<sup>28-32</sup> In particular, the energy of the next lowest unoccupied molecular orbital, electrophilicity and van der Waals surface area have shown to correlate with various biological activities, such as anticancer activities.<sup>28</sup>

In this chapter, we present the use of DFT based reactivity descriptors to study the structure, stability, and reactivity of artemisinin and some of its derivatives. Theoretically obtained values are compared with experimental data. Experimentally proposed mechanism of action of artemisinin has been established theoretically by verifying that O1 of the endoperoxide linkage of artemisinin is the preferred site of electrophilic attack by the heme iron. DFT based global reactivity descriptors, global softness and global electrophilicity, calculated at the optimized geometries are used to investigate the reactive nature of the molecules while local reactivity descriptors such as Fukui function and philicity are utilized for selecting the reactive site(s) in individual molecule. Multiple regression analyses were performed to build up a QSAR model based on DFT derived descriptors as well as molecular mechanics parameters for artemisinin to establish the importance of the descriptor in predicting antimalarial activity. The comparative QSAR study with the help of DFT techniques were performed in gas media and the training set

correlation coefficients and cross-validation (leave-one-out)  $q^2$  values were found to be significant.

The mode of action of artemisinin derivatives is different from other antimalarial drugs because of their unusual structures. Artemisinin is a sesquiterpene lactone with an endoperoxide group, and its unusual 1,2,4-trioxane ring system has been proven to be critical for the antimalarial activity.<sup>33</sup> It is ensured that the selected analogues act via similar mechanisms of action. Biological activity have been taken from reported control activity for artemisinin where the selected compounds have been tested using the same assay method, i.e., in vitro against the chloroquine-resistant, mefloquine-sensitive *P. falciparum* W-2 clone.<sup>11,34</sup> The relative activity (RA) was calculated from the experimentally derived  $IC_{50}$  of artemisinin divided by the  $IC_{50}$  of the analogue and corrected for molecular weight. Before inclusion into the spreadsheets, the RA was converted to the log RA as given below:

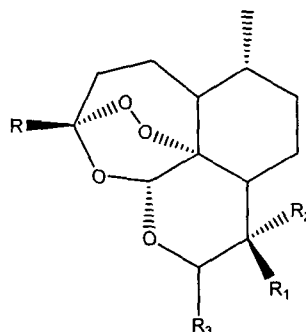
$$\log RA = \log[(IC_{50} \text{ of artemisinin}/IC_{50} \text{ of the analog}) \times (MW \text{ of the analog}/MW \text{ of artemisinin})]$$

## 5.2 Computational details

The artemisinin structure determined by X-ray crystallography<sup>35</sup> was considered as the reference structure to build up the analogues. Full unconstrained geometry optimization of artemisinins was carried out using the DMol<sup>3</sup> program. We used double numerical with polarization (DNP) basis set<sup>36</sup> in combination with several LDA and GGA exchange-correlation functionals like BLYP, BOP, HCTH, BP, PW91, PWC and VWN-BP. The other analogues of artemisinin considered for theoretical studies were optimized with most widely used exchange-correlation functional BLYP in combination with DNP basis set. The size of DNP basis set is comparable to the 6-31G\*\* basis of Hehre *et al.*<sup>37</sup> However, they are believed to be much more accurate than a Gaussian basis set of the same size.<sup>38</sup>

The structural variations of other 20 analogues of artemisinin due to the presence of various functional groups are presented in Table 5.1.

**Table 5.1** Artemisinin (molecule 1) and other derivatives with various functional groups.



Molecule	Substituent groups			
	R	R1	R2	R3
1	CH <sub>3</sub>	CH <sub>3</sub>	H	=O
2	CH <sub>3</sub>	H	CH <sub>3</sub>	=O
3	C <sub>2</sub> H <sub>5</sub>	H	H	=O
4	H	H	H	=O
5	C <sub>3</sub> H <sub>7</sub>	H	H	=O
6	CH <sub>3</sub>	=CH <sub>2</sub>	---	=O
7	CH <sub>3</sub>	=CHCH <sub>3</sub>	---	=O
8	CH <sub>3</sub>	=O	---	=O
9	CH <sub>3</sub>	C <sub>5</sub> H <sub>11</sub>	H	=O
10	CH <sub>3</sub>	C <sub>3</sub> H <sub>7</sub>	H	=O
11	CH <sub>3</sub>	CH <sub>3</sub>	H	H
12	CH <sub>3</sub>	CH <sub>3</sub>	H	OH
13	CH <sub>3</sub>	CH <sub>3</sub>	H	OEt
14	CH <sub>3</sub>	C <sub>4</sub> H <sub>9</sub>	H	OH
15	CH <sub>3</sub>	H	H	H
16	CH <sub>3</sub>	CH <sub>3</sub>	H	OMe
17	CH <sub>3</sub>	C <sub>4</sub> H <sub>9</sub>	H	H
18	CH <sub>3</sub>	C <sub>2</sub> H <sub>5</sub>	H	H
19	CH <sub>3</sub>	C <sub>3</sub> H <sub>7</sub>	H	OEt
20	CH <sub>3</sub>	H	H	OEt
21	CH <sub>3</sub>	C <sub>2</sub> H <sub>5</sub>	H	OEt

The global reactivity descriptors, such as chemical potential ( $\mu$ ), chemical hardness ( $\eta$ ), and electrophilicity ( $\omega$ ) have been calculated by using equations 2.12 and 2.13. Fukui function values were calculated using both Mulliken (MPA) and Hirshfeld population analysis (HPA). The molar refractivity parameter of carrier ligands and surface area of each complex were obtained from the MM+ computations with Hyperchem software.<sup>39</sup>

The optimized geometries of all the 20 analogues of artemisinin are presented in Figure 5.1.

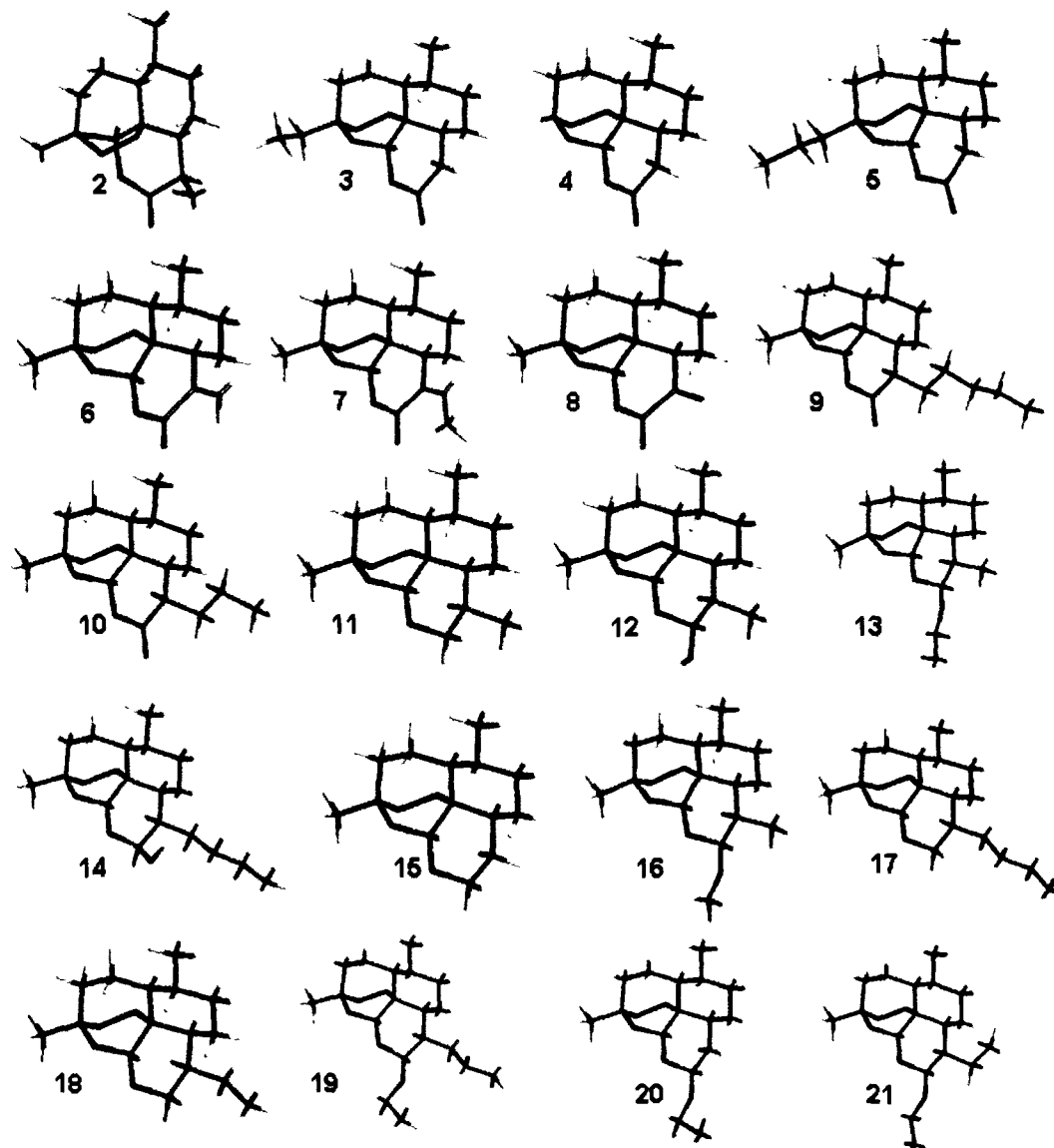


**Figure 5.1** Optimized geometries of 20 analogues of artemisinin.

### 5.3 Results and discussion

#### 5.3.1 Geometry of Artemisinin

The optimized geometry of artemisinin at BLYP/DNP level is shown in Figure 5.2 and its selected structural parameters obtained using DNP basis set in combination with several functional such as HCTH, BLYP, PW91, PWC, BOP, BP, VWN-BP are presented in Table 5.2. The available X-ray crystallographic<sup>35</sup> results of artemisinin are also presented in Table 5.2 structure.

It is seen from Table 5.2 that the geometric parameters of artemisinin calculated at various levels of theories are in good agreement with available experimental results.

**Table 5.2** Comparison of selected geometric parameters of artemisinin optimized at different theoretical levels with experimental results. Bond lengths are in Å, bond angles and dihedral angles are in degree.

Geometry	Exp.	HCTH	BLYP	PW91	PWC	BOP	BP	VWN-BP
<b>Bond length</b>								
C2C1	1.528	1.54	1.55	1.55	1.53	1.56	1.55	1.54
C3C2	1.559	1.53	1.55	1.54	1.52	1.55	1.54	1.54
C4C3	1.556	1.54	1.56	1.55	1.52	1.56	1.55	1.55
C5C4	1.521	1.56	1.57	1.56	1.53	1.57	1.56	1.56
C5O1	1.456	1.45	1.48	1.46	1.43	1.48	1.46	1.46
O1O2	1.478	1.46	1.51	1.49	1.45	1.51	1.49	1.49
O2C1	1.403	1.41	1.42	1.42	1.40	1.43	1.42	1.41
C1O8	1.437	1.45	1.47	1.46	1.43	1.47	1.46	1.46
O8C9	1.390	1.39	1.41	1.40	1.38	1.41	1.40	1.40
C9C5	1.529	1.53	1.54	1.54	1.52	1.55	1.54	1.54
<b>Bond angle</b>								
O1O2C1	107.5	108.4	107.7	107.8	107.7	107.9	107.8	107.7
O2C1O8	107.3	108.6	108.4	108.6	108.4	108.5	108.6	108.6
C1O8C9	114.1	113.8	114.0	113.8	113.0	114.0	113.4	113.4
O8C9C5	113.3	113.5	113.9	113.8	113.3	114.0	113.8	113.9
C9C5O1	111.0	111.4	111.7	111.8	111.8	111.6	111.8	111.8
C5O1O2	111.1	111.7	111.3	111.2	110.7	111.4	111.2	111.1
C9C5C4	111.6	111.1	111.2	111.0	110.4	111.3	111.0	111.0
O1C5C4	106.2	105.9	105.7	105.9	106.6	105.6	105.9	105.8
C5C4C3	112.2	112.1	112.2	112.1	112.0	112.2	112.1	112.0
C4C3C2	115.1	116.5	116.7	116.6	116.2	116.8	116.6	116.7
C3C2C1	112.6	114.3	114.6	114.4	113.8	114.7	114.4	114.4
C2C1O2	112.3	111.9	112.2	112.3	111.9	112.2	112.3	112.3
C2C1O8	110.6	109.4	109.4	109.3	109.3	109.4	109.3	109.3
<b>Dihedral angle</b>								
C5O1O2C1	47.4	47.1	46.9	47.4	49.5	46.5	47.4	47.8
O1O2C1O8		-73.7	-73.7	-74.2	-75.5	-73.4	-74.2	-74.4
O2C1O8C9		33.3	34.6	34.1	32.9	34.6	34.1	34.1
C1O8C9C5		26.9	26.5	26.8	28.0	26.4	26.8	26.9

Since no significant variation of bond lengths and bond angles from the experimental data have been noticed with DNP basis set and any of the functional,

the most popular exchange-correlation functional BLYP in combination with DNP basis set has been chosen for performing calculations for the remaining molecules.

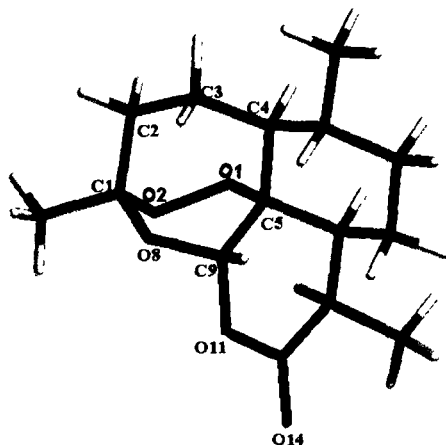


**Figure 5.2** Optimized geometry of artemisinin

### 5.3.2 Global Descriptors

Global reactivity parameters, chemical potential ( $\mu$ ), hardness ( $\eta$ ), and electrophilicity index ( $\omega$ ) of artemisinins have been calculated at the BLYP/DNP level and they are presented in Table 5.3. The variation of hardness ( $\eta$ ) calculated with BLYP/ DNP level for the molecules are shown in Figure 5.3.

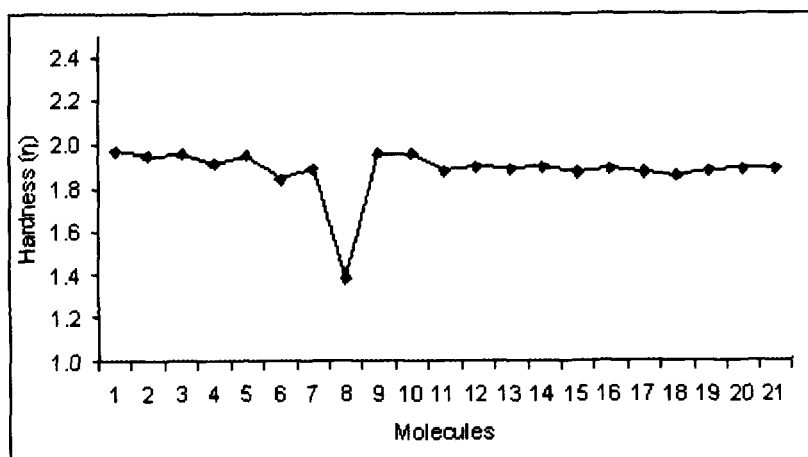


**Figure 5.3** Variation of hardness of the molecules calculated at BLYP/DNP level.

According to maximum hardness principle (MHP),<sup>40</sup> at constant external potential, stability of a molecule increases with hardness and with the increase in stability the reactivity decreases. It is seen from Table 5.3 that the molecule 8 has

the lowest chemical hardness ( $\eta$ ) value (1.379 eV) among all the modelled derivatives and hence is the most reactive one.

**Table 5.3** Comparison of the global reactivity descriptors,  $\mu$ ,  $\eta$ , and  $\omega$  of artemisinin and various derivatives calculated at BLYP/DNP theoretical levels.

Molecule	Chemical		
	Potential ( $\mu$ )	Hardness ( $\eta$ )	Electrophilicity ( $\omega$ )
1	-3.962	1.972	3.980
2	-3.969	1.944	4.052
3	-3.976	1.957	4.039
4	-4.114	1.909	4.433
5	-3.985	1.945	4.082
6	-4.097	1.836	4.571
7	-3.967	1.879	4.188
8	-3.471	1.379	4.368
9	-3.948	1.955	3.986
10	-3.955	1.955	4.001
11	-3.468	1.874	3.209
12	-3.573	1.894	3.370
13	-3.495	1.879	3.250
14	-3.611	1.891	3.448
15	-3.486	1.868	3.253
16	-3.510	1.885	3.268
17	-3.456	1.869	3.195
18	-3.477	1.853	3.262
19	-3.488	1.876	3.243
20	-3.502	1.882	3.258
21	-3.482	1.882	3.221

On the other hand, electrophilicity index ( $\omega$ ) is considered as a measure of electrophilic power of a molecular system towards a nucleophile. Larger the electrophilic power of a chemical system, higher is its reactivity as an electrophile. Conversely, lower is the electrophilic power of a chemical system higher is its reactivity as a nucleophile. The variation of electrophilicity index ( $\omega$ ) calculated at BLYP/ DNP level for the molecules is shown in Figure 5.4.

It can be seen from Figure 5.4 that molecule 6 has maximum electrophilicity value which is comparable to molecules 4 and 8. Thus from  $\omega$  values the molecules 4, 6 and 8 are found to be more reactive than the other compounds.

However, other global descriptor, chemical potential is observed to be less significant to predict any reactivity trend of the molecules correctly. Hence, there is a need for more reliable parameter to describe reactivity of these molecules.

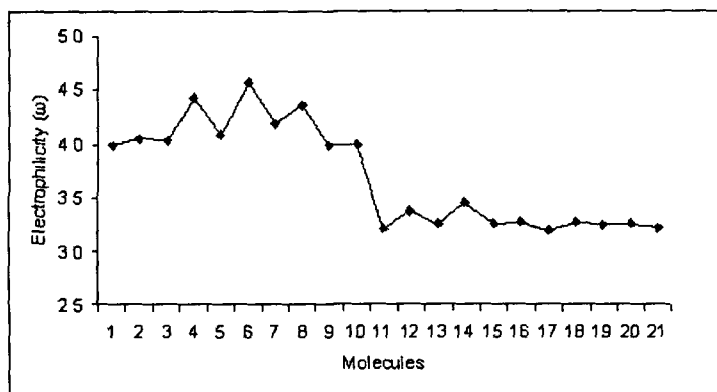


**Figure 5.4** Variation of electrophilicity of the molecules at BLYP/DNP levels.

### 5.3.3 Local Descriptors

Local reactivity parameters describe the relative reactivity and site selectivity of atoms in a molecule. The nucleophilic attack at a particular site of a system represents the sites with maximum values of Fukui function, ( $f_k^+$ ) and/or local philicity,  $\omega_k^+$ . Similarly, electrophilic attack at a particular site of a system represents the sites with maximum values of Fukui function,  $f_k^-$  and/or local philicity,  $\omega_k^-$ .

We calculated Fukui function for all the atoms of artemisinin and its derivatives to derive the most reactive atoms in each of the molecules. From the Fukui function values it was found that the atoms O1 and O2 shown in Figure 5.2 are the most reactive atoms in each of the molecule. Therefore, we considered Fukui function ( $f_k^+$ ), local philicity and relative electrophilicity values of O1 and O2 atoms for comparison.

#### 5.3.3.1 Fukui function, ( $f_k^+$ )

Fukui function values ( $f_k^+$ ) of O1 and O2 atoms of artemisinin and derivatives derived from MPA and HPA schemes using BLYP/DNP levels are listed in Table 5.4. It is seen from Table 5.4 that in all the molecules the value of



( $f_k^+$ ) is higher in case of atom O2 than that of atom O1. This indicates that atom O2 is the preferred site for nucleophilic attack which establishes the preference of heme iron to approach the O2 atom at the endoperoxide linkage of artemisinin compounds. While the  $f_k^+$  values of atom O2 are compared for all the molecules it does not show any significant variation. Similarly,  $f_k^+$  values of atom O1 also do not show any significant variation. Therefore, from  $f_k^+$  values of O2 and O1 atoms, it is difficult to compare the reactivity of the molecules.

### 5.3.3.2 Local philicity ( $\omega_k^+$ )

Philicity is considered as better intermolecular reactivity parameter than FF for analyzing electrophile-nucleophile interactions as it is the product of global and local parameter. Philicity ( $\omega_k^+$ ) values for O1 and O2 atoms of artemisinin and its derivatives derived from MPA and HPA schemes using BLYP/DNP levels are listed in Table 5.4. However, variation of philicity is also observed to be less significant to make a comparison among the molecules to predict their reactivity.

### 5.3.3.3 Relative electrophilicity, ( $f_k^+/f_k^-$ )

The variation of relative electrophilicity,  $f_k^+/f_k^-$ , calculated with BLYP/DNP level for the molecules are shown in Figure 5.5.

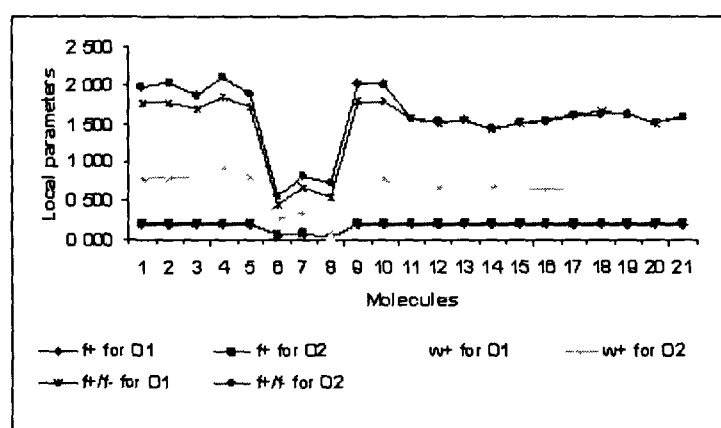


**Figure 5.5** Variation of local reactivity parameters of the O1 and O2 atoms of all 21 artemisinin derivatives calculated at BLYP/DNP level using HPA.

**Table 5.4** Fukui function ( $f_k^+$ ), local philicity ( $\omega_k^+$ ) and relative electrophilicity ( $f_k^+/f_k^-$ ) values for O1 and O2 atoms of artemisinin and derivatives calculated at BLYP/DNP level using HPA and MPA charges.

Molecule	Mulliken						Hirshfeld					
	$f_k^+$		$\omega_k^+$		$f_k^+/f_k^-$		$f_k^+$		$\omega_k^+$		$f_k^+/f_k^-$	
	O1	O2	O1	O2	O1	O2	O1	O2	O1	O2	O1	O2
1	0.214	0.222	0.852	0.884	1.698	2.075	0.189	0.198	0.752	0.788	1.766	1.980
2	0.215	0.220	0.871	0.891	1.720	2.115	0.187	0.198	0.758	0.802	1.781	2.041
3	0.213	0.222	0.860	0.897	1.626	1.982	0.189	0.196	0.763	0.792	1.703	1.867
4	0.219	0.222	0.971	0.984	1.780	2.155	0.194	0.210	0.860	0.931	1.848	2.100
5	0.212	0.222	0.865	0.906	1.643	1.982	0.188	0.196	0.767	0.800	1.709	1.885
6	0.061	0.067	0.279	0.306	0.436	0.549	0.053	0.063	0.242	0.288	0.442	0.553
7	0.079	0.083	0.331	0.348	0.681	0.830	0.067	0.078	0.281	0.327	0.677	0.830
8	0.009	0.024	0.039	0.105	0.474	0.750	0.011	0.022	0.048	0.096	0.550	0.733
9	0.215	0.222	0.857	0.885	1.720	2.114	0.189	0.198	0.753	0.789	1.783	2.020
10	0.215	0.222	0.860	0.888	1.720	2.114	0.189	0.198	0.756	0.792	1.783	2.020
11	0.217	0.219	0.696	0.703	1.497	1.659	0.190	0.197	0.610	0.632	1.570	1.563
12	0.217	0.219	0.731	0.738	1.447	1.634	0.191	0.197	0.644	0.664	1.516	1.539
13	0.217	0.219	0.705	0.712	1.486	1.659	0.190	0.196	0.618	0.637	1.557	1.556
14	0.215	0.220	0.741	0.758	1.352	1.507	0.189	0.197	0.652	0.679	1.410	1.428
15	0.218	0.219	0.709	0.712	1.444	1.599	0.191	0.197	0.621	0.641	1.516	1.504
16	0.217	0.219	0.709	0.716	1.466	1.647	0.191	0.197	0.624	0.644	1.553	1.539
17	0.217	0.219	0.693	0.700	1.550	1.724	0.190	0.196	0.607	0.626	1.624	1.607
18	0.217	0.219	0.708	0.714	1.572	1.738	0.190	0.197	0.620	0.643	1.652	1.628
19	0.216	0.218	0.700	0.707	1.543	1.730	0.190	0.196	0.616	0.636	1.624	1.620
20	0.217	0.219	0.707	0.714	1.447	1.610	0.191	0.197	0.622	0.642	1.516	1.515
21	0.217	0.218	0.699	0.702	1.517	1.690	0.190	0.196	0.612	0.631	1.597	1.581

The  $f_k^+/f_k^-$  values of O1 and O2 atoms of artemisinin and derivatives derived from MPA and HPA schemes at BLYP/DNP level are reported in Table 5.4. It is noticed from Table 5.4 that  $f_k^+/f_k^-$  values of O2 atom thus calculated increase in the order: molecule 10 = molecule 9 < molecule 4. Thus, reactivity of molecule 4 towards an electrophile is maximum followed by molecules 9 and 10.

### 5.3.4 QSAR studies

From the results of DFT calculations, various descriptors, such as energy of highest occupied molecular orbital ( $E_{HOMO}$ ), energy of lowest unoccupied molecular orbital ( $E_{LUMO}$ ), energy of the next lowest unoccupied molecular orbital ( $E_{NL}$ ), energy difference between LUMO and HOMO ( $\Delta_{L-H}$ ), dipole moments, electrophilicity ( $\omega$ ), hardness ( $\eta$ ), philicity ( $\omega^+$ ) etc were selected for QSAR modelling. In addition, the molecular mechanics parameters such as molar refractivity ( $MR$ ), van der Waals surface area ( $SA$ ), molecular volume, log of octanol/water partition coefficient ( $\log P$ ) of the whole molecule and molar refractivities ( $MR_R, MR_{R1}, MR_{R2}, MR_{R3}$ ) of the substituents ( $R, R_1, R_2, R_3$ ) were selected.

The logarithmic relative activity values ( $\log RA$ ) of compounds (1–21) were taken from the work of Avery *et al.*<sup>11</sup> The descriptors with greater correlation to  $\log RA$  with smaller auto correlation were selected out to perform the stepwise multiple linear regression. The QSAR equation having significant statistical parameters for 21 artemisinin analogues is represented by equation 5.1. The equation is obtained by considering the relative activity ( $\log RA$ ) as a dependent variable and electrophilicity ( $\omega$ ), energy of highest occupied molecular orbital ( $E_{HOMO}$ ),  $\log P$ , and molar refractivity of  $R_3$  group ( $MR_{R3}$ ) as independent variables, values of which are presented in Table 5.5.

$$\log RA = 13.912 - 0.871 \omega + 2.394 E_{HOMO} + 0.787 \log P - 0.0619 MR_{R3} \quad (5.1)$$

$$n = 21, r^2 = 0.795, SD = 0.515, F = 15.545, p < 0.05$$

Here,  $r^2$  is the square of correlation coefficient,  $SD$  is the standard deviations of regression,  $F$  is the overall  $F$ -statistics for the addition of each successive term, and  $p$  is the  $p$ -values using the  $F$  statistics. In general, a regression model is significant at  $p$ -value  $< 0.05$  using the  $F$  statistics<sup>41</sup> and so these models are statistically significant. However, according to the general

statistical standards, a model with  $r^2 > 0.80$ <sup>42</sup> is acceptable. Therefore this QSAR equation should be further improved to become a statistically significant model. To improve  $r^2$ , LOO (Leave One Out) method suggested by Dietrich *et al.* and Cornish-Bowden and Wang<sup>43,44</sup> was applied in which a compound is considered as outlier if its corresponding  $r^2$ , called jackknife  $r^2$  ( $r_j^2$ ) value obtained from the regression analysis after deleting the compound, is comparatively higher than the other  $r_j^2$  values. The calculated  $r_j^2$  values are presented in Table 5.5.

**Table 5.5** Parameters used to build the QSAR models along with the jackknife results for the selected set of artemisinin derivatives.

Molecule	$\omega$	$E_{HOMO}$	logP	$MR_{R3}$	Log RA	$r_j^2$
1	3.980	-5.933	4.71	1.95	0.00	0.796
2	4.052	-5.912	4.71	1.95	-0.17	0.794
3	4.039	-5.933	4.77	1.95	0.05	0.798
4	4.433	-6.023	3.59	1.95	-2.75	<b>0.821</b>
5	4.082	-5.929	5.17	1.95	0.83	0.817
6	4.571	-5.933	4.82	1.95	-0.89	0.789
7	4.188	-5.846	5.14	1.95	-0.36	0.808
8	4.368	-5.943	5.64	1.95	-2.47	0.782
9	3.986	-5.902	6.29	1.95	1.02	0.788
10	4.001	-5.910	5.50	1.95	1.13	0.808
11	3.209	-5.342	3.06	0.89	0.75	0.791
12	3.370	-5.467	2.85	2.56	0.55	0.811
13	3.250	-5.374	3.47	12.06	0.34	0.796
14	3.448	-5.502	4.04	2.56	0.96	0.790
15	3.253	-5.354	2.66	0.89	0.28	0.795
16	3.268	-5.395	3.13	7.32	0.28	0.795
17	3.195	-5.325	4.25	0.89	1.32	0.788
18	3.262	-5.330	3.46	0.89	0.67	0.797
19	3.243	-5.364	4.27	12.06	-0.04	<b>0.846</b>
20	3.258	-5.383	2.97	12.06	0.43	0.821
21	3.221	-5.364	3.87	12.06	0.50	0.794

It is clear that compounds 4, 19, 20 have higher  $r_j^2$  values where the values are same for compounds 4 and 20. We removed compound 19 and one of the other two compounds. But correlation is better for the QSAR equation obtained after removing molecules 4 and 19 compared to that obtained for 19 and 20. The QSAR equation obtained after deleting compounds 4 and 19 is given in equation 5.2.

$$\log RA = 8.868 - 0.875 \omega + 1.321 E_{HOMO} + 0.555 \log P - 0.033 MR_{R3} \quad (5.2)$$

$$n = 19, r^2 = 0.865, SD = 0.345, F = 22.572, p < 0.05$$

**Table 5.6** Experimental and calculated logRA values of artemisinin and derivatives from BLYP/DNP level.

Molecule	LogRA		
	Expt. <sup>11</sup>	Calculated	Residual
1	0.00	0.079	-0.079
2	-0.17	0.046	-0.216
3	0.05	0.063	-0.013
5	0.83	0.266	0.564
6	-0.89	-0.376	-0.514
7	-0.36	0.274	-0.634
8	-2.47	-2.594	0.124
9	1.02	1.049	-0.029
10	1.13	0.560	0.571
11	0.75	0.672	0.078
12	0.55	0.152	0.398
13	0.34	0.315	0.025
14	0.96	0.736	0.225
15	0.28	0.381	-0.101
16	0.28	0.289	-0.009
17	1.32	1.410	-0.090
18	0.67	0.878	-0.208
21	0.50	0.591	-0.091

Equations 5.1 and 5.2 reveal that increasing values of  $E_{HOMO}$  and  $\log P$  and decreasing values of  $\omega$  and  $MR_{R3}$  enhance the activity of artemisinin derivatives. Table 5.6 lists the experimental and calculated logRA values of the molecules.

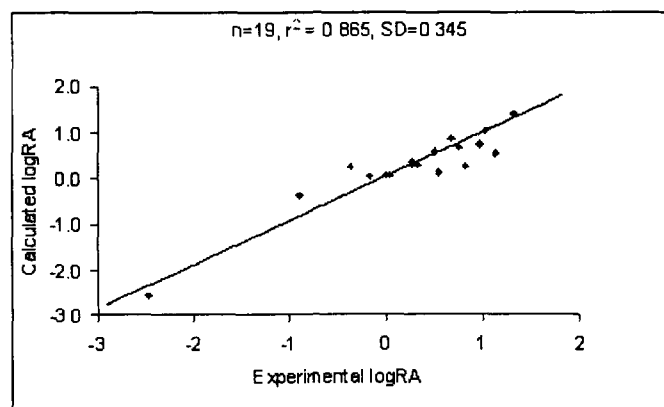


**Figure 5.6** A plot between experimental and calculated logRA values of all the derivatives of artemisinin.

A plot between the experimental and calculated logRA values (Figure 5.6) shows that the selected descriptors are capable of predicting the activity of artemisinin derivatives.

### 5.3.5 Conclusions

In this study we used DFT based reactivity descriptors to study the structure, stability, and reactivity of artemisinin and some of its derivatives. Comparison with experimental X-ray crystallographic structure data indicates that the optimized geometries of artemisinin obtained theoretically are in agreement with experimental values. One of the global descriptors, global hardness, reveals that molecule 8 is the most reactive one among the artemisinin derivatives. The electrophilicity value of molecule 6 is found to be maximum which is comparable with that of molecules 4 and 8. Fukui function ( $f_k^+$ ) values of all the atoms of each of the molecule show that atom O2 is the most reactive atom compared to other atoms. This also indicates that atom O2 is the preferred site for nucleophilic attack which reveals that heme iron prefers to approach the O2 atom at the endoperoxide linkage of artemisinin compounds in agreement with the experimentally proposed mechanism of action of artemisinin compounds. The relative electrophilicity, ( $f_k^+ / f_k^-$ ) shows that compound 4 has maximum reactivity followed by compounds 9 and 10. The comparative QSAR study with the help of DFT and MM techniques provide the importance of the selected descriptors in predicting activity of the artemisinin analogues.

### References

1. *Global burden of disease: 2004 update*. Geneva, World Health Organization, [www.who.int/healthinfo/bodestimates/en/index.html](http://www.who.int/healthinfo/bodestimates/en/index.html) (2008)
2. Roll Back Malaria, World Health Organization, and UNICEF, World Malaria Report (2005)
3. Liu, C.; Wang, Y.; Ouyang, F.; Ye, F., H.; Li, G. *Advances in artemisinin research*, *Huaxue Jinzhan* **11**, 41–48 (1999)

4. Vroman, J. A.; Gaston, A.; Avery, M.A. Current progress in the chemistry, medicinal chemistry and drug design of artemisinin based antimalarials, *Curr. Pharm. Des.* **5**, 101–138 (1999)
5. Tonmunphean, S.; Parasuk, V.; Kokpol, S. QSAR Study of Antimalarial Activities and Artemisinin-Heme Binding Properties Obtained from Docking Calculations, *Quant. Struct. Act. Relat.* **19**, 475–483 (2000)
6. Hansch, C; Fujita, T  $p$ - $\sigma$ - $\pi$  Analysis. A Method for the Correlation of Biological Activity and Chemical Structure, *J. Am. Chem. Soc.* **86**, 1616–1626 (1964)
7. Avery, M. A.; McLean, G.; Edwards, G.; Ager, A. Structure-activity relationships of peroxide-based artemisinin antimalarials, *Biol. Act. Nat. Prod.* **8**, 121–132 (2000)
8. Tonmunphean, S.; Parasuk, V.; Kokpol, S. Automated calculation of docking of artemisinin to heme, *J. Mol. Model.* **7**, 26–33 (2001)
9. Pinheiro, J. C.; Kiralj, R.; Ferreira, M. M. C. Artemisinin derivatives with antimalarial activity against *Plasmodium falciparum* designed with the aid of quantum chemical and partial least squares methods. *QSAR Comb. Sci.* **22**, 830–842 (2003)
10. Pinheiro, J. C.; Ferreira, M. M. C., Romero, O. A. S. Antimalarial activity of dihydroartemisinin derivatives against *P. falciparum* resistant to mefloquine: a quantum chemical and multivariate study *J. Mol. Struct. (Theochem)* **572**, 35–44 (2001)
11. Avery, M. A. *et al.* Structure-activity relationships of the antimalarial agent artemisinin. 6. The development of predictive in vitro potency models using CoMFA and HQSAR methodologies, *J. Med. Chem.* **45**, 292–303 (2002)
12. Silva, M. C.; Kiralj, R.; Ferreira, M. M. C. Estudo Teo'rico da Interacua~o Existente Entre a Artemisinina e Heme, *Quim. Nova* **30**, 25–31 (2006)
13. Cramer III, R.; Patterson, D.; Bunce, J. Comparative Molecular-Field Analysis (ComFA). 1. Effect of Shape on Binding of Steroids to Carrier Proteins, *J. Am. Chem. Soc.* **110**, 5959–5967 (1988)

14. Cheng, F. *et al.* Molecular docking and 3-D-QSAR studies on the possible antimalarial mechanism of artemisinin analogues. *Bioorg. Med. Chem.* **10**, 2883–2891 (2002)
15. Guha, R.; Jurs, P. C. The development of QSAR models to predict and interpret the biological activity of artemisinin analogues *J. Chem. Inf. Comput. Sci.*, **44**, 1440–1449 (2004)
16. Parr, R. G.; Pearson, R. G. Absolute hardness: comParrion parameter to absolute electronegativity, *J. Am. Chem. Soc.* **105**, 7512–7516 (1983)
17. Parr, R. G.; Donnelly, R. A.; Levy, M.; Palke, W. E. Electronegativity- the density functional viewpoint, *J. Chem. Phys.* **68**, 3801–3807 (1978)
18. Parr, R. G.; Szentpaly, L. V.; Liu, S. Electrophilicity Index, *J. Am. Chem. Soc.* **121**, 1922–1924 (1999)
19. Chattaraj, P. K.; Maiti, B.; Sarkar, U. Philicity: A Unified Treatment of Chemical Reactivity and Selectivity, *J. Phys. Chem. A* **107**, 4973–4975 (2003)
20. Chatterjee, A.; Balaji, T.; Matsunaga, H.; Mizukami F. A reactivity index study to monitor the role of solvation on the interaction of the chromophores with amino-functional silanol surface for colorimetric sensors, *J. Mol. Graph. Model.* **25**, 208–218 (2006)
21. Roy, R. K.; Usha, V.; Patel, B.; Hirao, K. Acetalization and thioacetalization of cabonyl compounds: a case study based on global and local electrophilicity descriptors, *J. Comp. Chem.* **27**, 773–780 (2006)
22. Parthasarathi, R.; Subramanian, V.; Roy, D. R.; Chattaraj, P. K. Electrophilicity index as a possible descriptor of biological activity, *Bioorg. Med. Chem.* **12**, 5533–5543 (2004)
23. Padmanabhan, J.; Parthasarathi, R.; Subramanian, V.; Chattaraj, P. K. QSPR models for polychlorinated biphenyls: *n*-Octanol/water partition coefficient, *Bioorg. Med. Chem.* **14**, 1021–1028 (2006)
24. Saha, S.; Roy, R. K. ‘One-into-Many’ Model: An Approach on DFT Based Reactivity Descriptor to Predict the Regioselectivity of Large System, *J. Phys. Chem. B* **111**, 9664–9674 (2007)



25. Proft, F. D.; Geerlings, P. Conceptual and Computational DFT in the Study of Aromaticity, *Chem. Rev.* **101**, 1451–1464 (2001)
26. Chattaraj, P. K.; Sarkar, U.; Roy, D. R. Electrophilicity Index, *Chem. Rev.* **106**, 2065–2091 (2006)
27. Roy, R. K. On the Reliability of Global and Local Electrophilicity Descriptors, *J. Phys. Chem. A* **108**, 4934–4939 (2004)
28. Sarmah, P.; Deka, R. C. Anticancer activity of nucleoside analogues: A density functional theory based QSAR study, *J. Mol. Model.* **16**, 411–418 (2010)
29. Sarmah, P.; Deka, R. C. DFT-based QSAR and QSPR models of several cis-platinum complexes: solvent effect, *J. Comp.-Aided Mol. Des.* **23**, 343–354 (2009)
30. Sarmah, P.; Deka, R. C. Solvent effect on the reactivity of cis-platinum(II) complexes : A density functional approach, *Int. J. Quant. Chem.* **108**, 1400–1409 (2008)
31. Wan, J.; Zhang, L.; Yang, G. F. Quantitative structure-activity relationships for phenyl triazolinones of protoporphyrinogen oxidase inhibitors: A density functional theory study, *J. Comput. Chem.* **25**, 1827–1832 (2004)
32. Srivastava, H. K.; Pasha, F. A.; Singh, P. P. Atomic softness-based QSAR study of testosterone, *Int. J. Quant. Chem.* **103**, 237–245 (2005)
33. Gu, J.; Chen, K.; Jiang, H.; Leszczynski, J. The Radical Transformation in Artemisinin: A DFT Study, *J. Phys. Chem. A* **103**, 9364–9369 (1999)
34. Milhous, W. K.; Weatherley, N.F.; Bowdre, J. H.; Desjardins, R. E. In vitro activities of and mechanisms of resistance to antifol antimalarial drugs, *Antimicrob. Agents. Chemother.* **27**, 525–530 (1985)
35. Lisgarten, J. N.; Potter, B. S.; Bantuzeko, C.; Palmer, R. A. Structure, absolute configuration, and conformation of the antimalarial compound, Artemisinin , *J. Chem. Cryst.* **28**, 539–543 (1998)
36. Delley, B. J. An all-electron numerical method for solving the local density functional for polyatomic molecules, *J. Chem. Phys.* **92**, 508–517 (1990)
37. Hehre, W. J.; Radom, L.; Schlyer, P. V. R.; Pople, J. A. *Ab Initio Molecular Orbital Theory* (Wiley, New York, 1986).

38. Delley, B. From molecules to solids with the DMol3 approach, *J. Chem. Phys.* **113**, 7756–7764 (2000)
39. HyperChem Release 7, Hypercube; <http://www.hyper.com> (2002)
40. Pearson, R. G. Recent advances in the concept of hard and soft acids and bases, *J. Chem. Educ.* **64**, 561–567 (1987)
41. Cho, D.H.; Lee, S.K.; Kim, B.T.; No, K.T. Quantitative Structure-Activity Relationship (QSAR) Study of New Fluorovinylloxyacetamides, *Bull. Korean Chem. Soc.* **22**, 388–394 (2001)
42. Yao, S.W. *et al.* Synthesis and QSAR Study of the Anticancer Activity of Some Novel Indane Carbocyclic Nucleosides, *Bioorg. Med. Chem.* **11**, 4999–5006 (2003)
43. Dietrich, S.W.; Dreyer, N.D.; Hansch, V.; Bentley, D.L. Confidence interval estimators for parameters associated with quantitative structure-activity relationships, *J. Med. Chem.* **23**, 1201–1205 (1980)
44. Bowden, A. C.; Wong, J. T. Evaluation of rate constants for enzyme-catalysed reactions by the jackknife technique. Application to liver alcohol dehydrogenase, *Biochem. J.* **175**, 969–976 (1978)

# 6

## DFT STUDIES ON HEME ARTEMISININ INTERACTION

---

### **Abstract**

A systematic DFT calculation has been performed to investigate the interaction of artemisinin with heme. Interaction energies, electronic states, and geometrical arrangements for the complexes between the heme and artemisinin have been determined. The antimalarial activity of artemisinin is supposed to be mediated by its interaction with intra-parasitic heme leading to free radicals which would be responsible for killing the parasite. Thus, the heme–artemisinin interaction constitutes the initial stage of the mechanism of action of artemisinin.

The results of theoretically calculated geometrical arrangements of the heme-artemisinin complex are found to be in good agreement with available experimental results. The most favorable heme-artemisinin interaction takes place in the most stable complex which is in triplet spin state. Calculated values of interaction energies and electronic states have provided an insight on the mechanism of action of artemisinin with heme.

## 6.1 Introduction

In the previous chapter we have studied the structure and chemical reactivity of artemisinin and some of its selected derivatives. DFT based reactivity descriptors have successfully describe the reactive sites of the molecules. A QSAR study was also performed using few selected descriptors to predict the activity of the artemisinin analogues.

We have already discussed the unique structure of artemisinin where the presence of endoperoxide group is responsible for the antimalarial activity. The interaction of this group with intracellular heme group of human hemoglobin constitutes the initial stage of the mechanism of action of artemisinin.<sup>1</sup> Recently, it has been established that heme reacts with artemisinin more efficiently than hemin, inorganic iron, or hemoglobin.<sup>2</sup>

The malaria parasite needs to synthesize its own protein for rapid development. In humans, malarial parasites digest more than 70% of hemoglobin within the infected red blood cell,<sup>3</sup> giving globin and heme as the products. Globin is hydrolyzed into amino acids which are used in protein synthesis by the parasite. The process also releases free heme (Fe(II) protoporphyrin-IX) which is toxic for the parasite. Malaria parasite detoxifies the toxic heme by its conversion into hemozoin through a specific mechanism called heme polymerization. The hemozoin formation involves the oxidation of heme to hemin (Fe(III) protoporphyrin-IX) by a mechanism that is not yet fully explored, but this step is presumed to involve molecular oxygen as the oxidizing agent.<sup>4</sup> Disruption of the hemozoin formation is the strategy most widely used for treating malaria.<sup>5</sup>

Several other molecular targets have been proposed apart from heme, for the reactive intermediates generated from artemisinin and its derivatives.<sup>6-12</sup> The reason why resistance has not yet developed against artemisinins is that, they exert their antimalarial effects not only by hitting a single biological target, but also by simultaneously hitting several targets with very high precision and efficiency.<sup>13,14</sup>

The mode of action of artemisinin has been suggested to involve at least two distinct steps.<sup>1,15,16,17</sup> In the first step, the activation step, one electron transfer from the heme Fe<sup>2+</sup> ion attacks and breaks the endoperoxide linkage of artemisinin. The cleavage of the endoperoxide generates oxygen centered radicals that immediately rearrange to carbon centered radicals. The transformation from the

oxygen to carbon-centered radicals can occur either from a homolytic cleavage of the C1-C2 bond or an intramolecular 1,5-H atom shift. These two pathways are presented in Figure 6.1. In the second step, such carbon radicals alkylate heme<sup>18,19</sup> disrupt the heme detoxifying process probably by preventing its polymerization into hemozoin.<sup>20</sup> This can cause the parasite death by a mechanism similar to that proposed for the quinoline-based antimalarials.<sup>21,22</sup>

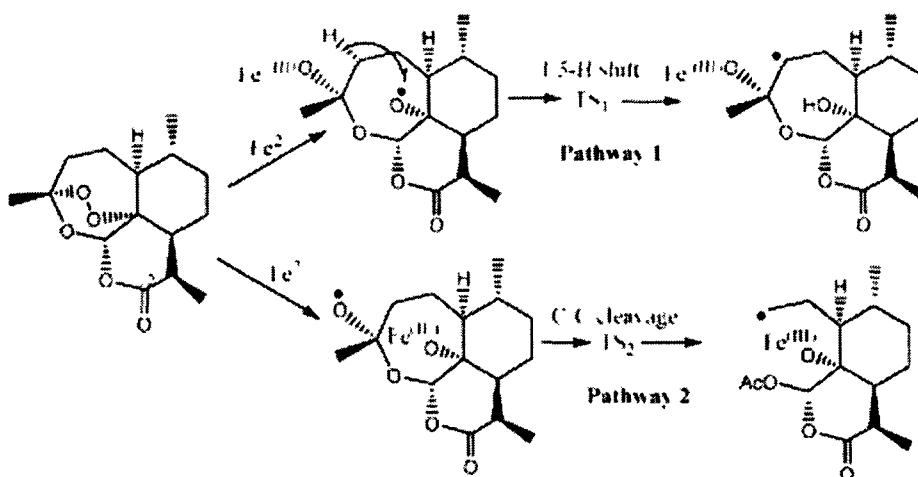


**Figure 6.1** Proposed mechanism of action of artemisinin

However, in spite of various mechanisms that have been proposed, the detailed mechanism of artemisinin action is not yet clear<sup>23,24</sup> and is still under debate.<sup>13,25-30</sup> It has been suggested that different reactive intermediates are generated in the decomposition of artemisinin and similar endoperoxide-based drugs and some of these could be the mediators of the antimalarial activity of this class of compounds.

The theoretical investigations on the reactions reveal that both the homolytic C–C cleavage reaction and the intramolecular 1,5-hydrogen shift process are important for antimalarial activities. The second pathway is found to be energetically more preferable.<sup>31</sup> On the other hand, other theoretical works performed utilizing docking approach between artemisinin compounds and heme illustrate the preference of heme iron to approach the O1 atom at the endoperoxide linkage of artemisinin compounds.<sup>32,33</sup>

The decomposition mechanism of artemisinin and other trioxanes induced by Fe(II)-containing species has been the subject of several studies during the past decade.<sup>34,35</sup> The mechanisms proposed by Cumming and Wu, have been combined and with slight modifications, are accepted as the reference. Definitive evidence for the generation of carbon radical intermediates during ferrous-mediated endoperoxide degradation of artemisinin and its derivatives was provided by EPR spin-trapping techniques.<sup>35-37</sup>

Apart from experimental studies, several theoretical investigations related to the antimalarial mode of action of artemisinin have been reported.<sup>31,33,38-56</sup> Gu *et al.*,<sup>57</sup> studied the reaction mechanism of the radical transformations in artemisinin by using a structurally similar model molecule, 6,7,8-trioxabicyclo[3,2,2]nonane. They predicted the transition state species and the details of the potential energy surfaces of the intramolecular 1,5-hydrogen shift and the homolytic cleavage of the C-C bond in artemisinin. The structural details of the O-centered radical and the corresponding low value of free energy of activation has been found for the intramolecular 1,5-hydrogen shift process in artemisinin. Recently, Moles *et al.*<sup>58</sup> have also reported similar theoretical study on the decomposition mechanisms of artemisinin, by using the same molecule as the molecular model for artemisinin. They could satisfactorily explain all relevant intermediates as well as the final products. However, several intermediates and radicals have been found as relatively stable species, thus giving support to the current hypothesis that some of these species can be responsible for the antimalarial action of artemisinin and its derivatives.

In a very recent paper, Moles *et al.*<sup>59</sup> have reported a theoretical study on the electronic and topological aspects on the reaction of dihydrated Fe(OH)<sub>2</sub> with 6,7,8-trioxabicyclo[3.2.2]nonane, as a model for the reaction of heme with artemisinin. The ferrous model was found to react preferably with the endoperoxide-containing species rather than with molecular oxygen. The reported results explain the affinity between Fe and the peroxide bond and suggest that artemisinin would compete with molecular oxygen in the very first step of hemozoin formation, killing the malaria parasite.

Drew *et al.*<sup>60</sup> investigated reactions of *seco* and *carba* analogues of artemisinin and arteether using DFT and found that addition of an electron leads to

scission of the O1–O2 bond and the energy barrier for subsequent 1,5-intramolecular hydrogen abstraction to produce a carbon-centred radical is similar to that for the parent compounds. Taranto *et al.*<sup>49,53</sup> studied the decomposition process at the semiempirical AM1 and PM3 levels. Tonmunphean *et al.*<sup>31</sup> also reported these steps by using artemisinin, dihydroartemisinin, deoxyartemisinin and another 12 antimalarial artemisinin derivatives.

A theoretical investigation at DFT/ZORA/TZP level, dealing with the interactions of several endoperoxides including artemisinin, with two possible sources of iron, namely the  $[\text{Fe}(\text{H}_2\text{O})_6]^{2+}$  ion and heme, has been reported.<sup>48</sup> The authors describe an initial formation of an Fe–O bond, followed by O–O cleavage, yielding the oxygen-radical species that subsequently transformed into the carbon-centered radicals.

In this chapter, we have presented a systematic study on interaction and geometrical arrangements of artemisinin with respect to heme by means of DFT calculations.

## 6.2 Computational Details

We performed full geometry optimizations with the isolated heme group and the artemisinin molecule. Then, the heme–artemisinin complex was fully optimized. We performed calculations for both heme and the heme–artemisinin complex for at least three different spin controlled electronic states. For heme, the states with singlet, triplet and quintet multiplicities ( $S = 0, 1$  and  $2$ , respectively) were calculated, while triplet, quintet, and septet states ( $S = 1, 2$ , and  $3$ , respectively) were calculated for the complex between heme and artemisinin.

All DFT calculations were performed using DMol<sup>3</sup> program package. The geometries of the heme group and of the artemisinin molecule were fully optimized at generalized gradient approximation (GGA)<sup>61</sup> with BLYP<sup>62</sup> functional as well as LDA with VWN functional. We used double numerical with polarization (DNP) basis set for optimization of the geometries of both artemisinin and the heme group. Similarly, calculations for the heme–artemisinin complex, with the  $d^6 \text{Fe}^{2+}$  ion (or  $d^5 \text{Fe}^{3+}$ ), were also performed at the same level of theory. The electronic populations are calculated using MPA and HPA.

## 6.3 Results and Discussion

### 6.3.1 DFT calculations of artemisinin

#### 6.3.1.1 Optimized geometry of artemisinin

The geometries of artemisinin optimized at BLYP/DNP level is shown in Figure 6.2.

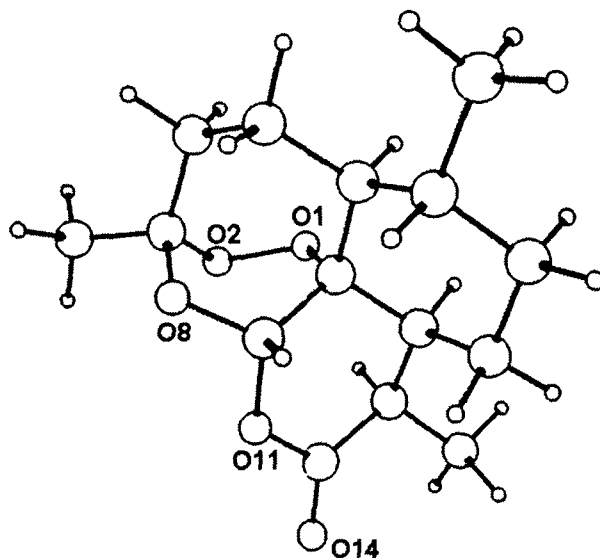


**Figure 6.2** The optimized geometry of artemisinin.

The selected geometric parameters of artemisinin obtained from BLYP/DNP and VWN/DNP levels of calculation are presented in Table 6.1. It is seen from Table 6.1 that the calculated O1—O2 bond lengths of peroxide moiety of all the theoretical calculations are found to be 1.390–1.510Å. These values are in good agreement with some of the available experimental and theoretical results.

It is also observed from Table 6.1 that the C5—O1 and C1—O2 distances fall into the interval of (1.435-1.476Å) and (1.399-1.424Å), respectively. These distances are in consistent with the experimentally determined values (1.450-1.461Å) and (1.469-1.474Å).



**Table 6.1** Selected geometric parameters of artemisinin calculated using BLYP/DNP and VWN/DNP levels. Some data from reference works are also indicated.

Functional /basis set	Geometric parameters (Å)		
	C5-O1	C1-O2	O1-O2
VWN/DNP	1.435	1.399	1.447
BLYP/DNP	1.476	1.424	1.510
HF/6-31G(d) <sup>52</sup>	1.429	1.396	1.390
HF/6-31G <sup>54</sup>	1.469	1.435	1.447
Experimental <sup>63</sup>	1.461	1.416	1.469
Experimental <sup>64</sup>	1.450	1.418	1.474

### 6.3.1.2 Atomic charges

Atomic charges of selected atoms of artemisinin calculated using both MPA and HPA are given in Table 6.2.

**Table 6.2** Mulliken and Hirshfeld atomic charge density for all the oxygen atoms of artemisinin calculated using BLYP/DNP and VWN/DNP level.

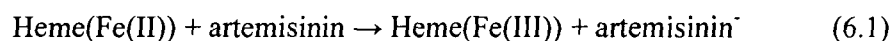
Atom	Atomic charges (e <sup>-</sup> )			
	BLYP/DNP		VWN/DNP	
	Mulliken	Hirshfeld	Mulliken	Hirshfeld
O1	-0.287	-0.080	-0.238	-0.058
O2	-0.256	-0.080	-0.213	-0.065
O8	-0.480	-0.145	-0.396	-0.124
O11	-0.431	-0.131	-0.340	-0.105
O14	-0.390	-0.255	-0.357	-0.248

As can be seen from Table 6.2, both MPA and HPA derived charges for different types of oxygen atoms have negative values. However, the charges on O8, O11 and O14 atoms are more negative compared to that on atoms O1 and O2.

Thus, our calculations show that the negative charge density of artemisinin concentrates not on the peroxide group but on the other oxygen atoms including that of the carbonyl group. Although these results may indicate a possible interaction of artemisinin with an electron poor group via the carbonyl group, this would have little effect on the peroxide group, well-known as the most relevant group in artemisinin for its antimalarial activity.

When analyzing the two oxygen atoms of the peroxide group the charge density on O1 is found to be less than that on O2, with both MPA and HPA. However, the values for Hirshfeld charge densities are much lower than those of Mulliken values. This leads to the possibility of interaction of the peroxide group of artemisinin with an electron rich atoms rather than with an electron poor one.

During interaction, heme reduces artemisinin. The electron transfer reaction may be represented by the general equation:



As depicted in equation 6.1, during interaction artemisinin receives an electron from  $\text{Fe}^{2+} \rightarrow \text{Fe}^{3+}$  conversion. Thus there is a nucleophilic attack on artemisinin.

### 6.3.1.3 Fukui function

Local reactivity parameter, Fukui function, describes the relative reactivity and site selectivity of atoms in a molecule. In conventional Fukui function computations, a value of 1.0 is used for  $\Delta N$ , i.e., one full electron is removed or added (equation 2.15) for the calculation of the charge density of the ions. DMol<sup>3</sup> can use fractional charges for this purpose. This yields faster SCF convergence, and results closer to the limit of  $\Delta N=0$  for which a value of 0.1 is recommended.

We present the Fukui function of all the oxygen atoms of artemisinin in Table 6.3. From the  $f_k^-$  values all the oxygen atoms it is found that the atoms O1, O2 and O14 shown in Figure 6.1 have the higher values of  $f_k^-$ . However, among the three atoms O14 shows the highest values of  $f_k^-$  in both MPA and HPA schemes and thus reflects the highest susceptibility to electrophilic attack on it.

**Table 6.3** Calculated Fukui function ( $f_k^-$ ,  $f_k^+$ ), relative nucleophilicity ( $f_k^-/f_k^+$ ) and relative electrophilicity ( $f_k^+/f_k^-$ ) values of all the oxygen atoms of artemisinin. These values are evaluated at BLYP/DNP, VWN/DNP levels using HPA and MPA charges.

Atom	$f_k^-$		$f_k^+$		$f_k^-/f_k^+$		$f_k^+/f_k^-$	
	MPA	HPA	MPA	HPA	MPA	HPA	MPA	HPA
<b>BLYP/DNP</b>								
O1	0.124	0.105	0.215	0.190	0.577	0.553	1.734	1.810
O2	0.105	0.098	0.223	0.200	0.471	0.490	2.124	2.041
O11	0.026	0.042	0.007	0.006	3.714	7.000	0.269	0.143
O13	0.049	0.043	0.039	0.027	1.256	1.593	0.796	0.628
O14	0.191	0.185	0.051	0.045	3.745	4.111	0.267	0.243
<b>VWN/DNP</b>								
O1	0.127	0.108	0.172	0.151	0.738	0.715	1.354	1.398
O2	0.104	0.099	0.180	0.160	0.578	0.619	1.731	1.616
O11	0.021	0.040	0.014	0.019	1.500	2.105	0.667	0.475
O13	0.042	0.038	0.032	0.024	1.313	1.583	0.762	0.632
O14	0.181	0.180	0.075	0.073	2.413	2.466	0.414	0.406

On the other hand, while the Fukui function values, ( $f_k^+$ ), of all the oxygen atoms are compared, it is seen from Table 6.3 that the value of  $f_k^+$  is higher in case of atoms O1 and O2, the later being the highest one. The rest of the oxygen atoms have significantly low values of  $f_k^+$ . This indicates that the heme-artemisinin interaction happens through nucleophilic attack on artemisinin. This also establishes that the heme iron prefers to approach the O2 atom at the endoperoxide linkage of artemisinin compounds. Therefore, from  $f_k^+$  values of O1 and O2 atoms, it is prominent that O2 is more susceptible for nucleophilic attack compared to O1 and other oxygen atoms in artemisinin.

#### 6.3.1.4 Relative electrophilicity, $(f_k^+/f_k^-)$

Other local reactivity descriptors, relative nucleophilicity,  $(f_k^-/f_k^+)$ , and relative electrophilicity,  $(f_k^+/f_k^-)$ , generate improved intramolecular as well as intermolecular reactivity trends than those obtained from condensed Fukui function. The relative nucleophilicity, and relative electrophilicity values of all the oxygen atoms of artemisinin derived from MPA and HPA schemes at BLYP/DNP and VWN/DNP level are reported in Table 6.3.

It is noticed from Table 6.3 that  $f_k^-/f_k^+$  values are maximum for O14 followed by atom O11. On the other hand, the relative electrophilicity,  $(f_k^+/f_k^-)$ , values of O2 are observed to be maximum followed by that of O1. The other oxygen atoms have significantly low  $f_k^+/f_k^-$  values. Thus relative electrophilicity values reveal O1 and O2 to be the preferred sites for nucleophilic attack in the artemisinin molecule. This also establishes that as the O2 atom is the most preferred site for nucleophilic attack, the heme–artemisinin interaction should preferentially involve oxygen O2 instead of O1.

### 6.3.2 DFT calculations for the heme group

The heme group has an  $\text{Fe}^{2+}$  ion coordinated to four pyrrolic nitrogen atoms making the porphyrin ring.<sup>65</sup> In order to study the interaction of artemisinin with heme, the coordination environment of hemoglobin is maintained as in the real system by adding a histidine residue to one of the pseudoaxial positions of the heme unit. The geometry of heme group in conjugation with the histidine residue optimized at BLYP/DNP level is shown in Figure 6.3.

It can be seen from Figure 6.3 that the minimum energy structure of heme has a conformation where the pairs of  $\alpha$  and  $\beta$  carbons forming the border of the pyrrolic rings are located up and down of the medium plane of porphyrin, respectively, while the meso carbon atoms are in the plane.<sup>66</sup>

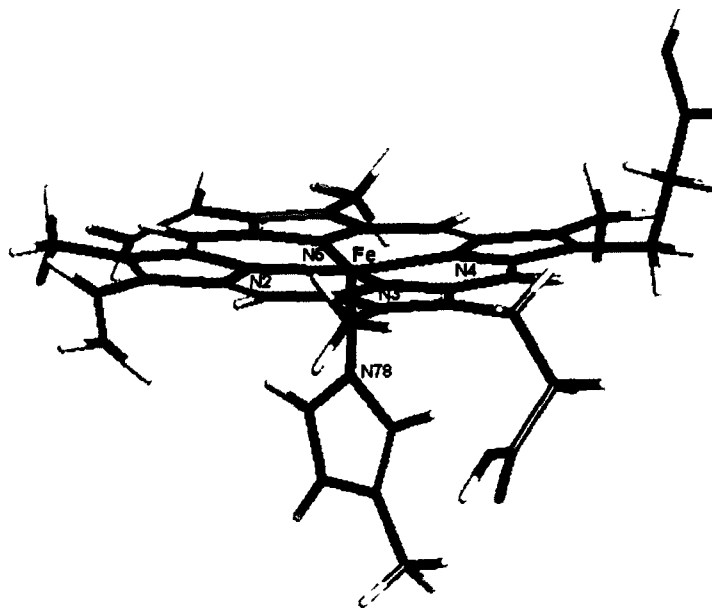


**Figure 6.3** The optimized geometry of heme group coordinated to a histidine residue.

### 6.3.2.1 Geometry

The coordination distance between iron and nitrogen are important geometric parameters to determine the structure of heme. The distances between  $\text{Fe}^{2+}$  and the imidazolic nitrogen of the histidine residue and the distances between the  $\text{Fe}^{2+}$  ion and the pyrrolic nitrogens calculated for various spin states are presented in Table 6.4. It is seen from Table 6.4 that in case of singlet, quintet and septet states, the distances between the  $\text{Fe}^{2+}$  ion and the imidazolic nitrogen of the histidine residue are higher than the distances between  $\text{Fe}^{2+}$  and the pyrrolic nitrogens. The trend is of reverse order in case of triplet state. The differences are, however, dependent on the spin state as well as the basis set. For instance, at the VWN/DNP level, the difference reduces from the singlet spin state to the quintet spin state, and increases from the quintet spin state to the septet spin state. Our observation is in good agreement with some of the experimental and theoretical results. However, in relation to the Fe–N distances, the BLYP/DNP results are closer to the experimental values.

**Table 6.4** Selected geometric parameters for heme group coordinated to a histidine residue, calculated at various spin states using BLYP/DNP and VWN/DNP levels. Some data from reference works are also indicated.

Structure	Functional /basis set	Geometric parameters				
		Fe-N5	Fe-N2	Fe-N78	N5-Fe-N3	N2-Fe-N4
Singlet	VWN/DNP	1.972	1.981	2.102	176.2	170.4
	BLYP/DNP	2.047	2.038	2.006	171.3	169.9
	Theoretical <sup>41</sup>	2.000	1.992	1.931	177.6	170.3
Triplet	VWN/DNP	1.979	1.969	1.867	174.2	171.1
	BLYP/DNP	2.047	2.034	1.985	170.3	168.7
	Theoretical <sup>41</sup>	1.993	2.017	2.249	173.1	170.8
Quintet	VWN/DNP	1.974	1.974	2.037	175.3	170.0
	BLYP/DNP	2.042	2.041	2.346	173.4	170.7
	Theoretical <sup>41</sup>	1.988	1.994	2.182	177.7	171.4
Septet	VWN/DNP	1.976	1.978	2.078	175.4	168.9
	BLYP/DNP	2.042	2.038	2.264	171.5	168.2
	Theoretical <sup>41</sup>	2.064	2.064	2.105	158.5	163.8
	Expt. <sup>67</sup>	2.061	2.052	2.233	152.1	152.1

### 6.3.2.2 Atomic charges and spin densities

The calculated charge densities of the pyrrolic nitrogen atoms of the heme group in conjugation with the histidine residue are presented in Table 6.5. It is seen from Table 6.5 that the charge densities on the pyrrolic nitrogen atoms are negative and almost evenly distributed. In contrast, the iron atom has positive charge density. The results obtained at BLYP/DNP and VWN/DNP levels show that the atomic charge values for triplet, quintet, and septet electronic states are similar, although there is a small increase in the positive charge on the Fe<sup>2+</sup> ion, with a corresponding increase in the negative charge on the nitrogens coordinated to it, when increasing the multiplicity from singlet, to triplet, quintet, and septet.

**Table 6.5** Atomic charges on selected atoms of the heme group calculated at BLYP/DNP and VWN/DNP levels.

Structure	Basis set/ functional	Fe		N2		N3		N4		N5		N78	
		MPA	HPA	MPA	HPA	MPA	HPA	MPA	HPA	MPA	HPA	MPA	HPA
Singlet	VWN/DNP	0.256	0.162	-0.410	-0.099	-0.409	-0.097	-0.412	-0.102	-0.419	-0.098	-0.295	-0.085
	BLYP/DNP	0.363	0.186	-0.459	-0.117	-0.472	-0.117	-0.465	-0.118	-0.470	-0.118	-0.318	-0.069
	Theoretical	1.196		-0.786		-0.767		-0.795		-0.773		-0.486	
Triplet	VWN/DNP	0.174	0.172	-0.415	-0.098	-0.412	-0.098	-0.413	-0.099	-0.419	-0.099	-0.190	-0.048
	BLYP/DNP	0.391	0.224	-0.474	-0.120	-0.483	-0.120	-0.478	-0.121	-0.484	-0.122	-0.317	-0.065
	Theoretical	1.182		-0.804		-0.775		-0.805		-0.790		-0.494	
Quintet	VWN/DNP	0.244	0.173	-0.410	-0.098	-0.414	-0.097	-0.412	-0.101	-0.423	-0.098	-0.279	-0.074
	BLYP/DNP	0.461	0.217	-0.470	-0.118	-0.481	-0.117	-0.473	-0.120	-0.480	-0.118	-0.382	-0.111
	Theoretical	1.353		-0.824		-0.831		-0.834		-0.836		-0.523	
Septet	VWN/DNP	0.296	0.211	-0.422	-0.102	-0.425	-0.100	-0.423	-0.105	-0.435	-0.102	-0.297	-0.082
	BLYP/DNP	0.507	0.275	-0.486	-0.123	-0.496	-0.122	-0.488	-0.125	-0.499	-0.123	-0.391	-0.104
	Theoretical	1.470		-0.858		-0.864		-0.859		-0.866		-0.576	

**Table 6.6** Spin densities on selected atoms of the heme group calculated at BLYP/DNP and VWN/DNP levels.

Structure	Basis set/ functional	Fe		N2		N3		N4		N5		N78	
		MPA	HPA	MPA	HPA	MPA	HPA	MPA	HPA	MPA	HPA	MPA	HPA
Triplet	VWN/DNP	0.433	0.416	0.017	0.019	0.012	0.015	0.021	0.023	0.016	0.017	-0.007	0.001
	BLYP/DNP	0.381	0.369	0.022	0.022	0.016	0.018	0.022	0.023	0.020	0.021	-0.006	0.000
	Theoretical	2.128		-0.030		-0.021		-0.031		-0.030		0.041	
Quintet	VWN/DNP	1.877	1.795	-0.011	0.006	-0.012	0.005	-0.008	0.009	-0.012	0.004	0.059	0.004
	BLYP/DNP	2.041	1.943	-0.025	-0.003	-0.026	-0.005	-0.025	-0.002	-0.025	-0.005	0.033	0.048
	Theoretical	2.886		-0.054		0.048		-0.051		0.044		0.083	
Septet	VWN/DNP	2.322	2.227	0.004	0.024	-0.001	0.019	0.006	0.026	0.000	0.020	0.091	0.096
	BLYP/DNP	2.363	2.269	0.001	0.020	-0.005	0.016	0.002	0.022	-0.001	0.018	0.055	0.069
	Theoretical	4.242		0.084		0.201		0.090		0.192		0.069	



### 6.3.2.3 Relative energies of heme

Calculated energies for several electronic states of heme group coordinated to a histidine residue are presented in Table 6.7. The corresponding relative energies calculated at BLYP/DNP and VWN/DNP levels of theory are also presented in Table 6.7. It is seen from Table 6.7 that the most stable electronic state of heme is the triplet state. The electronic states of heme are understandable if we analyze the  $\text{Fe}^{2+}$  electronic configuration. The quintet state originates from a  $3d^6$  electronic configuration on the  $\text{Fe}^{2+}$  ion, with the highest possible number of unpaired electrons. If the ligand field around the  $\text{Fe}^{2+}$  ion is weak, a high spin complex is obtained. In our calculation the quintet state is found to be significantly less stable. The septet state, on the other hand, is much less stable. The septet state may be obtained only by the promotion of one of the  $3d^6$  electrons to a higher energy level. It was calculated only to help comparison when the complex with artemisinin is formed.

**Table 6.7** Relative energies for heme group coordinated to a histidine residue calculated at BLYP/DNP and VWN/DNP levels of theory.

Structure	Energy (au)		Relative energies* (kcal/mol)		
	VWN/DNP	BLYP/DNP	VWN/DNP	BLYP/DNP	Theoretical <sup>41</sup>
Singlet	-2207.00244	-2224.48247	8.21	0.00	5.44
Triplet	-2207.01552	-2224.46182	0.00	12.95	0.95
Quintet	-2207.01526	-2224.46473	0.16	11.13	0.00
Septet	-2207.00721	-2224.45071	5.21	19.92	25.22

\* Larger positive values for Relative energy indicate weaker interaction

### 6.3.3 DFT calculations for heme–artemisinin complex

We performed full geometry optimization for the artemisinin–heme complex using BLYP/DNP and VWN/DNP levels of theory. The geometries of artemisinin–heme complex optimized at three electronic spin states triplet, quintet, and septet are presented in Figure 6.4 and 6.5. The important inter atomic

distances are indicated in the figures. It is observed from the Figure 6.4 that the distance between O1 and O2 has increased remarkably in the triplet spin state leading to the scission of the bond between them. Artemisinin molecule is closer to the heme moiety showing some sort of interaction between them. However, as can be seen distinctly from Figure 6.5, artemisinin is sufficiently away from the heme moiety in both quintet and septet spin states not to have any significant interaction.

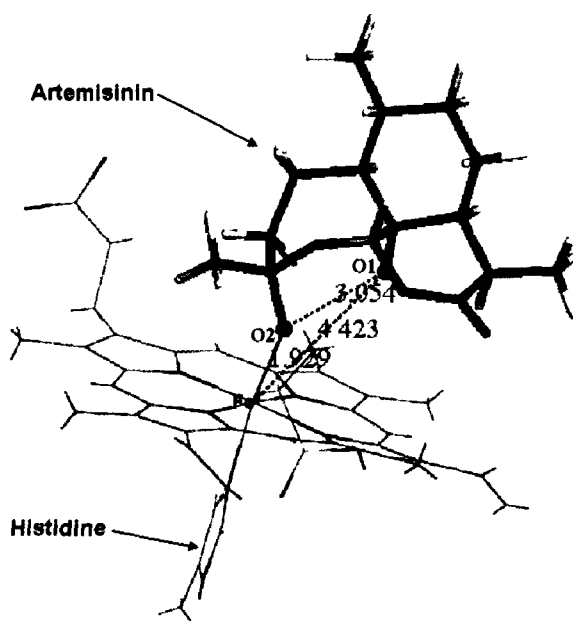


**Figure 6.4** Most stable complex between heme and artemisinin (triplet spin state).

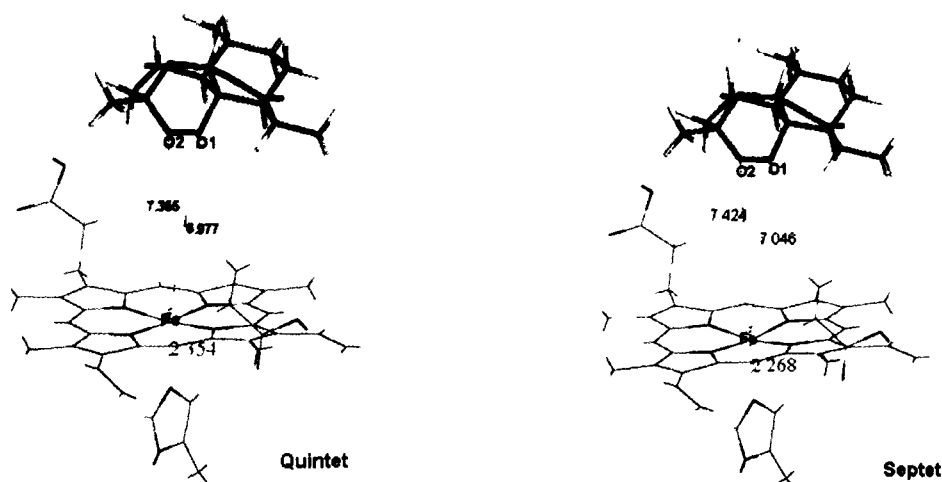


**Figure 6.5** Optimized complex between heme and artemisinin at quintet and septet spin state.

The selected geometric parameters for the optimized heme-artemisinin complexes are presented in Table 6.8. It is seen from Table 6.8 that O1-O2 distance is maximum in triplet state at BLYP/DNP level. This indicates the scission of the bond (which is not seen in quintet and septet spin states). The longer distance of O1-Fe compared to that of O2-Fe indicates that the heme iron interacts with the O2 atom of artemisinin to form a stable adduct in triplet spin state. Although the geometries can be predicted with both the functionals the results with BLYP functional are found to be closer to experimental as well as MP2 results in various compounds.<sup>68</sup>

On the other hand, for the quintet and septet states, it is observed that the O1-O2 retains the minimum distance without breaking the peroxide bond. However, the O1-Fe and O2-Fe distances are seen to get elongated which indicates that there is no interaction between artemisinin and heme. The distance between histidine N and heme Fe does not change significantly in any of the spin states. These results led us to conclude that heme-artemisinin adduct forms preferably at triplet spin state and the heme iron approaches O2 atom in the endoperoxide bond of artemisinin.

**Table 6.8** Geometric parameters calculated using BLYP/DNP and VWN/DNP level for the optimized heme-artemisinin complexes.

Structure	Functional/ basis set	Bond length (Å)			
		O1-O2	O1-Fe	O2-Fe	N78-Fe
Triplet	BLYP/DNP	3.054	4.423	1.929	2.101
	VWN/DNP	1.463	2.909	2.171	1.893
Quintet	BLYP/DNP	1.51	6.977	7.355	2.354
	VWN/DNP	1.444	6.969	7.383	2.088
Septet	BLYP/DNP	1.51	7.046	7.424	2.268
	VWN/DNP	1.445	6.967	7.382	2.081

### 6.3.3.1 Heme-artemisinin interaction energies

The interaction and relative energies for heme-artemisinin complexes calculated at BLYP/DNP and VWN/DNP levels of theory are presented in Table 6.9. It is seen from Table 6.9 that energetically, triplet state forms the most stable complex.

**Table 6.9** Interaction and relative interaction energies for heme-artemisinin complexes calculated at BLYP/DNP and VWN/DNP levels of theory.

Spin state	Interaction energy (kcal/mol)				Relative interaction energy* (kcal/mol)			
	BLYP/DNP		VWN/DNP		BLYP/DNP		VWN/DNP	
	UR	R	UR	R	UR	R	UR	R
Triplet	-177.02	-178.16	-69.43	-69.63	0.00	0.00	0.00	0.00
Quintet	0.97	0.19	30.99	30.96	177.99	178.35	100.42	100.59
Septet	19.41	19.55	47.77	47.76	196.43	197.71	117.20	117.39

UR= Unrestricted; R= Restricted

\* Larger positive values of Relative interaction energy indicate weaker interactions

In the final fully optimized geometry of the adduct, the difference between interaction energies of the triplet and the quintet states is more than 177.99 kcal/mol in the BLYP/DNP and more than 100 kcal/mol in VWN/DNP.

The septet state is the least stable. The quintet spin state is only 18.44 kcal/mol more stable than the septet spin state. These results accord to the expectation of yielding two unpaired electrons if we consider oxidation of the heme group and reduction of artemisinin. Therefore, the septet spin state should result from a  $d^5$  electronic configuration of the  $Fe^{3+}$  ion of the heme group summed up with an unpaired electron on the O1 oxygen atom of artemisinin.

Although some of the previous calculations indicated the quintet as the lowest state,<sup>69</sup> later studies for model systems reported the triplet state as the most stable<sup>60</sup> which in good agreement with results given in the present work.

#### 6.4 Conclusions

Theoretically calculated selected geometric parameters of artemisinin, heme group coordinated to a histidine residue and heme-artemisinin complex are in good agreement with those of the available experimental values.

The DFT calculations for artemisinin attribute higher charge density on O8, O11, and O14 and lower charge density on the peroxide group. Thus, there is a possibility of interaction of artemisinin with an electron poor group via the

carbonyl group possessing the highest charge density. This also leads to the possibility of interaction of the peroxide group, the most relevant group in artemisinin for its antimalarial activity, with an electron rich rather than with an electron poor group.

DFT based local reactivity descriptor, Fukui function showed that the heme-artemisinin interaction happens through nucleophilic attack on artemisinin where the heme iron prefers to approach the O2 atom of the endoperoxide linkage. Another descriptor, relative electrophilicity further establishes these facts.

For heme, the DFT calculations show that the triplet spin state is more stable than the singlet, quintet and septet spin states. The results also show the septet spin state as the most distorted one. Negative charge densities are evenly concentrated on the pyrrolic nitrogen while the iron atom has positive charge density. The spin densities for the triplet and quintet states are completely concentrated on the iron atom of heme while some spin density is also found on the nitrogen atoms in case of the septet state.

It could be predicted that for artemisinin–heme interactions the most stable state is the triplet one. The quintet spin state is slightly more stable than the septet spin state. This result is in good agreement with some of the earlier results performed at low level of theory.

Thus, we could find that heme–artemisinin interaction preferentially involve oxygen O2 instead of O1. It may be confirmed in the present study that after artemisinin reduction, a 1,5-hydride transfer from carbon C4 to oxygen O1 is the most probable pathway in the mode of action of artemisinin.

This leads to a better understanding of antimalarial mechanism and thereby provides guidelines to design new artemisinin analogues with better activity.

## References

1. Meshnick, S. R.; Jefford, C. W.; Posner, G. H.; Avery, M. A.; Peters, W. *Parasitol.* Second-generation antimalarial endoperoxides, *Today*. **12**, 79–82 (1996)
2. Zhang, S.; Gerhard, G. S. Heme Mediates Cytotoxicity from Artemisinin and Serves as a General Anti-Proliferation Target, *Bioorg. Med. Chem.* **16**, 7853–7861 (2008)

3. Francis, S. E.; Sullivan, D. J.; Goldberg, D. E. Hemoglobin metabolism in the malaria parasite, *Plasmodium falciparum*, *Ann. Rev. Microbiol.* **51**, 97–123 (1997)
4. Egan, T. J. Haemozoin formation, *Mol. Biochem. Parasitol.* **157**, 127–136 (2008)
5. Rathore, D.; McCutchan, T. F.; Sullivan, M.; Kumar, S. Antimalarial drugs: current status and new developments, *Expert. Opin. In Vestig. Drugs.* **14**, 871–873 (2005)
6. Eckstein-Ludwig, U. *et al.* Artemisinins target the SERCA of *Plasmodium falciparum*, *Nature.* **424**, 957–961 (2003)
7. Bhisutthibhan, J.; Meshnick, S. R. Immunoprecipitation of [<sup>3</sup>H]Dihydro artemisinin Translationally Controlled Tumor Protein (TCTP) Adducts from *Plasmodium falciparum*-Infected Erythrocytes by Using Anti-TCTP Antibodies, *Antimicrob. Agents Chemother.* **45**, 2397–2399 (2001)
8. Pandey, A. V.; Tekwani, B. L.; Singh, R. L.; Chauhan, V. S. Artemisinin, an Endoperoxide Antimalarial, Disrupts the Hemoglobin Catabolism and Heme Detoxification Systems in Malarial Parasite, *J. Biol. Chem.* **274**, 19383–19388 (1999)
9. Asawamahasakda, W.; Ittarat, I.; Pu, Y. M.; Ziffer, H.; Meshnick, S. R. Reaction of antimalarial endoperoxides with specific parasite proteins, *Antimicrob. Agents Chemother.* **38**, 1854–1858 (1994)
10. Bhisutthibhan, J.; Philbert, M. A.; Fujioka, H.; Aikawa, M.; Meshnick, S. R. The *Plasmodium falciparum* translationally controlled tumor protein: subcellular localization and calcium binding, *Eur. J. Cell Biol.* **78**, 665–670 (1999)
11. Yang, Y. Z.; Little, B.; Meshnick, S. R. Effects of heme, pH, and drug structure, *Biochem. Pharmacol.* **48**, 569–573 (1994)
12. Yang, Y. Z.; Asawamahasakda, W.; Meshnick, S. R. Alkylation of human albumin by the antimalarial artemisinin, *Biochem. Pharmacol.* **46**, 336–339 (1993)

13. O'Neill, P. M.; Posner, G. H. A Medicinal Chemistry Perspective on Artemisinin and Related Endoperoxides, *J. Med. Chem.* **47**, 2945–2964 (2004)
14. Ridley, R. G. Malaria: To kill a parasite, *Nature*. **424**, 887–889 (2003)
15. Vyas, N.; Avery, B.; Avery, M. A.; Wyandt, C. M. Carrier-mediated partitioning of artemisinin into *Plasmodium falciparum*-infected erythrocytes, *Antimicrob. Agents Ch.* **46**, 105–109 (2002)
16. Kamchonwongpaisan, S.; Meshnick, S. R. The mode of action of the antimalarial artemisinin and its derivatives, *Gen. Pharmacol.* **27**, 587–592 (1996)
17. Borstnik, K.; Paik, I. H.; Shapiro, T. A.; Posner, G. H. Antimalarial chemotherapeutic peroxides: Artemisinin, yingzhaosu A and related compounds, *Int. J. Parasitol.* **32**, 1661–1667 (2002)
18. Selmeczi, K.; Robert, A.; Claparols, C.; Meunier, B. Alkylation of human hemoglobin A0 by the antimalarial drug artemisinin, *FEBS Lett.* **556**, 245–248 (2004)
19. Rodriguez, M.; Bonnet-Delpon, D.; Begue, J.-P.; Robert, A.; Meunier, B. Alkylation of manganese(II) tetraphenylporphyrin by antimalarial fluorinated artemisinin derivatives, *Bioorg. Med. Chem. Lett.* **13**, 1059–1062 (2003)
20. Pagola, S.; Stephens, P. W.; Bohle, D. S.; Kosar, A. D.; Madsen, S.K. The structure of malaria pigment beta-haematin, *Nature*. **404**, 307–310 (2000)
21. Cazelles, J.; Robert, A.; Meunier, B. Alkylating Capacity and Reaction Products of Antimalarial Trioxanes after Activation by a Heme Model, *J. Org. Chem.* **67**, 609–616 (2002)
22. Robert, A.; Cazelles, J.; Meunier, B. Characterization of the alkylation product of heme by antimalarial drug artemisinin, *Angew. Chem., Int. Ed.* **40**, 1954–1957 (2001)
23. Fidock, D. A.; Rosenthal, P. J.; Croft, S. L.; Brun, R.; Nwaka, S. Antimalarial drug discovery: efficacy models for compound screening, *Nat. Rev.* **3**, 509–520 (2004)

24. Haynes, R. K. *et al.* Highly Antimalaria-Active Artemisinin Derivatives: Biological Activity Does Not Correlate with Chemical Reactivity, *Angew. Chem., Int. Ed. Engl.* **43**, 1381–1385 (2004)
25. Taranto, A. G.; Carneiro, J.W. d. M.; de Oliveira, F. G.; de Araujo, M. T.; Correa, C. R. The Role of C-Centered Radicals on the Mechanism of Action of Artemisinin, *J. Mol. Struct. (Theochem)* **580**, 207–215 (2002)
26. Robert, A.; Dechy-Cabaret, O.; Cazelles, J.; Meunier, B. From Mechanistic Studies on Artemisinin Derivatives to New Modular Antimalarial Drugs, *Acc. Chem. Res.* **35**, 167–174 (2002)
27. Robert, A.; Benoit-Vical, F. ; Claparols, C. ; Meunier, B. The antimalarial drug artemisinin alkylates heme in infected mice, *Proc. Natl. Acad. Sci. U.S.A.* **102**, 13676–13680 (2005)
28. Tang, Y. *et al.* Dispiro-1,2,4-trioxane Analogs of a Prototype Dispiro-1,2,4-trioxolane: Mechanistic Comparators for Artemisinin in the Context of Reaction Pathways with Iron (II), *J. Org. Chem.* **70**, 5103–5110 (2005)
29. Messori, L. *et al.* The reaction of artemisinins with hemoglobin: a unified picture, *Bioorg. Med. Chem.* **14**, 2972–2977 (2006)
30. Golenser, J.; Waknine, J. H.; Krugliak, M.; Hunt, N. H.; Grau, G. E. Current perspectives on the mechanisms of action of artemisinins, *Int. J. Parasitol.* **36**, 1427–1441 (2006)
31. Tonmunpheap, S.; Parasuk, V.; Kokpol, S. Effective Discrimination of Antimalarial Potency of Artemisinin Compounds Based on Quantum Chemical Calculations of Their Reaction Mechanism, *Bioorg. Med. Chem.* **14**, 2082–2088 (2006)
32. Tonmunpheap, S.; Parasuk, V.; Kokpol, S. QSAR study of antimalarial activities and artemisinin-heme binding properties obtained from docking calculations, *Quant. Struct. Act. Rel.* **19**, 475–483 (2000)
33. Tonmunpheap, S.; Parasuk, V.; Kokpol, S. Automated calculation of docking of artemisinin to heme, *J. Mol. Model.* **7**, 26–33 (2001)



34. Cumming, J. N.; Ploypradith, P.; Posner, G. H. Antimalarial activity of artemisinin (qinghaosu) and related trioxanes: mechanism(s) of action, *Adv. Pharmacol.* **37**, 253–297 (1997)
35. Wu, W.-M. *et al.* Unified mechanistic framework for the FeII-induced cleavage of qinghaosu and derivatives/analogues. The first spin-trapping evidence for the previously postulated secondary C-4 radical, *J. Am. Chem. Soc.* **120**, 3316–3325 (1998)
36. O'Neill, P. M. *et al.* Biomimetic Fe(II)-mediated degradation of arteflene (Ro-42-1611). The first EPR spin-trapping evidence for the previously postulated secondary carbon-centered cyclohexyl radical, *J. Org. Chem.* **65**, 1578–1582 (2000)
37. Butler, A. R. *et al.* EPR evidence for the involvement of free radicals in the iron-catalysed decomposition of qinghaosu (artemisinin) and some derivatives; antimalarial action of some polycyclic endoperoxides, *Free Rad. Res.* **28**, 471–476 (1998)
38. Drew, M. G. B.; Metcalfe, J.; Dascombe, M. J.; Ismail, F. M. D. Reactions of Artemisinin and Arteether with Acid: Implications for Stability and Mode of Antimalarial Action, *J. Med. Chem.* **49**, 6065–6073 (2006)
39. Pereira, M. S. C.; Kiralj, R.; Ferreira, M. M. C. Theoretical Study of Radical and Neutral Intermediates of Artemisinin Decomposition, *J. Chem. Inf. Model.* **48**, 85–98 (2008).
40. Gu, J.; Chen, K.; Jiang, H.; Leszczynski, J. The Radical Transformation in Artemisinin, *J. Phys. Chem. A.* **103**, 9364–9369 (1999)
41. Araujo, J. Q.; Carneiro, J. W. d. M.; de Araujo, M. T.; Leite, F. H. A.; Taranto, A. G. Interaction between artemisinin and heme. A Density Functional Theory study of structures and interaction energies, *Bioorg. Med. Chem.* **16**, 5021–5029 (2008)
42. Nosoongnoen, W. *et al.* Elucidation of the natural artemisinin decomposition route upon iron interaction: a fine electronic redistribution promotes reactivity, *Phys. Chem. Chem. Phys.* **10**, 5083–5093 (2008)

43. Galasso, V.; Kovac, B.; Modelli, A. A theoretical and experimental study on the molecular and electronic structures of artemisinin and related drug molecules, *Chem. Phys.* **335**, 141–154 (2007)
44. Drew, M. G. B.; Metcalfe, J.; Dascombe, M. J.; Ismail, F. M. D. De novo identification and stability of the artemisinin pharmacophore: Studies of the reductive decomposition of deoxyartemisinins and deoxyarteethers and the implications for the mode of antimalarial action, *J. Mol. Struct. (Theochem)* **823**, 34–46 (2007)
45. Wiwanitkit, V. Quantum chemical analysis of alternative pathways for iron activation step for artemisinin, a new antimalarial drug, *J. Infect.* **53**, 148–151 (2006)
46. Taranto, A. G.; Carneiro, J. W. d. M.; de Araujo, M. T. DFT Study of the Reductive Decomposition of Artemisinin, *Bioorg. Med. Chem.* **14**, 1546–1557 (2006)
47. De Araujo, M. T.; de Carneiro, J. W.; Taranto, A. G. Solvent effects on the relative stability of radicals derived from artemisinin: DFT study using the PCM/COSMO approach, *Int. J. Quantum Chem.* **106**, 2804–2810 (2006)
48. Drew, M. G. B.; Metcalfe, J.; Ismail, F. M. D. Antimalarial drugs based on artemisinin: DFT calculations on the principal reactions, *J. Mol. Struct. (Theochem)* **756**, 87–95 (2005)
49. Arantes, C.; de Araujo, M. J.; Taranto, A. G.; de Carneiro, J. W. Relative stability of radicals derived from artemisinin: A semiempirical and DFT study, *Int. J. Quantum Chem.* **103**, 749–762 (2005)
50. Tonmunphean, S.; Parasuk, V.; Kokpol, S. Theoretical Investigations on Reaction Mechanisms of Antimalarial Artemisinin Compounds: Effect of Structure on Kinetic Energy Profile and Antimalarial Activity, *J. Mol. Struct. (Theochem)* **724**, 99–105 (2005)
51. Rafiee, M. A.; Hadipour, N. L.; Naderi-manesh, H. The Role of Charge Distribution on the Antimalarial Activity of Artemisinin Analogues, *J. Chem. Inf. Model.* **45**, 366–370 (2005)

52. Pinheiro, J. C.; Kiralj, R.; Ferreira, M. C. Artemisinin derivatives with antimalarial activity against *Plasmodium falciparum* designed with the aid of quantum chemical and partial least squares methods, *QSAR Comb. Sci.* **22**, 830–842 (2003)
53. Taranto, A. G.; Carneiro, J. W. d. M.; de Oliveira, F. G.; de Araujo, M. T.; Correa, C. R. The Role of C-Centered Radicals on the Mechanism of Action of Artemisinin, *J. Mol. Struct. (Theochem)* **580**, 207–215 (2002)
54. Pinheiro, J. C.; Ferreira, M. M. C.; Romero, O. A. S. Antimalarial activity of dihydroartemisinin derivatives against *P. falciparum* resistant to mefloquine; a quantum chemical and multivariate study, *J. Mol. Struct. (Theochem)* **572**, 35–44 (2001)
55. Gu, J. D.; Chen, K. X.; Jiang, H. L.; Leszczynski, J. A model molecule study of the O-centered and the C-centered free radical intermediates of artemisinin, *J. Mol. Struct. (Theochem)* **491**, 57–66 (1999)
56. Moles, P.; Oliva, M.; Safont, V. S. A theoretical study on the decomposition mechanism of artemisinin, *Tetrahedron*. **64**, 9448–9463 (2008)
57. Gu, J.; Chen, K.; Jiang, H.; Leszczynski, J. The Radical Transformation in Artemisinin: A DFT Study, *J. Phys. Chem. A*. **103**, 9364–9369 (1999)
58. Moles, P.; Oliva, M.; Safont, V. S. Modeling the Decomposition Mechanism of Artemisinin, *J. Phys. Chem. A*. **110**, 7144–7158 (2006)
59. Moles, P.; Oliva, M.; Gonzalez, A. S.; Safont, V. S. A Topological Study of the Decomposition of 6,7,8-Trioxabicyclo[3.2.2]nonane Induced by Fe(II): Modeling the Artemisinin Reaction with Heme, *J. Phys. Chem. B*. **114**, 1163–1173 (2010)
60. Drew, M. G. B.; Metcalfe, J.; Ismail, F. M. D. A DFT study of free radicals formed from artemisinin and related compounds, *J. Mol. Struct. (Theochem)* **711**, 95–105 (2004)
61. White, J. A.; Bird, D. M.; Implementation of gradient-corrected exchange-correlation potentials in Car-Parrinello total-energy calculations, *Phys Rev B*. **50**, 4954–4957 (1994)

62. Becke, A. D. Density-Functional Thermochemistry .3. the Role of Exact Exchange, *J. Chem. Phys.* **98**, 5648–5652 (1993)
63. Lisgarten, J. N.; Potter, B. S.; Bantuzeko, C.; Palmer, R. A. Structure, absolute configuration, and conformation of the antimalarial compound, Artemisinin, *J. Chem. Crystallogr.* **28**, 539–543 (1998)
64. Leban, I.; Golic, L.; Japelj, M. Crystal and molecular structure of qinghaosu: a redetermination, *Acta Pharm. Jugosl.* **38**, 71–77 (1988)
65. Cowan, J. A. *Inorganic Biochemistry: An Introduction* (VHC Publishers, New York, 1993)
66. Munro, O. Q. *et al.* Molecular mechanics study of the ruffling of metalloporphyrins, *J. Am. Chem. Soc.*, **114**, 7218–7230 (1992)
67. Frier, J. A.; Perutz, M. Structure of human foetal deoxyhaemoglobin, *J. Mol. Biol.* **112**, 97–112 (1977)
68. Wang, Z.; Day, P.N.; Pachter, R. A density functional and Hartree-Fock study of pyran and 2,4-pentadienals, *Chem. Phys. Lett.*, **237**, 45-52 (1995)
69. Choe, Y.-K.; Nakajima, T.; Hirao, K.; Lindh, R. Theoretical study of the electronic ground state of iron(II) porphine II, *J. Chem. Phys.* **111**, 3837–3845 (1999)

# 7

## GENERAL CONCLUSIONS

In this thesis, several molecular modeling techniques have been systematically used to investigate structure and properties of two categories of organic bio-active molecules having antitubercular and antimalarial activities. The work presented in various chapters and subsequent outcome are summarized in the following section:

Structure, reactivity and mode of action of drug molecules with the active sites of biological system are very crucial to have insights into the activity of molecules. These properties can be properly described theoretically utilizing molecular modeling techniques, based on quantum mechanics. Due to the advance in computational processing power and their implementation in software during the last few years, more refined techniques of sufficient accuracy for making quantitative predictions have become available. DFT methods have been established as one of the main methods for calculations on organic molecules. However, QM cannot be utilized to study large system because of the involvement of higher computational cost. Such limitations are overcome by using hybrid QM/MM methods which treats a part of a large system at a very accurate QM level and the rest with molecular mechanics. Docking is the computational technique that helps exploration of the possible binding modes of a substrate to a given receptor, enzyme or other binding site and thus plays an important role in rational drug design. Another method QSAR is utilized for estimating structure related properties of molecules.

In chapter 1, we present a general overview of TB and malaria diseases, some of the important drug molecules used for their treatment and a brief review of the theoretical works carried out in this field. The theory of several molecular modeling methods adopted in this thesis are detailed under the title “Theoretical methods of quantum chemistry” in chapter 2.

The third chapter of the thesis deals with the study of antitubercular drug molecules. DFT calculated optimized geometries of anti-tubercular agents INH and PZA are found to be in good agreement with available experimental data. The molecular structure of novel molecule MHI is predicted on this basis. Reactivity comparison performed with DFT based reactivity descriptors has established MHI to be the most reactive one.

Chapter 4 uses docking experiments to find out the most favorable binding mode among the antitubercular drug molecules. Energetically more favorable docking are found with adducts in the sequence INH-NAD>PZA-NAD>NADH. Subsequent use of hybrid QM/MM methods to study the changes of geometry in various environments and their compatibility with experimental values establishes the accuracy of the method. Both INH and PZA drug molecules show similar types of interactions and the interaction energy values reveal that INH interacts more favorably with the relevant bio-molecule compared to PZA.

In Chapter 5, we focus on reactivity of antimalarial drug, artemisinin and some of its derivatives. DFT based reactivity descriptors along with some MM parameters are utilized to build up a statistically significant QSAR equation. Biological activities of theoretically designed artemisinins can be predicted with the help of this equation.

The heme–artemisinin interaction plays an important role in understanding the mechanism of action of artemisinin. Our quantum chemical studies on heme–artemisinin interaction are presented in chapter 6. Endoperoxide oxygens (O1 and O2) are found to be the most reactive atoms in artemisinins. Between the most reactive atoms, heme–artemisinin interaction is found to preferentially involve oxygen O2 instead of O1. This is in excellent agreement with the experimentally proposed mechanism of action of artemisinin compounds. It is also found that, triplet spin state form the most favorable complex rather than quintet and septet states.

While the present chapter (Chapter 7) provides the overall summary and conclusions of this thesis, the specific conclusions derived from each chapter are summarized at the end of those chapters. In general, it is seen that the combination of several molecular modeling techniques along with experiment may be of

significant help in understanding and thus designing a drug molecule for a particular disease.

**Future scopes:**

- The present study on antitubercular drug molecules can be extended up to few more theoretical derivatives of INH.
- For further insight of the mode of action the antitubercular drugs, the ease of forming adduct with NAD by INH derivatives can be studied.
- In case of antimalarial drugs, Docking, QM/MM and FMO studies of various artemisinin derivatives with hemoglobin will be useful in predicting reactivity based on their mode of action.

# List

## OF PUBLICATIONS

### In Journals

1. **Kalyan K. Hazarika**, Nabin C. Barua and Ramesh C. Deka “Interaction of some anti-tuberculosis drug molecules and their NAD adducts to the active site of the *Mycobacterium tuberculosis* enoyl-ACP reductase (InhA): A hybrid QM-MM and docking approach” (under preparation)
2. **Kalyan K. Hazarika**, Pubalee Sarmah, Nabin C. Barua and Ramesh C. Deka “Density Functional Theory Studies on Reactivity of Artemisinin and Some of its Derivatives” (under revision)
3. **Kalyan K. Hazarika**, Nabin C. Barua and Ramesh C. Deka, “Molecular Structure and Reactivity of Anti-tuberculosis Drug Molecules Isoniazid, Pyrazinamide and 2-Methylheptylisonicotinate: a Density Functional Approach” *Struct. Chem.* **2009**, *20*, 1079–1085.
4. P. Mondal, **K.K. Hazarika**, A. Deka and R. C. Deka, “Density functional studies on Lewis acidity of alkaline earth metal exchanged faujasite zeolite”, *Mol. Simul.* **2008**, *34*, 1121–1121.
5. P. Mondal, C. Arunabhiram, **K.K. Hazarika** and R.C. Deka, “Quantum chemical studies on acidity of isomorphously substituted ZSM-5 zeolite”, *Bull. Catal. Soc. Ind.* **2004**, *3*, 82–93.
6. Paritosh Mondal, **Kalyan K. Hazarika** and Ramesh Ch. Deka, “Reactivity of  $\alpha,\beta$ -unsaturated carbonyl compounds towards nucleophilic addition reaction: a local hard-soft acid-base approach”, *Phys. Chem. Commun.* **2003**, *6*, 24–27.



### In Conferences

1. **Kalyan Kr. Hazarika**, Nabin Ch. Barua, Ramesh Ch. Deka, "Density functional comparison of reactivity of anti-tuberculosis drug molecules" *42<sup>nd</sup> IUPAC Congress: Chemistry Solutions, August 02-07, 2009, SECC, Glasgow, United Kingdom.*
2. **Kalyan Kr. Hazarika**, Nabin Ch. Barua and Ramesh Ch. Deka, "Reactivity comparison of Artemisinin and its synthetic Derivatives: A DFT Approach", *the Eighth Triennial Congress of the World Association of Theoretical and Computational Chemists, WATOC 2008" September 14-19, 2008, Sydney, Australia.*
3. **Kalyan Kr. Hazarika**, Nabin Ch. Barua and Ramesh Ch. Deka, "Artemisinin and synthetic derivatives: a DFT based comparison" *10th CRSI National Symposium at Indian Institute of Science, Bangalore from 31-01-08 to 03-02-08.*
4. **Kalyan Kr. Hazarika**, Nabin Ch. Barua and Ramesh Ch. Deka, "Reactivity of new synthetic derivatives of Artemisinin: a DFT based comparison", *International conference organized by The Royal Society of Chemistry "Faraday Discussion 135: Chemical Concepts from Quantum Mechanics", September 04-06, 2006, University of Manchester, United Kingdom.*
5. **Kalyan Kr. Hazarika**, Ramesh Ch Deka and Nabin Ch Barua, "Molecular modeling studies on 2-methylheptylisonicotinate: designing of new anti-TB drug lead for synthesis", *7<sup>th</sup> National Symposium in Chemistry organized by Chemical Research Society of India held at the Indian Association for the Cultivation of Science, Kolkata, February 4-6, 2005.*
6. **Kalyan Kr. Hazarika**, Ramesh C. Deka and N. C. Barua, "Theoretical investigation on binding site interaction of Artemisinin and its derivatives with Heme", *National Symposium on Current Trends in Chemical Research, February 27-28, 2004, Department of Chemistry, Gauhati University, Guwahati*